AD-753 056

REMOVAL AND SEPARATION OF PARTICLES BY CRYSTALLIZATION

Vincent H. S. Kuo

University of Southern California

Prepared for:

Advanced Research Projects Agency

February 1973

USCEE Report 435

UNIVERSITY OF SOUTHERN CALIFORNIA

REMOVAL AND SEPARATION OF PARTICLES BY CRYSTALLIZATION

Vincent H. S. Kuo

November 1972

A Dissertation Presented in Partial Fulfillment of the Requirements for the Degree of Doctor of Philosophy in Chemical Engineering.

This research was supported by Grant No. 4528-AC6 from the Petroleum Research Fund (administered by the American Chemical Society) and by Grant No. DAHC15-72-G7 from the Advanced Research Projects Agency of the Department of Defense.

ELECTRONIC SCIENCES LABORATORY

182

Engineering

UNCLASSIFIED
Security Classification

DOCUMENT CONTROL DATA – R & D
(Security classification of title, body of abstract and indexing annotation must be entered when the overall report is classified)

ORIGINATING ACTIVITY (Corporate author)
Electronic Sciences Laboratory
University of Southern California
Los Angeles, California 90007

2a. REPORT SECURITY CLASSIFICATION
Unclassified

2b. GROUP

3. REPORT TITLE
REMOVAL AND SEPARATION OF PARTICLES BY CRYSTALLIZATION

4. DESCRIPTIVE NOTES (Type of report and inclusive dates)
Dissertation (Sept. 1969 - Nov. 1972)

5. AUTHOR(S) (First name, middle initial, last name)
Vincent H. S. Kuo

6 REPORT DATE	7a. TOTAL NO OF PAGES	7b. NO OF REFS
November 1972	180	76

8a. CONTRACT OR GRANT NO
~~PRF4528-AC6~~; DAHC15-72-G7
b. PROJECT NO. DAHC15-72-G-XXX
ARPA Order No. 1623
c.
d.

9a. ORIGINATOR'S REPORT NUMBER(S)
USCEE Report 435

9b. OTHER REPORT NO(S) (Any other numbers that may be assigned this report)

10 DISTRIBUTION STATEMENT
Approved for public release; distribution unlimited.

11 SUPPLEMENTARY NOTES

12. SPONSORING MILITARY ACTIVITY
Advanced Research Projects Agency

13 ABSTRACT

Pushing and incorporation of foreign particles during solidification were studied. Trapping was favored by rapid freezing, a small amount of stirring, and the presence of gas bubbles at the interface, and by formation of an acute angle between the interface and the container. With faceted growth, trapping differed from grain to grain and was sometimes favored at a grain boundary. The temperature gradient had no effect on particle trapping. Particle mixtures were separated by slowly increasing the freezing rate. This is called particle chromatography. A theory was developed for nucleation of gas bubbles during crystallization.

Details of illustrations in this document may be better studied on microfiche

14. KEY WORDS:
Particles, solidification, freezing, bubbles, mixtures, separation, chromatography, nucleation, crystallization.

1a

DD FORM 1 NOV 65 1473

UNCLASSIFIED
Security Classification

REMOVAL AND SEPARATION OF PARTICLES BY CRYSTALLIZATION

by

Vincent H. S. Kuo

A Dissertation Presented to the

FACULTY OF THE GRADUATE SCHOOL

UNIVERSITY OF SOUTHERN CALIFORNIA

In Partial Fulfillment of the

Requirements for the Degree

DOCTOR OF PHILOSOPHY

(Chemical Engineering)

February 1973

UNIVERSITY OF SOUTHERN CALIFORNIA
THE GRADUATE SCHOOL
UNIVERSITY PARK
LOS ANGELES, CALIFORNIA 90007

This dissertation, written by

Vincent H. S. Kuo

under the direction of his Dissertation Committee, and approved by all its members, has been presented to and accepted by The Graduate School, in partial fulfillment of requirements of the degree of

DOCTOR OF PHILOSOPHY

Charles G. Mayo

Dean

Date February 1973

DISSERTATION COMMITTEE

William W. Wilcox
Chairman

Stephen M. Copley

Charles J. Pebert

ACKNOWLEDGMENTS

I wish to gratefully acknowledge my advisor, Dr. W. R. Wilcox, for his advice, guidance and encouragement throughout this work, and also for his warm personal concern during the course of this study.

I also wish to acknowledge my committee members, Dr. C. J. Rebert and Dr. S. M. Copley, for their interest and constructive suggestions. Dr. R. C. Binder served the committee until his retirement (August 1972).

Special thanks are due Professor N. Kharasch for permitting me to use his gas chromatograph; to Mr. P. Weidman for the helpful discussions on rotation of the fluid; and to Messrs. G. Mueller, J. Emerson and J. Scott for assisting in construction of the experimental apparatus.

This research was financially supported by the Petroleum Research Fund (1969-1971), administered by the American Chemical Society; and by the Advanced Research Projects Agency (1971-1972) of the Department of Defense under Grant No. DAHC 15-72-G7.

The πMC particle size distributions were kindly performed by the Millipore Corporation, and the scanning electron micrographs of the carbon particles were taken by the Aerospace Corporation.

Preparation of the final manuscript by Mrs. Shari Wilcox, and the rough draft by Mrs. Georgia Lum are thankfully acknowledged.

Finally, I am particularly grateful to my wife, Jane, for her encouragement and understanding during the course of this work. She

assumed part of the financial responsibility and full responsibility for taking care of our two children, so that I could concentrate on pursuing my research and interests.

TABLE OF CONTENTS

Page

Page

LIST OF FIGURES

LIST OF TABLES

ABSTRACT

Foreign particles are present in nearly all solid organic chemicals, including laboratory-grade chemicals. Metals may similarly contain particles of slag and furnace refractories following extractive metallurgical processes. These particles are not only sources of impurities but may induce defects and change many properties of a solid.

It has been known for many years that growing crystals sometimes reject and push foreign particles in addition to segregation of soluble impurities. The actual interaction between particles and a solid-liquid interface was recently studied experimentally and theoretically, and some particle pushing and trapping phenomena clarified. At sufficient low growth rates, nearly all particles were pushed by a freezing interface. As the growth rate was increased, a critical velocity V_c was reached beyond which particles started being trapped into the growing crystal. The measured values of V_c were different for each particle-matrix material system and possessed no discernible pattern. Prior to the present work, insufficient information was known about particle pushing to permit design of a separation process for producing particle-free ultrapure materials.

Two different experimental methods were employed in this study. An improved Bridgman-Stockbarger apparatus was first constructed permitting microscopic observation of particle pushing and trapping at the freezing interface. Interface shape, growth container, growth orientation, and presence of bubbles all significantly influenced V_c.

For the carbon-naphthalene system V_c was 21 mm/hr., but it was reduced to 18 mm/hr. when the particles were trapped next to the tube wall with a convex interface. For the copper-naphthalene system V_c was about 18 mm/hr. The interfacial temperature gradient had no discernible effect on V_c. The formation of bubbles was prevented by evacuating the growth container. In an attempt to increase V_c by stirring of the melt, insertion of a propeller or paddle agitator was found to be impractical.

Horizontal zone-refining with rotation was then adopted to increase V_c. This apparently was the first time this technique was applied for removing particles. This method eliminated the detrimental effects resulting from settling of the particles and formation of bubbles which were encountered in the first method. Thus, the measured values of V_c were increased 300% for copper and 50% for carbon particles in naphthalene. This new separation process has proven to be simple, effective and economical (product cost is about 22 cents per gram for particle-free naphthalene). Furthermore, horizontal zone-refining with rotation and vertical Bridgman technique were used to separate carbon particles from a mixture of carbon and copper particles in naphthalene by taking advantage of their difference in V_c. This new separation technique is christened "particle chromatography."

The measured figures of V_c were in good agreement with those calculated by Bolling and Cisse's equation. Theoretical treatments on formation of air bubbles, effect of crystal dimension on the interfacial temperature gradient, effect of temperature gradient and

horizontal rotation on particle pushing were made in this study. In general, they agreed with the present experimental results and previous data.

At least three objectives have been accomplished in this dissertation. (1) Discovery of some important phenomena leading to better understanding of pushing of particles by a freezing interface. (2) The development of a new separation process enabling economical removal of foreign particles from organic compounds. (3) The invention of a new technique to separate mixtures of different particles, opening up a potentially new field--particle chromatography.

CHAPTER I

INTRODUCTION

The demand for highly pure solid materials is continuously growing for research and applications, particularly in the fields of semiconductors and pharmaceuticals. While separation of soluble impurities has been extensively investigated during the past two decades, removal of insoluble impurities has been largely neglected. Foreign particles are present in nearly all organic compounds, including laboratory-grade chemicals. Metals may similarly contain particles of slag and furnace refractories following extractive metallurgical processes. These particles are not only source of impurities but may induce defects such as dislocations [1], and change many properties of a solid.

It has been known for many years that growing crystals sometimes reject and push foreign particles in addition to segregation of soluble impurities [2]. This observation suggested the possibility of removing particles by solidification processes [3]. The actual interaction between particles and a freezing interface has recently been studied [4-10], and some particle pushing phenomena have been clarified. At sufficiently low crystal growth rates, nearly all particles were observed to be pushed by the solid-liquid interface. As the growth rate was increased, a critical velocity V_c was reached beyond which all particles of a particular type were trapped. The measured values of V_c were different for each particle-matrix material system, and possessed no discernible pattern. Prior to the present

study insufficient information was known about particle rejection to permit engineering design of such a separation process.

The purpose of this research was to learn more about the fundamental nature of particle pushing and trapping phenomena, and to study the effects of some of the design variables of a separation process. Selected particles were mixed in transparent organic melts. In order to measure the critical rate for trapping, the solidification rate was gradually increased. Two different techniques were employed. An improved vertical Bridgman-Stockbarger growth apparatus was first set up for direct observation of the particle pushing and trapping at the solid-liquid interface. A horizontal zone-refiner with rotation was then employed. Since some of the organic compounds used here froze non-faceted like most metals [11], the results of this work should be equally applicable to removal of particles from metals.

In the next chapter the prior literature is critically reviewed, and some theoretical considerations needed for this work are described. This is followed by Chapter III which describes the detailed experimental methods and materials employed for the research. Chapter IV shows the experimental results. Chapter V explores potential applications with some experimental evidence and also gives economic aspects of the developed process. Interpretation of experimental results is given in Chapter VI. Accomplishments and important results drawn from this research are summarized in Chapter VII. Finally, the extension of the present work to several fields is suggested in the last chapter.

CHAPTER II

LITERATURE STUDIES

This chapter consists of two sections: a review of previous work and some theoretical considerations required for the present work. The prior literature is reviewed in chronological order. Earlier work is discussed under "Crystallization Pressure", since before 1960 many investigators interpreted that a growing crystal could exert a force which pushed an external body. This is followed by a review of more recent papers in which the interaction between particles and a solid-liquid interface was examined. Of these recent studies, the work of Bolling and Cisse [8,9,10] appears most significant for particle pushing and trapping. Their theory is thus reviewed in detail. Some theoretical considerations needed for this research are discussed in the second section of this chapter, such as the structure of a solid-liquid interface and the interfacial temperature gradient.

A. Review of Previous Work

1. Crystallization Pressure

It has been known for many years that in addition to segregation of soluble impurities, a growing crystal either repels or entraps foreign solids [2,4]. Many interesting examples have been observed [12]. Crystals of epsomite ($MgSO_4 \cdot 7H_2O$) grown on the bottom of salt lakes repelled particles of mud and were therefore colorless and

transparent. On the other hand, crystals of astrakanite ($Na_2SO_4 \cdot MgSO_4 \cdot 4H_2O$) formed under similar conditions were usually dark colored due to entrapment of mud particles. Gypsum crystals ($CaSO_4 \cdot 2H_2O$) growing in clay rejected the particles in their proximity and were often clear, while the same crystals formed in sand exhibited abundant inclusions of sand particles. These phenomena of particle repulsion or entrapment may be related to a force exerted by the crystal on the particle during crystallization.

Becker and Day [14] were the first to perform experiments in 1905. They put forward the view that a crystal could exert a pressure when growing. They placed a loaded glass plate on the top face of an alum crystal. The crystal continued growing even when the load was increased to one kilogram. They attributed the effect to a "linear crystallization force". The crystallization pressure was defined as the maximum pressure exerted by a crystal at which the growth ceased at a given supersaturation (or supercooling). Since then many investigators have pursued the measurement of crystallization pressure, but have not agreed on the values of the pressures that might occur. Some found values of about 20 Kg/cm^2 [4,14,15,16] while others found only a few g/cm^2 [17,18]. The former used Becker and Day's method, the latter used Shubnikov's method [16]. Shubnikov used a growing crystal to encounter a glass ball which was attached to a spring. The crystallization pressure was determined when the ball began entering the crystal. Those who took the pressure to be large, related the pushing force to the energy of the phase change. Those who took the pressure to be small explained the effect as a surface interaction.

In fact, the supply of supersaturated solution to the contact region is the limiting process in the latter case.

Correns and Steinborn [19] thermodynamically related the crystallization pressure to the supersaturation. The conditions for reaching equilibrium were obtained by calculating in two different ways the amount of work needed to transform a supersaturated solution into a saturated solution. The maximum work W gained to perform this transformation isothermally and reversibly is

$$W = N\,kT\,\ell n\,\frac{C}{C_\infty} \tag{2-1}$$

where C is the actual concentration, C_∞ is the saturated concentration, N is the number of molecules transformed, k is the Boltzmann's constant and T is the absolute temperature. The crystal grows under a load B and the work gained by lifting the load for a distance of d is

$$W = Bd = PAd = PN\,v_s \tag{2-2}$$

where P is the crystallization pressure, A is the contact area between the load and crystal, v_s is the molecular volume of the crystal. Equating the above two equations, the crystallization pressure is obtained as

$$P = \frac{kT}{v_s}\,\ell n\,\frac{C}{C_\infty} \quad . \tag{2-3}$$

The above relation indicates the crystallization pressure increases with the supersaturation. Experimental results [4,19] on alum

covered by a glass plate confirmed the relation at small and medium supersaturation ($C/C_\infty \leq 1.2$). However, the theoretical prediction was too large at high supersaturation [P = 55 Kg/cm^2 for theoretical, while 42 Kg/cm^2 was measured on a (111) face and 32 Kg/cm^2 on a (110) face]. The (100) face of alum gave zero pressure at all supersaturations [19,20]. It was also found that the pressure depended on the nature of the external body. Alum covered by mica yielded zero pressure for (111), (110) and (100) faces at all supersaturations. Therefore, the crystallization pressure cannot be described entirely by the above relation. It depends not only on supersaturation, but also on the type of crystal, on the solvent, on the external body, and on the transport conditions at the contact area between the crystal and the external body.

Khaimov-Mal'kov [21] also studied crystallization pressure thermodynamically. Although his theoretical relation included the anisotropy effects of elastic behavior, these effects became appreciable only at pressures of geological order (greater than 1000 Kg/cm^2).

2. Correns' Phase-Boundary Force

As indicated above, a (111) face of alum pushes a glass plate while a (100) face sticks to such a plate. Further, both faces stick to a mica plate. These experimental results give the impression that the crystallization pressure might be related to surface energies. Correns [22] established another condition to show whether or not an

external body could be pushed. When a particle (p) is in intimate contact with a crystal (s) in liquid (ℓ), an amount of work is necessary to separate the particle from the crystal. Work has to be done against the surface energies in order that two new solid-liquid and particle-liquid interfaces appear and the original particle-solid interface disappears. If the surface energy between the solid and particle is σ_{sp}, the surface energy between the solid and liquid is $\sigma_{s\ell}$, and the surface energy between the particle and liquid is $\sigma_{p\ell}$, the work done is

$$W = (\sigma_{sp} - \sigma_{s\ell} - \sigma_{p\ell})\, A \quad . \tag{2-4}$$

If $\sigma_{sp} > \sigma_{s\ell} + \sigma_{p\ell}$, then W is positive and work is gained so that the crystal will lift the particle, provided that sufficient solution (or melt) enters into the contact region between the crystal and the particle. On the other hand, when $\sigma_{sp} < \sigma_{s\ell} + \sigma_{p\ell}$ is valid, the particle simply adheres to the crystal.

Unfortunately, there are no experimental data available for σ_{sp}. There are few values available for $\sigma_{p\ell}$ and $\sigma_{s\ell}$[23]. The relationship $\sigma_{sp} > \sigma_{s\ell} + \sigma_{p\ell}$ only indicates whether or not it is possible for the growing crystal to push the external body.

3. Work of Corte

Corte [5] investigated pushing of seven different particles by upward freezing of water. For each particle it was found that trapping occurred only when critical freezing rate was exceeded. Using

different shapes of silica (glass bead, broken glass and quartz), it was demonstrated that an important factor in particle repulsion and capture was the shape of the particle. Glass beads, having the smallest contact area, showed the smallest freezing rate for trapping. Broken glass and quartz, having a greater contact area, were pushed at larger rates. Mica particles, which had the largest contact area of the particles (all 0.15 mm in diameter), exhibited the greatest critical freezing rate.

The relation of critical freezing rate to particle size was also studied. Fine particles migrated under a wide range of rates of freezing, while coarse particles migrated at slower and narrower ranges of rates of freezing. He pointed out that a layer of water must be continuously present between the particle and the ice front during particle migration.

4. Work of Uhlmann, Chalmers, and Jackson

Uhlmann, Chalmers, and Jackson [6] studied the interaction between particles and an advancing solid-liquid interface both experimentally and theoretically. They observed the pushing of eleven different types of particles in three organic compounds contained as a thin film (300-500 μm) between glass slides. They also found that for each particle-melt combination a critical velocity V_c existed, below which the particles were rejected by the interface, and above which they were trapped in the crystal. The dependence of V_c on various properties of particles and matrix material was studied.

A theory was developed based on the assumptions of a particle-interface repulsion (due to the difference of surface energies, $\Delta\sigma_o = \sigma_{sp} - \sigma_{s\ell} - \sigma_{p\ell}$) combined with diffusion of melt into the contact region. The critical trapping velocity for a smooth spherical particle on a planar interface was expressed as

$$V_c = \frac{1}{2}(n+1)(La\, v_\ell D/kT\, R^2) \qquad (2\text{-}5)$$

where D is the diffusion coefficient, L the latent heat of fusion, v_ℓ the atomic volume of melt, a the molecular diameter, R the radius of particle, k the Boltzmann's constant, and n a constant which is an exponent relating variation of $\Delta\sigma_o$ with separation distance.

They also treated the problem in more detail, including the effects of viscous drag and particle roughness. However, the results were not satisfactory. One of the reasons is a lack of microscopic properties for the supercooled thin film between the particle and the freezing solid. In their calculations, they had to assume a diffusion coefficient 400 times smaller than the value in the bulk liquid in order to obtain agreement with the experiment results.

Table 1 summarizes their measured V_c, along with those observed by others [5,7,9,10,24].

5. Work of Hoekstra and Miller

Hoekstra and Miller [7] postulated that the transport of water in a thin film between a glass particle and ice is by diffusion. They took the free energy gradient as a driving force and related it to the temperature gradient, deriving

TABLE 1

SUMMARY OF CRITICAL VELOCITIES FROM PREVIOUS STUDIES

Investigators	Particles	V_c, mm/hr. Salol	Thymol	Orthoterphenyl	Diphenylamine	Water
Uhlmann, Chalmers & Jackson Ref. 6	AgI	not pushed	21.6	not pushed		
	Fe_2O_3	9.0	7.2	9.0		
	MgO	10.8	28.8	1.8		
	Ni	8.3	28.8	7.2		
	Si	2.9	36.0	2.9		
	Sn	3.6	14.4	3.6		
	Zn	25.2	21.6	9.0		
	Diamond (0-2 μm)	7.2		4.7		
	Diamond (3-5 μm)	7.6	32.4	5.0		
	Graphite	not pushed	43.2	1.1		
	Silt	2.5	57.6	2.5		

TABLE 1 (continued)

SUMMARY OF CRITICAL VELOCITIES FROM PREVIOUS STUDIES

		V_c, mm/hr.				
Investigators	Particles	Salol	Thymol	Orthoterphenyl	Diphenylamine	Water
Pikunov Ref. 24	Al_2O_3	7			35	
	Cr_2O_3	7				
	Coal	7				
	Lycopodium	7				
Corte Ref. 5	Mica					0.4 - 3.2 (1 - 0.15 mm)
	Shale					0.2 - 1.1 (1 - 0.15 mm)
	Quartz					0.2 - 0.7 (1 - 0.15 mm)
	Rutile					0.2 - 0.7 (0.6 - 0.15 mm)
	Calcite					0.3 - 0.6 (0.6 - 0.15 mm)
	Broken Glass					0.1 - 0.5 (0.6 - 0.15 mm)

TABLE 1 (continued)

SUMMARY OF CRITICAL VELOCITIES FROM PREVIOUS STUDIES

Investigators	Particles	V_c, mm/hr. Salol	Thymol	Orthoterphenyl	Diphenylamine	Water
Hoekstra and Miller Ref. 7	Glass Beads					0.1 - 1.3 (230 - 120 μm)
	Glass Cylinders					0.5 - 3.0 (270 - 160 μm)
Cisse and Bolling Ref. 9 & 10	SiO_2	0.6 - 1.1 (90 - 35 μm)				1.4 - 2.3 (100 - 40 μm)
	Cu	0.6 - 1.1 (80 - 10 μm)				0.6 - 18 (125 - 5 μm)
	W	0.6 - 1.3 (10 - 7 μm)				0.7 - 12 (60 - 5 μm)
	W_2C	0.6 - 1.1 (20 - 10 μm)				
	Aℓ	0.6 - 1.1 (80 - 10 μm)				
	Ag	0.6 (80 μm)				

$$V_c = \frac{2d\lambda c\rho_\ell}{kT \cdot \rho_s} \left(\frac{1}{R}\right) \frac{dT}{dr} \qquad (2\text{-}6)$$

where d is the thickness of the thin film, λ is the mobility of the liquid film, ρ_s is the density of ice, ρ_ℓ is the density of water, and c is a constant.

Their experiments, executed like Corte's [5], confirmed the linear relationship between V_c and 1/R for both glass beads and glass cylinders. The glass cylinders gave higher values for V_c than did the glass beads. However, they did not test experimentally the dependence of V_c on the temperature gradient.

6. Work of Bolling and Cisse

Bolling and Cisse [8,9] combined fluid-flow viscous drag and diffusion considerations to derive theoretical relations for V_c. They also considered the indentation of the interface shape generated by the interaction between the particle and the interface. Using an upward moving interface to push four different particles by freezing water, their experimental results [9] supported well the deduced relations. They established a simple inverse power law between V_c and size for smooth particles. When the theory was made more complex by considering the effects of particle roughness, gravity and thermal conductivities, the fit with experiment was improved. As predicted by their theory, the ratio V_c: $\sqrt{2}\ V_c$: $\sqrt{3}\ V_c$ was measured for the critical velocities when trapping of the same type and size of particles occurred at a grain surface, a grain boundary groove and a grain

boundary triple point.

Their theoretical development appeared to be significant for understanding trapping and rejection of insoluble particles, but it is very difficult to follow and understand. Thus, the study of their theory became part of the task of this dissertation. Part of the theory relevant to this work is explained here in detail for a better understanding of the phenomena of particle pushing.

The steady-state interface shape during the pushing of a foreign particle depends on the interaction between the particle and the freezing interface. The interface must be responsive to all forces exerted on the particle such as gravity and viscous drag. This quite often results in a smooth shallow indentation in the interface adjacent to the particle. Crystal growth can be described by specifying the solid-liquid interface temperature as a function of position. For the simplest case of pure growing material and an inert smooth particle of the same thermal conductivity as the solid and melt, the interfacial temperature T_i can be expressed as

$$T_i = T_m - \Delta T_s - \Delta T_c - \Delta T_i \qquad (2\text{-}7)$$

where T_m is the melting temperature of pure material, ΔT_s is the supercooling needed to provide a driving force for crystal growth and is a function of growth rate V, $\Delta T_c = \sigma \bar{K}/\Delta S$ is the temperature depression due to curvature effects, ΔS is the entropy of fusion per unit volume, $\bar{K}$ is the total curvature at any point on the interface, and ΔT_i is the temperature change due to interaction of the particle with

the interface and is evaluated as follows.

The thermodynamic criteria for equilibrium requires that the free energies of the two phases (solid and liquid) are equal at the melting point. The fundamental relation for a small change in free energy of the system dG is expressed as

$$dG = -SdT + V\,dP \tag{2-8}$$

where S is the entropy of system, V the volume, and P the pressure. It follows that the condition for equilibrium between two phases is that $dG_s = dG_\ell$, or

$$-S_s\,dT_s + V_s\,dP_s = -S_\ell\,dT_\ell + V_\ell\,dP_\ell \tag{2-9}$$

where the subscripts s and ℓ refer to solid and liquid respectively. If we assume that the liquid pressure in the particle-interface contact area is similar to the bulk pressure, then the $V_\ell\,dP_\ell$ may be neglected. Further, $T_s = T_\ell$ at the equilibrium state. Thus, the above equation becomes

$$\Delta T_i = \left(\frac{V_s}{S_s - S_\ell}\right)\Delta P\ . \tag{2-10}$$

If we substitute $\Delta S = S_s - S_\ell/V_s$, and $\Delta P = F/\pi r_o^2$ into the equation, the temperature change due to a force acting on the crystal is

$$\begin{aligned} \Delta T_i &= \frac{F}{\Delta S \pi r_o^2} \qquad \text{if } r \leq r_o \\ &= 0 \qquad\quad \text{if } r > r_o \end{aligned} \tag{2-11}$$

where r_o is an effective contact radius beyond which no interaction occurs between the particle and the interface, as defined by Uhlmann et al. [6]. F is the interacting force within r_o.

The search for a complete solution of F is the next step in development of the theory. The viscous drag on the particle, which produces a force on the freezing interface, is considered next. A hydrodynamic approach is used to solve the problem of flow around a sphere to a nearby uniform sink (interface). Figure 1 shows a schematic cross section of a spherical particle in contact with an interface. The contact region within r_o is expanded. The formula for viscous drag F_c for the plane sink ($\theta = 0$) as derived in Uhlmann's dissertation by G. Carrier [25] is

$$F_c = 6\pi\eta V R^2/d \tag{2-12}$$

which gives the viscous drag upon a sphere of radius R located a distance d from a plane interface advancing at growth rate V. The problem considered here requires a sink which is concave due to interaction within the contact area $r \leq r_o$. The separation distance h between particle and interface at any point in the contact region is

$$h = d + R - (R^2-r^2)^{1/2} - E(r) \tag{2-13}$$

where E(r) is the vertical distance between a concave interface and its lowest point, and is a function of the radial distance. For the case of $r << R$, $(R^2-r^2)^{1/2}$ is approximately equal to $R - r^2/2R$ by a MacLaurin's series and thus

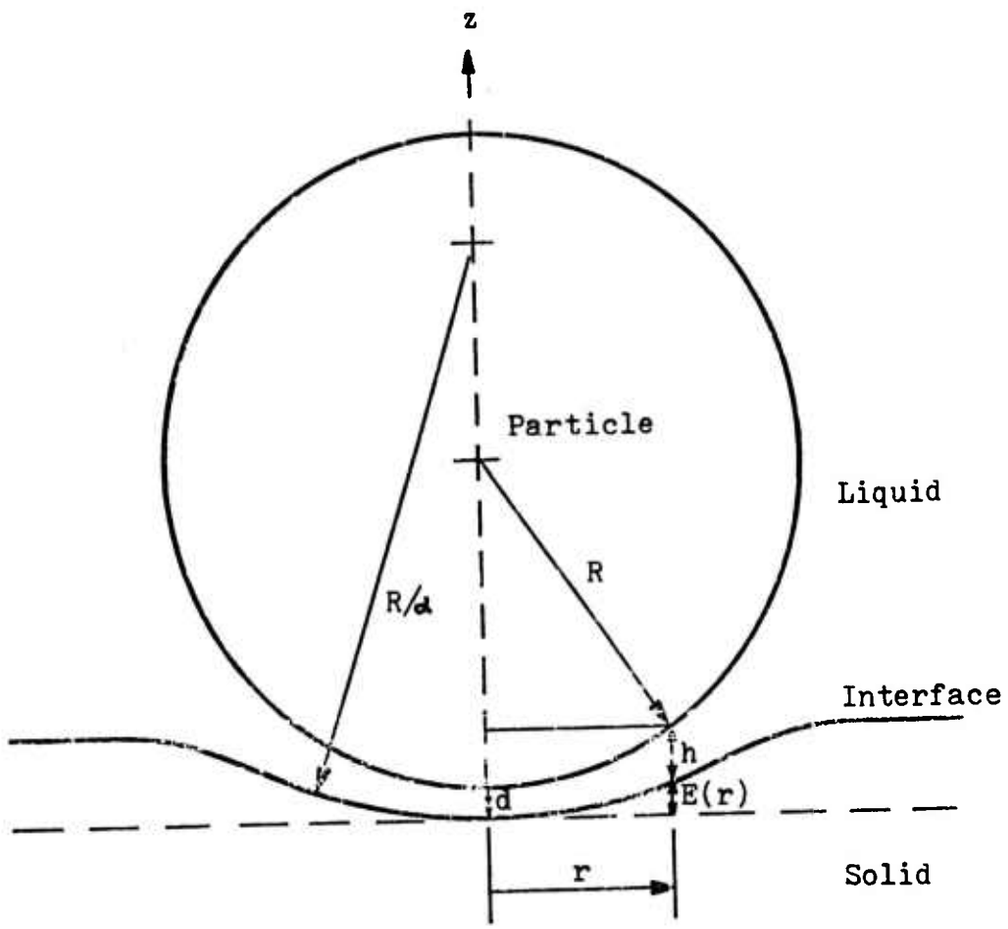

Figure 1 Schematic cross section of a spherical particle in contact with a solid-liquid interface with a magnified contact area.

$$h \approx d + r^2/2R - E(r) \quad . \tag{2-14}$$

A parabolic velocity profile U is assumed for the flow in the contact region, with zero tangential velocity at the solid-liquid interface ($z = E(r)$) and the particle-liquid interface ($z = h + E(r)$). That is,

$$U = C(r) \left(z - E(r)\right) \left(z - h - E(r)\right) \quad . \tag{2-15}$$

Consider the region of contact as a sort of cylinder with a radius of r. Conservation of mass requires that the liquid entering the cylindrical walls equals that leaving at the bottom of the cylinder under the steady state conditions.

$$\int_{E(r)}^{h+E(r)} 2\pi\, rU\, \rho_\ell\, dz = \pi r^2\, V\, \rho_s \quad . \tag{2-16}$$

Substituting Eq. (2-15) into the above equation and integrating the left-hand side, the function C(r) is found to be

$$C(r) = \frac{3rV}{h^3}\left(\frac{\rho_s}{\rho_\ell}\right) \quad . \tag{2-17}$$

Hence, the complete expression for U is

$$U = \frac{3rV}{h^3}\left(\frac{\rho_s}{\rho_\ell}\right)\left(z - E(r)\right)\left(z - h - E(r)\right) \quad . \tag{2-18}$$

The pressure gradient in the r direction is found from the Navier-Stokes equation for a fluid in steady-state laminar motion [26] to be

$$\frac{dP}{dr} = \eta \frac{d^2U}{dz^2} = \frac{6\eta r V}{h^3}\left(\frac{\rho_s}{\rho_\ell}\right) \quad . \tag{2-19}$$

The pressure difference ΔP between the inside of the contact region and the outside of the contact region is

$$\Delta P = P(r) - P(R) = \int_R^r \frac{6\eta r V}{h^3}\left(\frac{\rho_s}{\rho_\ell}\right) dr \quad . \tag{2-20}$$

Since h increases with r in real situations, dP/dr in Eq. (2-19) increases from zero and then decreases, approaching zero again as r approaches R. On the other hand, ΔP is the largest at r = 0 and decreases as r increases. Their variations are shown schematically in Figure 2. These trends, as given by Eqs. (2-19) and (2-20), hold whether the approximate formula Eq. (2-14) is employed or not. In either case r/h^3 approaches zero as r approaches R. The major contribution to the integral Eq. (2-20) comes from the region $r << R$.

Because the hydrostatic pressure P(R) can be considered constant over the surface of a small particle, ΔP is essentially the net pressure exerted on the particle in the vertical direction. This pressure is multiplied by the projected area of the particle, and thus gives a net force F, which is

$$F = \int_R^0 2\pi r\Big(P(r)-P(R)\Big)\, dr$$

$$= \int_R^0 2\pi r \int_R^r \frac{6\eta V x}{\left(d+x^2/2R-E(x)\right)^3}\left(\frac{\rho_s}{\rho_\ell}\right) dx\, dr \quad . \tag{2-21}$$

Since we have assumed $r << R$, we may well take the lower limit as

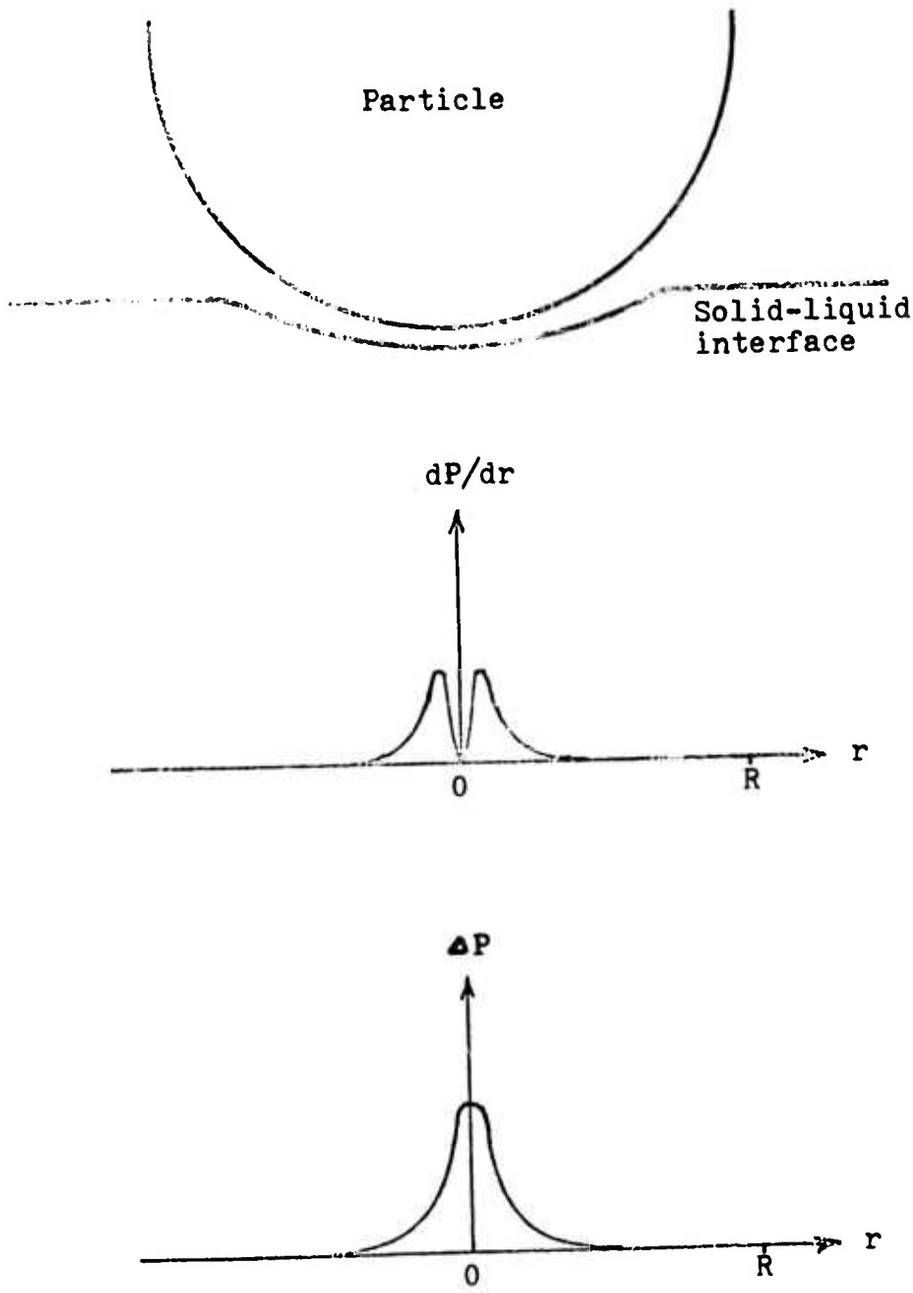

Figure 2 Sketch showing variations of dP/dr and ΔP with respect to r in the contact region.

∞ for R to obtain

$$F \approx \int_{\infty}^{0} 2\pi r \int_{\infty}^{r} \frac{6\eta\, Vx}{\left(d + \frac{x^2}{2R} - E(r)\right)^3} \left(\frac{\rho_s}{\rho_\ell}\right) dx\, dr \quad . \tag{2-22}$$

The above equation cannot be integrated unless we know the function $E(r)$. Because we are searching for an outer bound, it is possible to find a limit for this function which may give a maximum force. At the limit $r = 0$ and $z = 0$, the contact region between the particle and interface may approximate a part of a sphere, and $E(r)$ has a maximum value if the interface would closely contact with a spherical particle with a radius of R/α where $\alpha \leq 1$. At the limit $d \approx h$, we obtain from Eq. (2-14)

$$E(r) \approx \frac{\alpha\, r^2}{2R} \quad . \tag{2-23}$$

Equation (2-22) is then integrated by substituting the above relation for $E(r)$ to obtain

$$F(\alpha) \approx \frac{6\pi\eta\, V\, R^2}{d(1-\alpha)^2} \left(\frac{\rho_s}{\rho_\ell}\right) \tag{2-24}$$

where $F(\alpha) \geq F$.

When α has a value of zero, the interface is a plane sink and not responsive to the presence of the particle. Equation (2-24) thus becomes Eq. (2-12) of Carrier's expression for viscous drag. At the other extreme, when α has a value of unity, the interface and the particle are in an intimate contact, and Eq. (2-24) yields an extremely large force. Therefore, we have to limit the use of $F(\alpha)$, particularly as α approaches unity.

The viscous drag derived above appears to depend on the separation distance d at r = 0. The value of d is difficult to evaluate so that we may relate it to some system parameters. The interface discussed here is responsive to the existence of the nearby particle; and therefore d has an influence on the interface shape. If we relate the interface shape parameter α to some characteristic value of d, let us say at the value of Na_0 where a_0 is the interatomic distance and N is a number depending on a system parameter β (β is some characteristic only of the liquid for inert particle but of liquid and particle if there is a chemical interaction), and choose a decay function to represent the variation between the two limits for α (α = 0 and 1), we obtain

$$\alpha = \exp\left[-(d-\beta a_0)/a_0\right] \quad , \tag{2-25}$$

which gives a planar interface (α = 0) at $d \gg \beta a_0$ and intimate contact (α = 1) between the particle and the interface at $d = \beta a_0$. Rearranging the above relation we obtain

$$d = a_0(\beta - \ell n\ \alpha) \quad . \tag{2-26}$$

Thus, Eq. (2-24) can be expressed in terms of β by means of Eq. (2-26)

$$F(\alpha) = \frac{6\pi\ \eta\ V\ R^2}{(1-\alpha)^2(\beta-\ell n\ \alpha)a_0}\left(\frac{\rho_s}{\rho_\ell}\right) \quad . \tag{2-27}$$

We just completed the hydrodynamic approach to the transport problem in the contact region. Uhlmann et al. [6] treated the same transport problem from a diffusion viewpoint. If there is a diffusion

limit, Eq. (2-24) may be used to compare with this diffusion limit. For the purpose of comparison, $F(\alpha)$ is mathematically manipulated with the assumption of $w = r^2(1-\alpha)/2R$,

$$F(\alpha) = -\frac{6\pi\,\eta\,V\,R^2}{(1-\alpha)^2}\left(\frac{\rho_s}{\rho_\ell}\right)\int_\infty^o \frac{dw}{(d+w)^2}$$

$$= -\frac{6\pi\,\eta\,V\,R^2}{(1-\alpha)^2}\left(\frac{\rho_s}{\rho_\ell}\right)\left[\int_\infty^{r_o} \frac{dw}{(d+w)^2} + \int_{r_o}^o \frac{dw}{(d+w)^2}\right] . \qquad (2\text{-}28)$$

The force $F(\alpha)$ is divided into two portions. One arises within the contact region $r \leq r_o$, the other one from the region $r > r_o$. Now we may compare $F(\alpha)$ with a supposed force which is required for the diffusion process,

$$F_{virtual} = -\frac{6\pi\,\eta\,V\,R^2}{(1-\alpha)^2}\left(\frac{\rho_s}{\rho_\ell}\right)\int_\infty^{r_o} \frac{dw}{(d+w)^2} + F_D \qquad (2\text{-}29)$$

where F_D is the force needed for diffusion in the contact area $r \leq r_o$. This force is less than that for flow within the same region, or flow would occur. Thus, $F(\alpha) \geq F_{virtual}$. If we work at the limit, it becomes immaterial to distinguish between flow and diffusion. The movement of molecules on the surface following a random walk with no preferred direction is [27]

$$\overline{\Delta r}^2 = 4\,Dt \qquad (2\text{-}30)$$

where t is the time necessary for a mean displacement $\overline{\Delta r}$. If we assume that b is the height for growth of a monoatomic layer, then the time required for molecules to diffuse into the contact region

(with an effective radius r_o) is $t = b/V$. The least advantageous diffusion sequence is then

$$r_o^2 \leq 4\ D\ b/V \quad . \tag{2-31}$$

If we relate fluid flow and diffusion by means of the Stokes-Einstein equation, that is, $D = kT/3\pi\eta a_o$, the above relation becomes

$$r_o^2 \leq \frac{4\ kT}{3\pi\ \eta\ V} \quad . \tag{2-32}$$

With this relation in mind, we may determine the conditions under which the force $F(\alpha)$ is dominant during particle pushing. The force within $r \leq r_o$ where the diffusion might occur can be evaluated from the second term of Eq. (2-28)

$$F(\alpha)_{o \text{ to } r_o} = -\frac{6\pi\ \eta\ V\ R^2}{(1-\alpha)^2}\left(\frac{\rho_s}{\rho_\ell}\right)\int_{r_o}^{o}\frac{dw}{(d+w)^2}$$

$$= \frac{6\pi\ \eta\ V\ R^2}{(1-\alpha)}\left(\frac{\rho_s}{\rho_\ell}\right)\frac{r_o^2}{2Rd[d+(1-\alpha)r_o^2/2R]} \quad . \tag{2-33}$$

The force $F(\alpha)_{o \text{ to } r_o}$ is sensibly the force $F(\alpha)$ of Eq. (2-24) if

$$\frac{r_o^2(1-\alpha)}{2R} >> d \quad . \tag{2-35}$$

At the limit of the diffusion sequence, the above relation when combined with Eq. (2-32) becomes

$$\frac{2kT\ (1-\alpha)}{3\pi\ \eta\ V\ R} >> d \ . \tag{2-35}$$

Based on Eq. (2-24), the viscous drag increases with increase of the growth rate or the interface curvature. $F(\alpha)$ reaches a maximum when the growth is at the critical trapping velocity. At this point the region of close contact gives a maximum radius R/α. If we equate the effect of the maximum force to that of the maximum possible curvature, or $\Delta T_c = \Delta T_i$, we obtain the conditions for initiation of particle trapping. Thus

$$\frac{F(\alpha)}{\Delta S \, \pi \, r_o^2} = \frac{2\sigma}{\Delta S} \frac{\alpha}{R}$$

or

$$r_o^2 = \frac{3\eta \, V_c R^3}{\sigma a_o} \left[\frac{1}{\alpha(1-\alpha)^2(\beta - \ell n \, \alpha)} \right] \quad . \tag{2-36}$$

If Eq. (2-35) holds, we are allowed to use Eq. (2-32) to evaluate the quantity r_o^2 while maintaining the conditions of maximum force and critical trapping velocity. That is,

$$V_c^2 = \frac{4 \, kT \, \sigma a_o}{9\pi \, \eta^2 \, R^3} \phi(\alpha) \left(\frac{\rho_\ell}{\rho_s} \right) \tag{2-37}$$

where $\phi(\alpha)$ is $\alpha(1 \, \alpha)^2(\beta - \ell n \, \alpha)$. This is the final equation to be used for prediction of the critical trapping velocity.

The relation of α and β is found at the extremum of $\phi(\alpha)$, or at the condition of $d\phi(\alpha)/d\alpha = 0$. They are

$$\beta = \ell n \, \alpha + (1-\alpha)/(1-3\alpha) \tag{2-38}$$

and

$$\phi(\alpha)_{max} = \alpha(1-\alpha)^3/(1-3\alpha) \quad . \tag{2-39}$$

The above relations restrict the quantity α, which must be less than 1/3 or else the curvature of the interface would be large enough to engulf the particle. If we apply this limitation to Eq. (2-25), a useful relationship is obtained as

$$\exp\left(\frac{d - \beta a_o}{a_o}\right) > 3$$

or

$$d > (1.1 + \beta)a_o \ . \tag{2-40}$$

The above relation gives the thickness of the thin film existing between the particles and interface. Since the thin film consists of several interatomic layers, it is logical to assume a minimum of unity for β to solve the problem.

The relationship between d and α can be obtained from Eqs. (2-26) and (2-38),

$$d = (1-\alpha)a_o/(1-3\alpha) \ . \tag{2-41}$$

The inequality presented in Eq. (2-35) to be evaluated then becomes

$$VR << 2(1-3\alpha)kT/3\pi\ \eta\ a_o \ . \tag{2-42}$$

If we choose $\beta = 1$, the value of α gives 0.229 at $\phi(\alpha) = \phi(\alpha)_{max}$. For water as a matrix material, $a_o \cong 3.8 \times 10^{-8}$ cm, $\eta = 1.8$ c.p., $T = 273°K$, and $VR \leq 3.7 \times 10^{-6}$ cm^2/sec. This requirement was met by several different particles in freezing of water [7,9].

Equation (2-27) was derived without accounting for effects of gravity and particle roughness. Cisse and Bolling [9] studied smooth

spherical tungsten and copper particles in water. The data supported Eq. (2-37) quite well for the small particles with $R < 10$ μm.

B. Some Theoretical Considerations

1. Structure of the Solid-Liquid Interface

The importance of interface morphology to this study is obvious, since the solid-liquid interface was employed to reject and push foreign particles. The nature of the interface is known to have a decisive influence on the kinetics and morphology of crystal growth. According to one viewpoint, all molecules either clearly belong to the crystal or to the melt, yielding a sharp well-defined interface between the two. Such an interface may either be atomically smooth or atomically rough. These two possible interfaces are shown in Figure 3 where the white spheres represent the atoms of the melt, the black spheres are the crystal atoms. Figure 3(A) is an atomically smooth interface, while (B) represents a rough interface.

With the present knowledge of crystal growth, two possible growth mechanisms have been discussed [28,29]. A crystal whose equilibrium interface is atomically smooth grows by the formation and lateral growth of layers. In a perfect crystal, new layers are formed discontinuously by two-dimensional nucleation. When one or more screw dislocations are present, new layers may be formed continuously. Rapid lateral growth of layers leads to formation of macroscopic facets.

When, on the other hand, the equilibrium interface is atomically

(A) Atomically smooth interface.

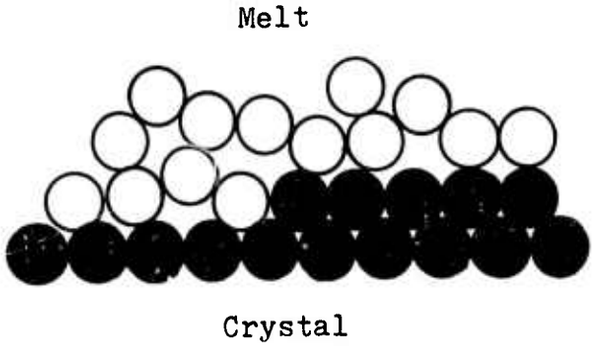

(B) Atomically rough interface.

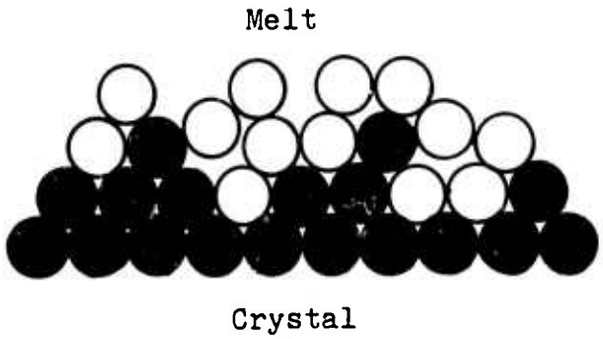

Figure 3 Atomic solid-liquid interface.

rough, the crystal can grow without formation of new layers. The interface advances uniformly and is not faceted.

The theory of the equilibrium interface roughness was satisfactorily examined by Jackson in 1958 [30]. He considered an initially atomic smooth interface and calculated the change in surface free energy on adding extra molecules. The results of his elementary statistical thermodynamic approach predicted that the equilibrium interface should be atomically rough and non-faceted for materials having entropies of fusion (ΔS_f) less than 2R or 16.8 J/mole°K (where R is the gas constant). For $\Delta S_f > 4R$ the interface was predicted to be atomically smooth, faceted and essentially crystallographically perfect. Most metals and certain organic compounds have low entropies of fusion ($\Delta S_f < 16.8$ J/mole°K). Their non-faceted and planar interfaces were confirmed by recent experiments [29,31].

A different approach to the problem of the structure of the interface was discussed by Cahn [32] who assumed a diffuse interface of finite thickness. The transition from crystal to melt takes place over several layers of atoms. According to the theory, lateral growth occurs at low undercooling, but continuous growth takes place at high undercooling. A transition from lateral growth kinetics to continuous growth kinetics was predicted for all materials. Unfortunately, there is no known way of determining the diffuseness of the interface, so that a test of the theory is impossible.

2. Interfacial Temperature Gradient

The temperature gradient at the solid-liquid interface is an

important parameter in the growth of crystals. It influences the perfection and properties of crystals [33], eutectic structures [34], the microscopic shape stability of the interface [35], and interface faceting [36]. The role of temperature gradient in pushing and trapping is not clear. Hoekstra and Miller [7] predicted that V_c should be proportional to the temperature gradient. However, theoretical treatments by other workers [6,8] did not consider this term. The importance to this work is discussed below.

Interface Stability. Even so-called "pure" materials are not completely pure. Traces of impurities are always present. If, for example, the concentration of the solute (impurity) in the solid is less than that of the liquid from which it is forming, there is a rejection of solute into the liquid at the solid-liquid interface. The liquid in the vicinity of the interface becomes enriched in solute. Unless the growth rate is slower than the diffusion rate of solute in the liquid, a concentration gradient develops in the liquid ahead of the interface. Since the presence of solute in the melt lowers the freezing points, the freezing temperature increases from the interface while the impurity concentration decreases as shown in Figure 4. The imposed temperature normally increases as one moves into the melt. When the slope of this actual temperature is less than the slope of the freezing point, the melt ahead of the interface is below its normal freezing temperature. This excess supercooling, termed constitutional supercooling [37], is a direct result of the concentration gradient which exists in the melt. Under such conditions

(A) Solute distribution during normal freezing.

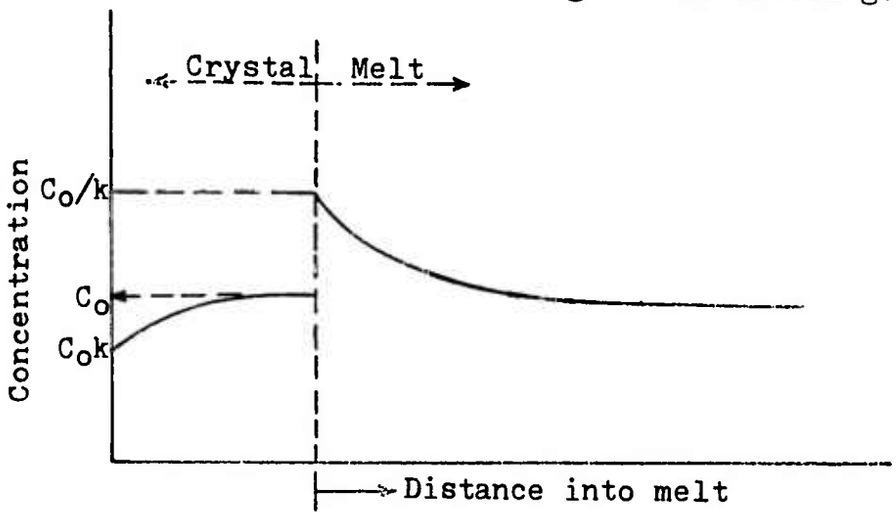

(B) Corresponding equilibrium freezing temperature distribution.

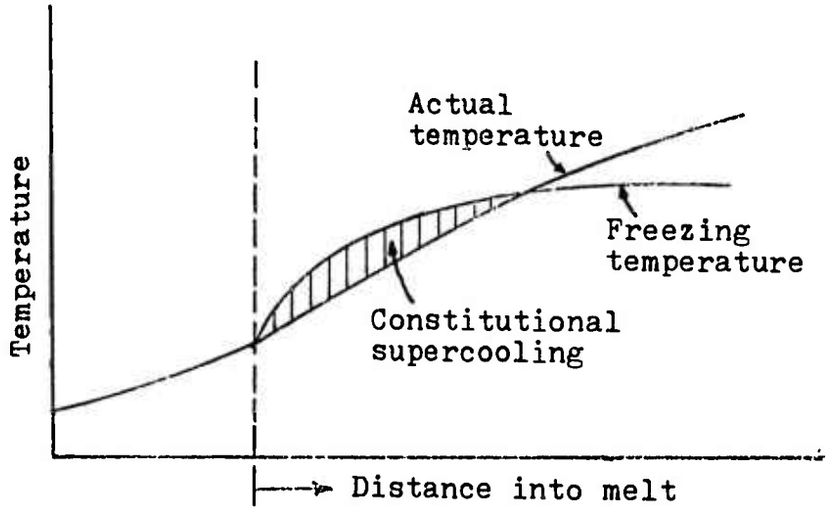

Figure 4 Constitutional supercooling.

the interface is unstable with respect to small perturbation. The supercooling can be relieved by the growth of small projections into the melt. A freezing interface which is rough on an atomic scale may develop pox structures, elongated cells, hexagonal cellular structures, or even dendrites, depending on the degree of constitutional supercooling. Such interface breakdown has a detrimental influence on the process of particle pushing and therefore was avoided in this work.

The conditions for the onset of constitutional supercooling may be expressed in simple mathematical terms [38,39]. When the imposed temperature gradient is less than the gradient of equilibrium freezing temperature at the interface, the following relationship between the imposed growth conditions and the system parameters is obtained for the critical condition of supercooling if there is no liquid mixing in the liquid phase.

$$\left(\frac{dT}{dz}\right)_{z=0} \leq m\left[(C_s)_i - \frac{\rho_s}{\rho_\ell}(C_\ell)_i\right]\frac{V}{D} \qquad (2\text{-}43)$$

where $(C_s)_i$ and $(C_\ell)_i$ are the interfacial solute concentrations in the solid and the melt, and m is the slope of the liquidus line on the phase diagram. Some quantitative studies [40,41] have verified the above relationship. In order to avoid the effects of constitutional supercooling, the imposed temperature gradient should be increased to exceed the gradient of freezing temperature at the interface.

Interface Faceting. Jackson's theory of interface roughness was derived for an isothermal and equilibrium environment. In real solidification situations, the system is neither isothermal nor at

equilibrium. Wilcox's theoretical discussions [36] pointed out that crystals predicted to grow in a faceted manner (high entropy of fusion materials) would grow non-faceted in the presence of a sufficiently large temperature gradient. From equilibrium considerations, faceting in a temperature gradient would exist only if the edge energy was considered in addition to the surface energy and the bulk free energy. From the standpoint of kinetic effects, faceting is favored by anisotropic growth kinetics and rapid growth. There is widespread qualitative experimental evidence to support the effect of temperature gradient on interface faceting.

CHAPTER III

EXPERIMENTAL

Two crystal growth methods were employed for this experimental work. A vertical Bridgman-Stockbarger technique was first used to investigate the fundamental nature of particle pushing and trapping phenomena. Horizontal zone-refining with rotation was then employed to study some of the design variables for a separation process. Uhlmann, et al. [6] conducted particle pushing experiments by means of a horizontal thin film (held between glass slides) with a vertical freezing interface. Their results might have been strongly influenced by the glass slides and not characteristic of bulk materials. Others [5,7,9,10] used Bridgman-Stockbarger growth with the solid-liquid interface moving upward, reducing the possibility of the particles dragging on the glass wall. We incorporated facilities for direct observation and temperature measurements. This was the first time that a horizontal zone-refiner with rotation was used to investigate removal of particles from the matrix materials.

Following the description of the two experimental techniques, the materials used for this study are presented, including the particles and the organic compounds. The treatment of solidified products is then discussed. The final section of this chapter is devoted to a description of the zone-refining of organic compounds.

A. Bridgman-Stockbarger Technique

1. Apparatus

A Bridgman-Stockbarger apparatus was constructed as shown in Figure 5. This unit was designed to provide an upward moving solid-liquid interface which could be constantly observed with a microscope. Essentially the unit consisted of a heater, a cooler and a tube lowering mechanism. The heater was made by winding nichrome wire on a piece of flanged Pyrex glass tube, which was insulated by another glass tube. The cooler was constructed similar to a laboratory condenser, as shown in Figure 6. The cooling fluid was circulated from a refrigerated constant temperature bath (0 to -30°C), passed through the annular space of the cooler, and returned to the circulator. A crystal-growth tube travelling through the heater steadily displaced the heat-transfer fluid which overflowed from a side tube. This fluid was placed in the inner tube of the cooler to eliminate the air gap between the inner tube and the crystal-growth tube, thus improving the heat transfer. The circulating fluid and the heat-transfer fluid were not mixed, but both consisted of 50 volume % ethylene glycol-water. The position of the side tube was adjustable, so that the level of the fluid in the inner tube could be controlled. Two variable-speed motors provided lowering rates of 1 to 15 mm/hour and 10 to 80 mm/hour. The heater power was controlled by an auto-transformer which was connected to a Sola constant-voltage transformer (30 VA, Harmonic Neutralized Type CVS) to obtain a constant voltage A.C. input. The power (3 to 12 watts) was

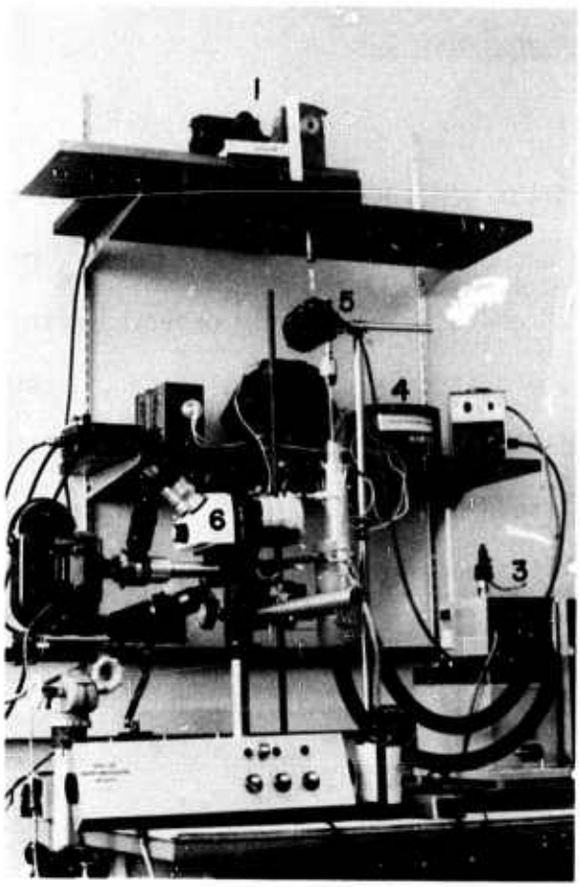

Figure 5 Bench-scale unit of improved Bridgman-Stockbarger technique.

(1) Drive mechanism

(2) Heater and cooler (Details shown in Fig.6)

(3) Constant temperature circulator

(4) Wattmeter

(5) Electronic controlled stirrer

(6) Microscope

(7) Movie camera equipped with time-lapse controller

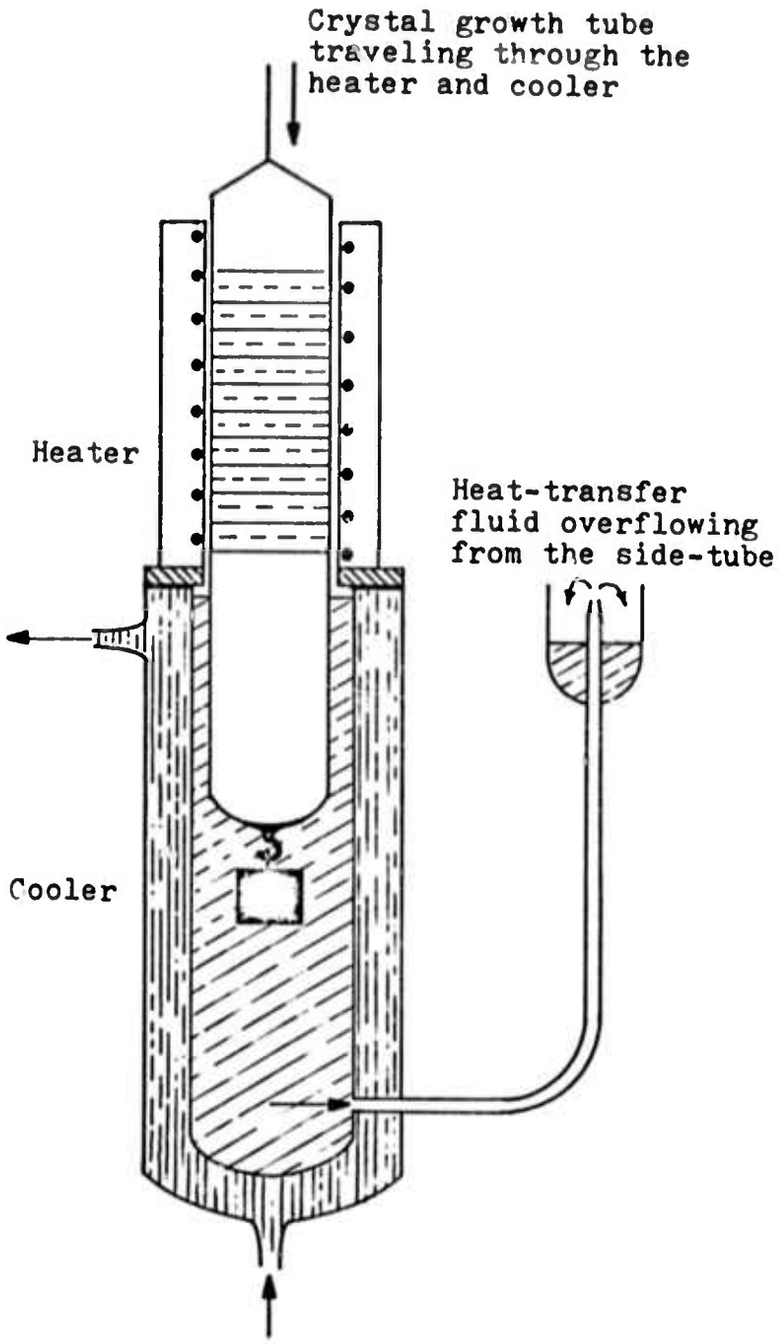

Figure 6 Schematic diagram of the heater and the cooler.

monitored by a wattmeter placed between the heater and the auto-transformer.

Most runs were performed with a cooler made of brass (37 mm I.D. x 17 cm long for the inner tube) while a few runs were made with a small glass cooler (17 mm I.D. x 15 cm long for the inner tube). Two heaters were employed--one small (13.5 mm I.D. x 12 cm long for the inner tube) and one large (31 mm I.D. x 14 cm long for the inner tube). The large heater was used for some runs with a glass stirrer inserted into the growth tube. The stirring motor was placed on a adjustable stepless platform in order that the distance between the stirring blade and the freezing interface could be controlled.

2. Sample Preparation

The solidification tube was made from Pyrex glass tubing with a weight attached to the round bottom to keep the growth tube vertical. Most runs were made with 10.5 mm I.D. (13 mm O.D.) x 10 and 15 cm long tubes. Some runs with stirring used large tubes, 26.5 mm I.D. (30 mm O.D.) x 22 cm long. In the early experiments, particles were directly added into an organic melt and the mixture then poured into the growth tube. As described in Section C, these particles were agglomerates. They should have been broken into individual particles before using for particle pushing study. In later experiments the particle-melt mixture was first poured into a 10 cc cylindrical Pyrex bottle, sealed with a screw cap, and then placed in an ultrasonic cleaner containing hot water in order to keep

the organic molten. The mixture was ultrasonically vibrated about 2 minutes, and then transferred into the growth tube by a dropping pipet.

Molten organic chemicals dissolve gases and release them as bubbles at the freezing interface during solidification. These bubbles were found to seriously interfere with the particle pushing process. Bubbles were avoided in later experiments by the following procedure: A pressure slightly less than one atmosphere was applied to the organic melt in a tube so as to gently degas the melt. The organic was then solidified and a vacuum (50 Torr) applied to the tube, which was sealed with a torch. Gas bubbles were not generated during solidification in these vacuum-sealed tubes. Gas bubbles are further discussed in Chapters IV and VI.

3. Experimental Procedure

A solidification tube containing a mixture of particles and organic compound was placed in the growth unit as illustrated in Figure 6. The length of the tube submerged in the cooler was initially about one tube diameter. The reason for this is described in the next chapter. As soon as a steady solid-liquid interface covered with a layer of particles was established, the tube was lowered at a predetermined rate. The interface was observed through a stereoscopic microscope at 10-50 X and the interface position determined by the eyepiece. Each run started with a low lowering rate (about 6 mm/hour) which was increased step by step (about 2 mm/hour every 30 minutes) until all particles were trapped by the growing solid.

For some time after each increase in lowering rate the growth rate was less than the lowering rate. Relative to the observer, the interface moved slowly downward after a rate change until a new steady-state position was reached (stationary with respect to the heater and cooler). Under this steady-state condition, the growth rate and the lowering rate were equal. Normally, this transient period was 20 to 30 minutes in length. The minimum growth rate for particle trapping, V_c, was usually determined by direct observation of pushing and trapping, but sometimes it was estimated by microscopic examination of the solidified product. The errors in such measurements were less than 10%.

Motion pictures were taken of interesting phenomena at the freezing interface, such as bubble formation and surface-driven flows using a 16 mm movie camera on the microscope, as shown in Figure 5. Time-lapse cinematography was employed for very slow particle pushing processes. To avoid large disturbance of the heat balances at the advancing interface, a water cell was placed in front of the 500-watt photo lamp. Water flowed through the cell continuously and absorbed heat generated from the lamp. The time-lapse movie showed that the travelling motion of the growth tube was not smooth, presumably because of backlash in the gearing. Additional weight was placed between the motor and the tube to reduce this problem.

4. Temperature Measurements

Thin 36-gauge copper and constantan thermocouple wires were employed to measure the temperature distribution in the Bridgman

growth of naphthalene. These thin wires were supported by a capillary tube and positioned at the center of the cross section of the growth container as shown in Figure 7(A). The thermocouple emf was measured by a millivolt recorder against an ice bath junction.

Because the thermocouple was fixed in the growth container, it travelled with the container as the latter passed through the growth unit (Figure 6). Therefore, temperature measurements started in the melt, reached the solid-liquid interface, and finished in the solid. The temperature versus time was continuously recorded. The rate of change of temperature divided by the growth rate yielded the temperature gradient. Thus, for measuring temperature gradients at the interface, knowledge of the time at which the thermocouple was at the interface was required. For instance, if the thermocouple joint was 0.5 mm in diameter and the growth rate was 10 mm/hour, it took 3 minutes for the interface to pass by the thermocouple. This made it difficult to determine the interface from the temperature recording, particularly for experiments at very slow growth rates. With the help of microscopic observation, the interface position was determined when the thermocouple was contacting the interface. The errors in the temperature measurements were less than 0.1°C, but they might be up to 20% in the temperature gradients.

Another factor influencing the accuracy of the above measurements was heat conduction down the thermocouple wires, so that the measured temperatures were higher than they should have been. An improved measuring technique was therefore developed as shown in

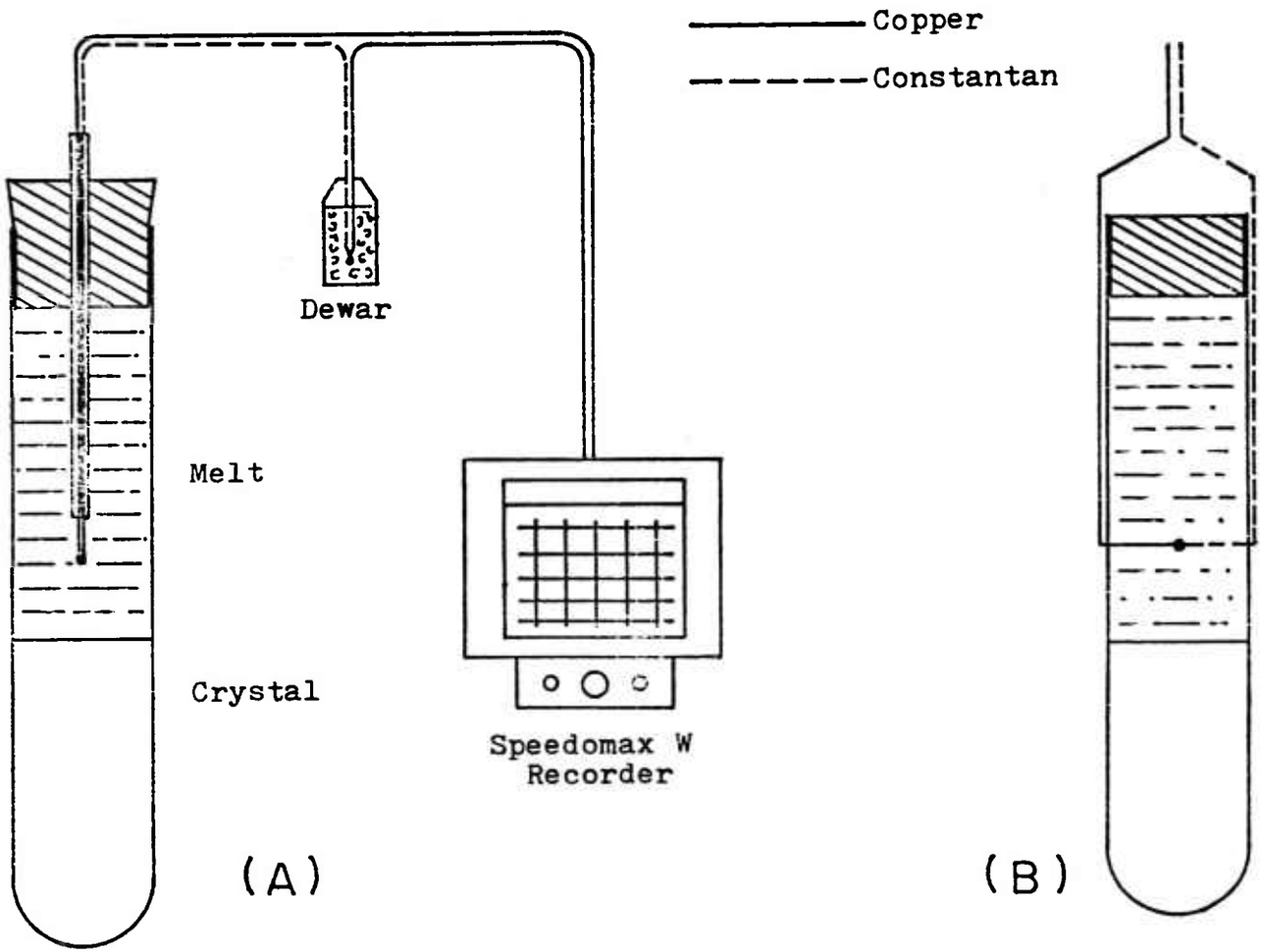

Figure 7 Temperature measurements by thermocouples during Bridgman-Stockbarger crystal growth.

Figure 7(B). The bare thermocouple wires were stretched across the cross section of the container with the welded junction positioned at the center.* The wires were passed through two opposing small holes in the container tube and the holes were sealed with epoxy cement. This improved method was not actually used in the present study because preliminary results based on the method of Figure 7(A) indicated that the critical velocity V_c does not depend on the temperature gradient. However, the method was used in this laboratory by Chong E. Chang. The results were quite satisfactory even at very slow growth rates, less than 1 mm/hour.

B. Horizontal Zone Refining with Rotation

Some experiments were made in the vertical Bridgman apparatus by inserting a stirrer in the growth tube (Figure 6). The purpose of stirring of the melt was to increase the critical trapping velocity. However, this method of stirring made operation quite difficult. It was impossible to keep the distance between the stirrer and the freezing interface close and constant. If the distance was large, stirring would not be expected to influence V_c. If the stirrer and the interface contacted each other, either the stirrer or the growth tube was damaged. A different method of stirring was needed. The method of horizontal zone-refining with rotation was thus adopted to study stirring effect on rejection of particles.

*44-gauge copper-constantan thermocouple with 0.15 mm welded junction diameter.

1. Apparatus

The method of horizontal zone-refining with rotation was developed in 1966 by Pfann, Miller and Hunt [42]. In this technique a horizontal tube is rotated about the tube axis. If particles are present in the molten zone, they move with the melt. The particles are suspended in the zone and are not always in contact with the freezing interface. A Lepel floating zone refiner (model FLZ-100) was modified to suit the present investigation. The molten zone was heated with a loop of nichrome wire (3 mm width) which was passed around the rotating tube, as shown in Figure 8. Two heaters, which could be controlled independently, were needed to control the shape of the freezing interface. One was used to heat the zone; the other to control the heat flow from the interface into the growing crystal. The electrical circuit for the heating system was similar to the one used in the Bridgman-Stockbarger apparatus, except that a step-down transformer (5.2 volts c.p. - 24A) was placed between the constant voltage transformer and the auto-transformer.

2. Sample Preparation

Two sizes of Pyrex tube (13 and 22 mm O.D.) with 30 cm length were used to study the effect of tube diameter on particle pushing with stirring. As shown in Figure 9, a mixture of ultrasonically dispersed particles and organic melt was poured into a tube with a slidable Teflon plug about 3 cm above the sealed bottom. Organic melt without particles was then poured on top of this mixture which

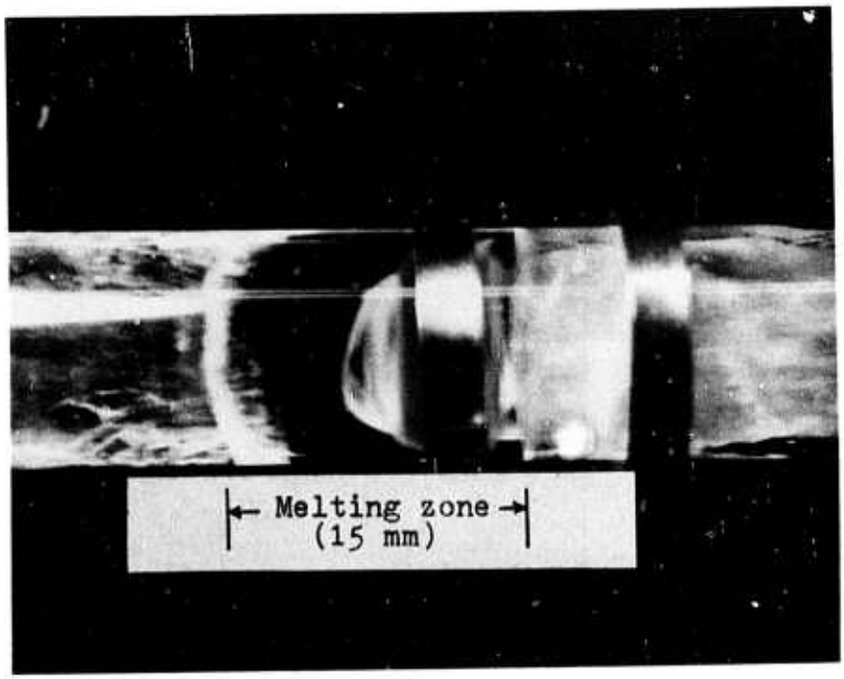

Figure 8 A naphthalene molten zone containing carbon particles traveling in the right-hand direction with a concave freezing interface (Only left-hand heater used, the white material appearing in the melting zone is part of the heater support).

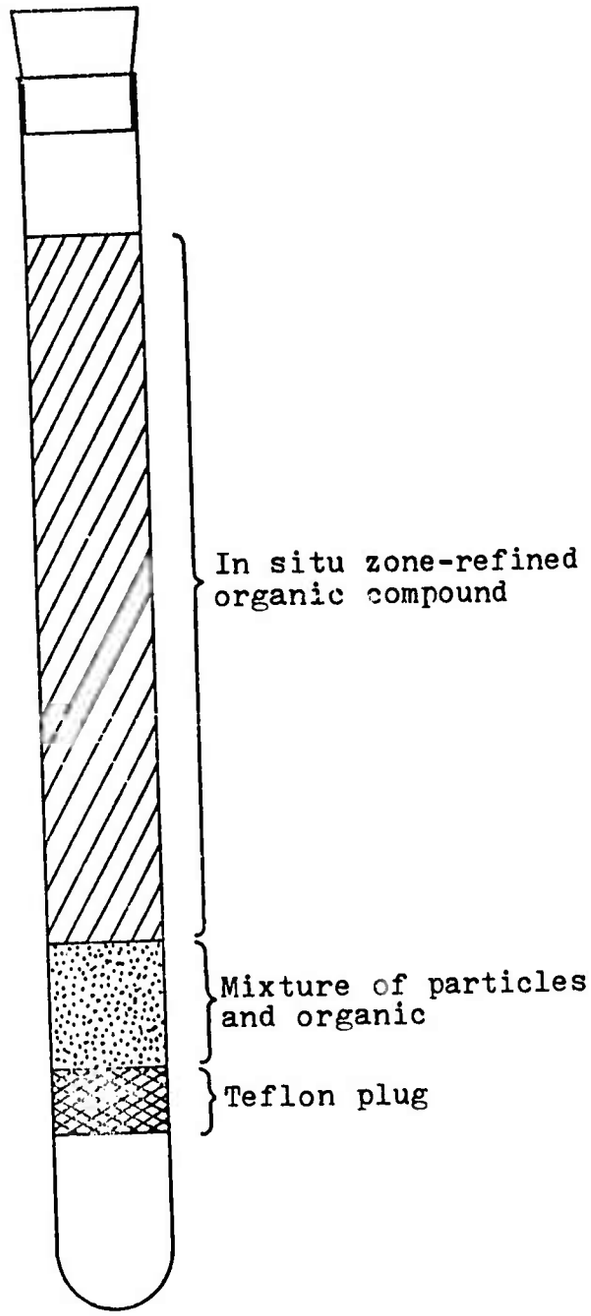

Figure 9 Preparation of the solid charge for horizontal zone-refining with rotation.

had solidified. The purpose of the slidable plug was to prevent tube breakage [42] due to increases in volume upon melting.

Because the initial solid charge was porous, a bubble or void appeared at the top of the molten zone during horizontal zone-refining with rotation. As the zone advanced, the porous solid was melted and a nonporous solid formed behind the zone. The void thus gradually increased in size and eventually occupied more than half of the zone at the end of the run. The void adversely affected the particle separation process when it occupied more than one-third of the zone volume. Preliminary in-situ zone-melting of the particle-free portion of the solid charge (see Figure 9) was therefore used prior to the particle-pushing experiments in order to reduce and control the size of the void.

3. Experimental Procedure

For a typical experiment, a charge tube prepared as above was placed horizontally, rotated about its own axis, and moved through a stationary heater. The particles were suspended in the molten zone and moved with it at travel rates below V_c. The crystal growth rate equalled the movement rate under steady-state conditions. The growth rates would have some fluctuation due to drafts in the laboratory. The rates were increased step by step (about 3 mm/hour every 20 minutes) with particle trapping again observed both by microscopic observations and by sectioning of the solidified material. The errors in the measured V_c were less than 5%.

C. Materials

1. Particles

Properties of the particles employed for these experiments are summarized in Table 2. Carbon particles (bone black) were extensively used as foreign particles in this study because they appear to be one of the common impurities in organic compounds. Scanning electron micrographs of these particles are shown in Figure 10. Special preparations were needed to take these pictures. The carbon sample was placed on a piece of brass which was coated with a 300-500 Å gold film. It appears that the carbon particles were actually agglomerates of very small particles. The agglomerates were porous and of irregular shape. The individual particles were not spherical and their surfaces were not smooth. These agglomerates were directly added into organic melts for early Bridgman-Stockbarger runs. Later, the carbon was dispersed into the melt using ultrasonic vibrations, which broke the agglomerates into individual particles and removed most of the gases entrapped in the carbon.

Copper and red iron oxide were also studied extensively in the naphthalene melt for experiments of horizontal zone-refining with rotation. Other types of particles such as silver, zinc and silicon were also used for some preliminary studies.

The size distributions of ultrasonically dispersed carbon, iron oxide and copper particles were determined by a Millipore πMC particle measurement computer system [45]. Figures 11 and 12 show the distributions based on a count. The average diameters were 1.0, 1.7 and

TABLE 2

PROPERTIES OF THE PARTICLES

Material	Size Range μm	Shape	Density[1] g/cc	Thermal[1] Conductivity cal/cm sec °C	In Melt of Naphthalene	Source
C[2]	<13	Irregular	1.8 - 2.1 (amorphous)	0.057	Fines suspended	Matheson Coleman & Bell
Cu	<80	Irregular & Spherical	9.0	0.94	All particles settled	Alcan, MD-301
Fe_2O_3 (red)	< 3	Spherical	5.2		Fines suspended	Pfizer, R2200
Ag	<74	Spherical	10.5	1.0	-	Alcan, MD-201-S
Zn			7.1	0.27	-	Mallinckrodt, AR
Si	<150		2.3	0.2	-	Alcan, MD-101

(1) Data from Reference 43.

(2) Density from 1.03 to 1.55 and thermal conductivity from 0.004 to 0.012 for carbon with a porosity of 48 to 23%. Data from Reference 44.

(A) Carbon particles showing agglomeration, 300X.

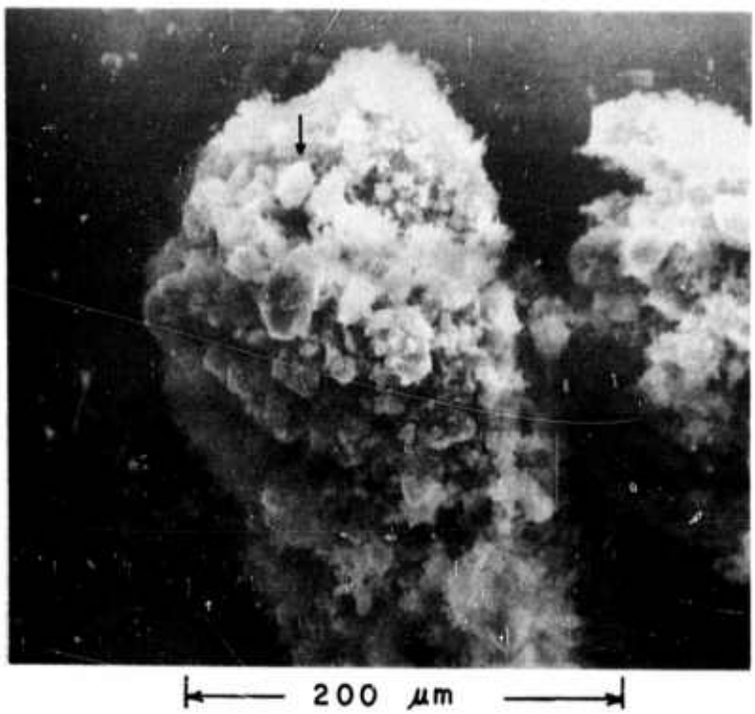

(B) Carbon particle enlarged from (A) at arrow, 6000X.

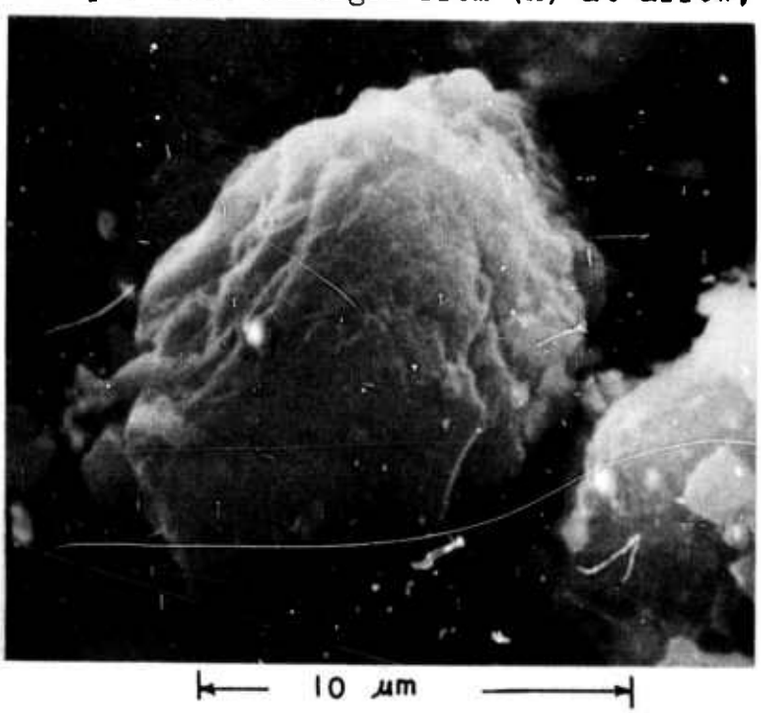

Figure 10 Micrographs of carbon particles.

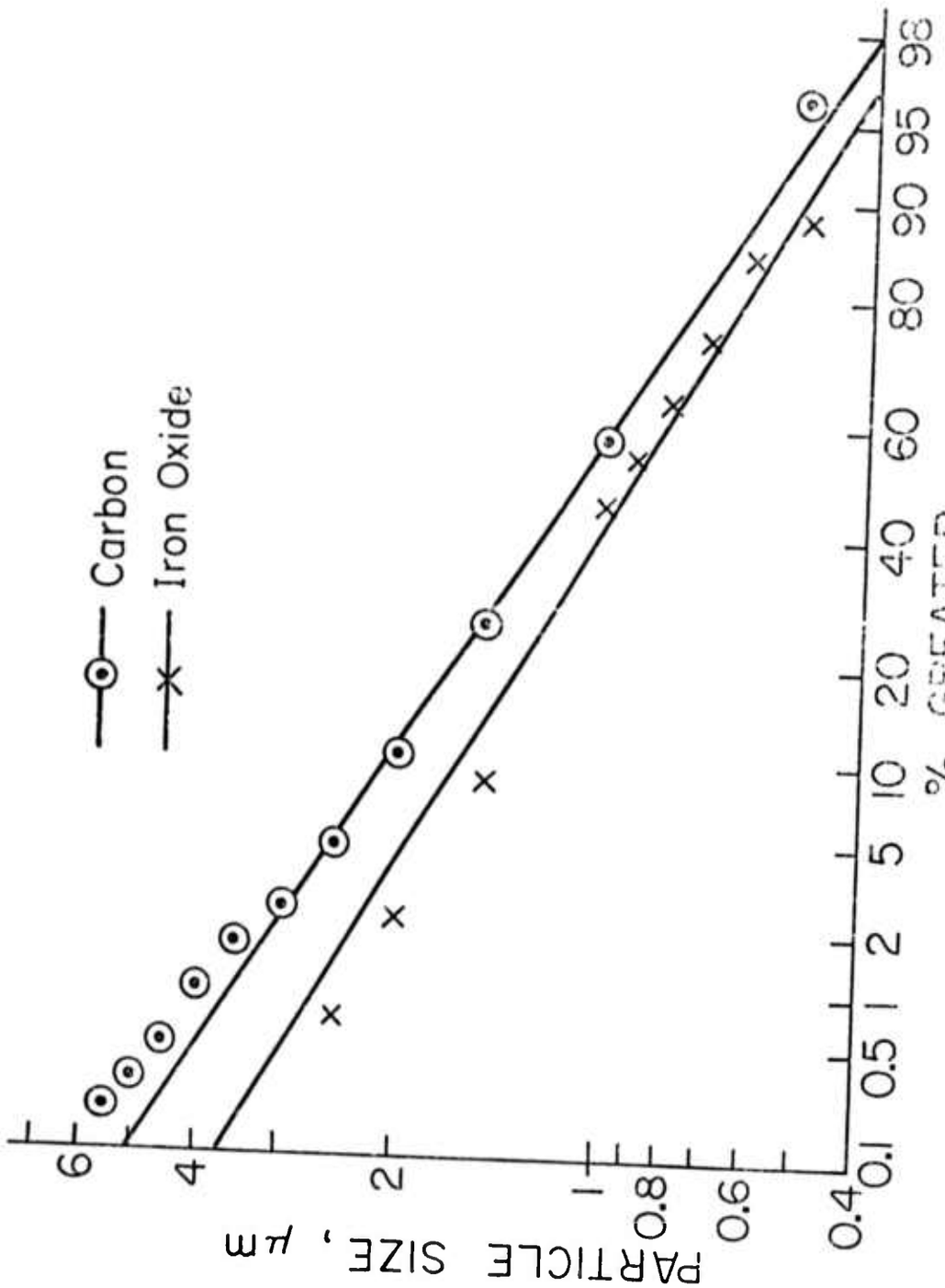

Figure 11 Size distribution for carbon and iron oxide particles.

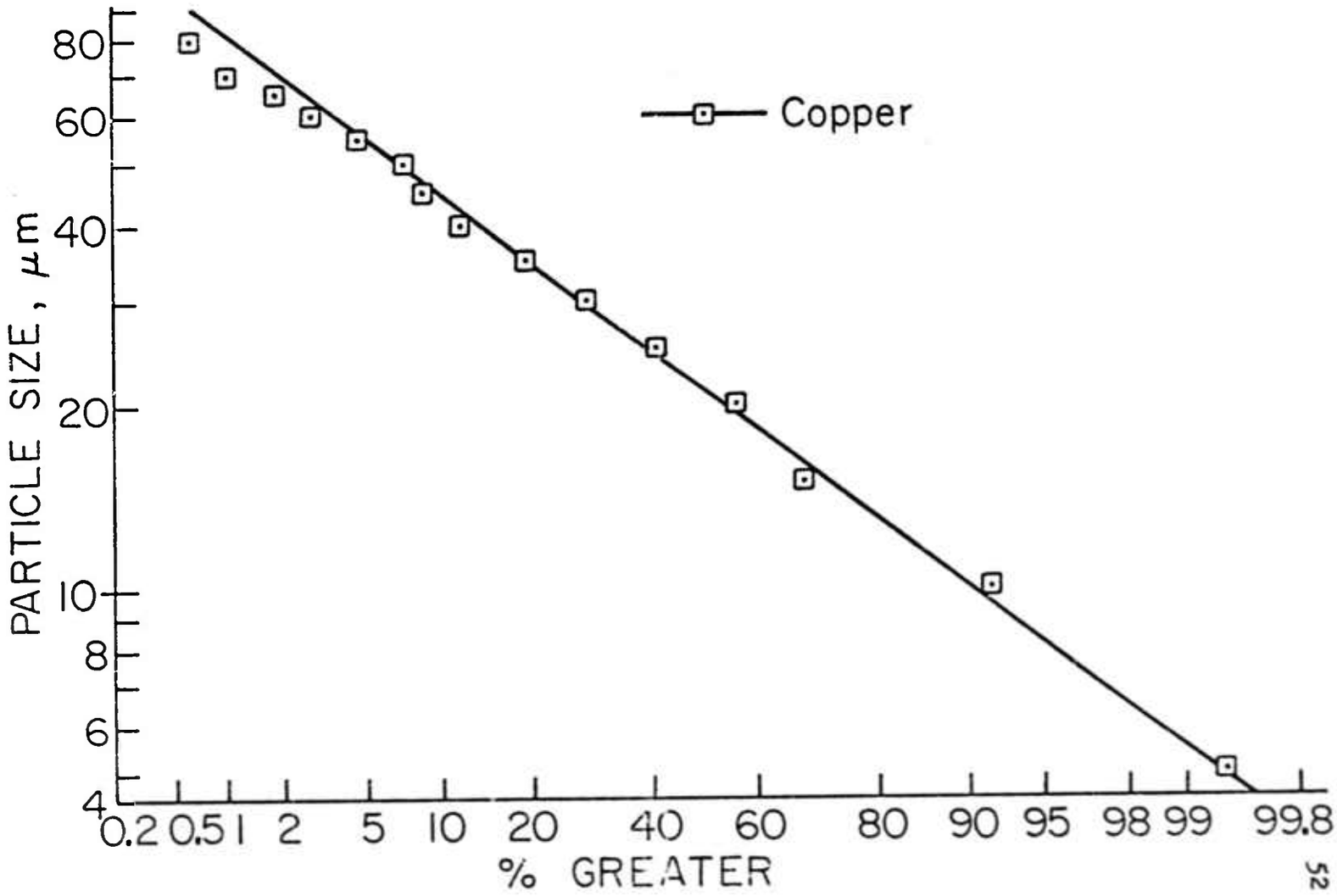

Figure 12 Size distribution for copper particles.

26.0 μm for iron oxide, carbon and copper, respectively.

2. Organic Compounds

The organic compounds studied as matrix materials were naphthalene, camphor, salol and benzophenone. Their properties are summarized in Table 3. Preliminary results indicated that only naphthalene could readily push these particles and thus it was used for most of the experiments. Initially, an attempt was made to zone refine naphthalene and camphor, but ironically the very small native particles present in the reagents were difficult to remove thereby. Therefore, these chemicals were used directly in experiments without further purification. Some of these native particles collected from naphthalene in solidification run BNA-11B are shown in Figure 13. Fortunately, such particles differed sufficiently from those added that no difficulty was encountered in measuring V_c of added particles. Details of zone-refining camphor and naphthalene are discussed in the next section, along with gas chrcmatographic analyses of these compounds and their refined products. No impurities were detected in Baker reagent grade naphthalene by conventional gas chromatography.

D. Solidified Products

In addition to direct observation during the solidification experiment, the solidified products in their glass containers were examined microscopically (up to 500 X) both through the glass tube and after sectioning to determine critical velocities and particle

TABLE 3

ORGANIC COMPOUNDS[1]

Material	Melting Point °C	Density g/cc		Thermal[2] Conductivity cal/cm sec °C		Viscosity (at M.P.), cp	Source
		Melt	Solid	Melt	Solid		
Naphthalene	80.2	0.98	1.03	0.00032	0.00068	0.97	Baker analyzed reagent
Camphor	179.8		0.99			5.0[3]	Baker, Baker grade
Salol	42.0		1.25			8.5[4]	Mallinckrodt N.F.
Benzophenone	48.1		1.15			5.7[4]	Matheson Coleman & Bell

[1] Data from REference 46 and 47.

[2] Data from Reference 48.

[3] Estimated by the present author.

[4] Obtained from Figure 38.

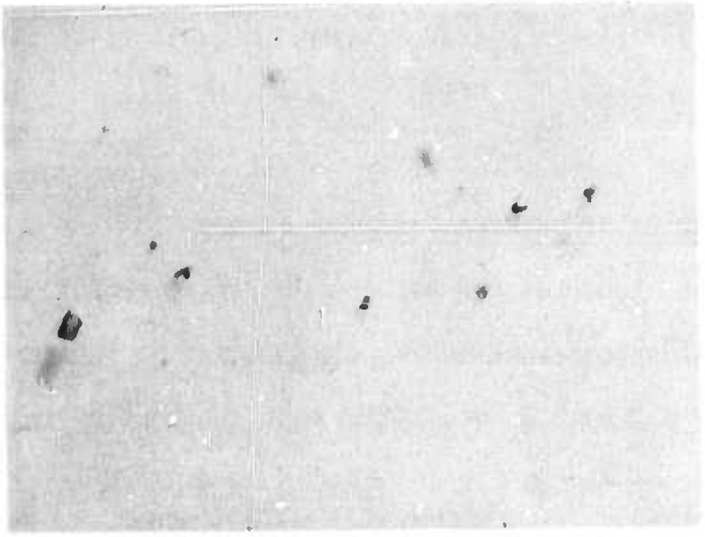

Figure 13 Native particles collected from naphthalene (Baker analyzed reagent), 50X.

trapping characteristics. Samples were cut either traversely or longitudinally by means of a rotating blade which is mounted on a Micro-Matic Precision Wafering Machine (Micromech Mfg. Corp.). Sometimes the naphthalene slices were dissolved in acetone and the solution filtered through a 1 μm Millipore filter. The filter plus collected particles was placed between two glass slides and examined under the microscope.

E. Zone-Refining of Organic Compounds

A Fisher zone refiner was used to purify organic compounds for the particle-pushing experiments. Camphor and naphthalene were zone-refined using a 2 cm O.D. glass tube with two heaters travelling upward at low speeds (2.5 to 10 mm/hour).

1. Camphor

Air oxidation of camphor occurred during the initial melting and tube filling and during the first few zone passes. The brown-colored oxidation products were readily removed as zone-refining continued. Filling the tube with argon did not completely prevent the discoloration, because some air was entrapped in the camphor.

When the melt was uncolored, the freezing interface was planar and smooth if the growth rate was less than 10 mm/hour. Above this rate the interface became dendritic. Cells were observed on the interface when the melt was colored and the growth rate exceeded 2.5 mm/hour. Foreign particles originally present in the reagent were very difficult to remove. Most of these particles were at first

pushed by the planar interface at 9.7 mm/hour, but were then subsequently incorporated into the crystal after less than 10 mm of pushing. The particle separation was not greatly improved when the average zoning rate was decreased to 2.5 mm/hour, which indicates that there was a fluctuating freezing rate due to drafts in the room, power fluctuations, and the intermittent motion of the heater.

Analyses by gas chromatography indicated that the Baker-grade DL-camphor contained about five different trace impurities. Three of these impurities were removed by zone-refining at 2.5 mm/hour (RC-7). We identified one of the remaining impurities as camphene, the content of which was lower in the refined camphor. The concentration of one other impurity was higher in the product than in the starting material. The chromatograms of Baker, refined and colored camphor are shown in Figure 14. The colored oxidation products did not show up in the chromatograms. However, they coagulated as brownish flocs in the CS_2 solution used for chromatography, after the solution had stood for several weeks. When reheated in air, the zone-refined camphor became yellow while no change occurred if oxygen was excluded, proving that air oxidation is the origin of the colored material.

2. Naphthalene

This compound is much more stable than camphor when heated in air. At a zone speed of 4 mm/hour (RN-6), the native particles present in Baker-analyzed reagent were difficult to remove. The freezing interface was smooth and planar. Occasionally, surface-

(A) DL-Camphor (Baker grade, 97.3 mg/100 cc CS_2).

(B) Zone-refined portion (105.4 mg/100 cc CS_2).

(C) Colored portion (105.4 mg/100 cc CS_2).

Figure 14 Chromatograms of camphor (Aerograph HY-F1, Model 600, column 5 ft x 1/8 in, 5% SE-30 60/80 A/W DMCS Chrome W, each injection 4.5 μl).

driven flows caused particles to vigorously circulate around bubbles. Gas chromatographic analyses revealed no impurities in the naphthalene (Figure 15), even with the use of a boosting technique and high temperature (360°C) injection. Thus, the impurity content must be less than 0.1%, which is the minimum detectable value for this gas chromatograph. The zone-refined (bottom) and slightly yellow (top) portions (RN-9) gave chromatograms similar to the reagent, with no impurity peak. When 0.5 wt % of anthracene, a likely impurity, was added to the naphthalene, the peak showed up as shown in Figure 15(B).

(A) Naphthalene (Baker analyzed reagent, high concentration in CS_2).

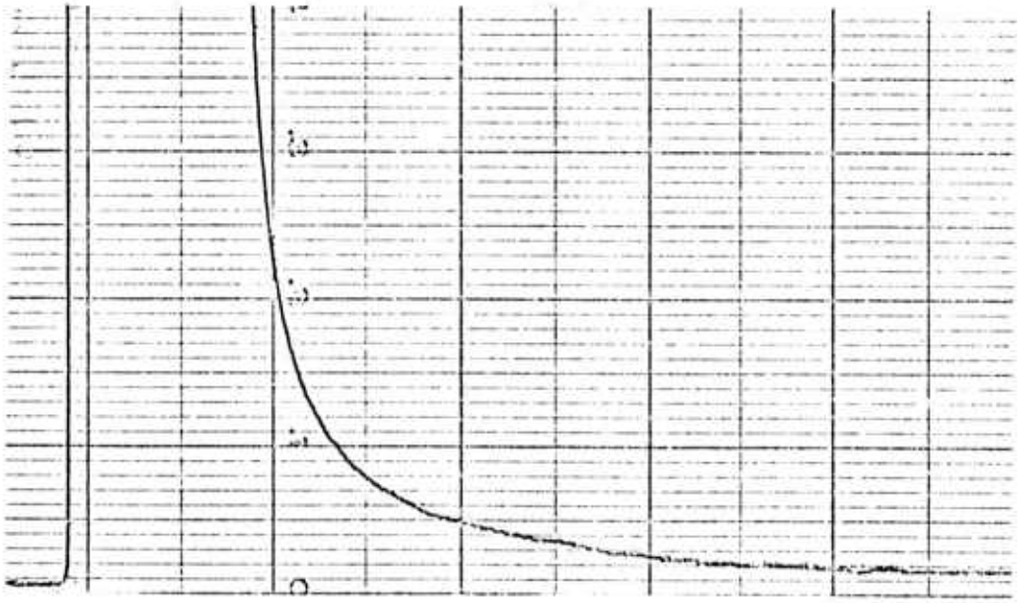

(B) Anthracene (0.5 wt %) added to naphthalene (High concentration in CS_2).

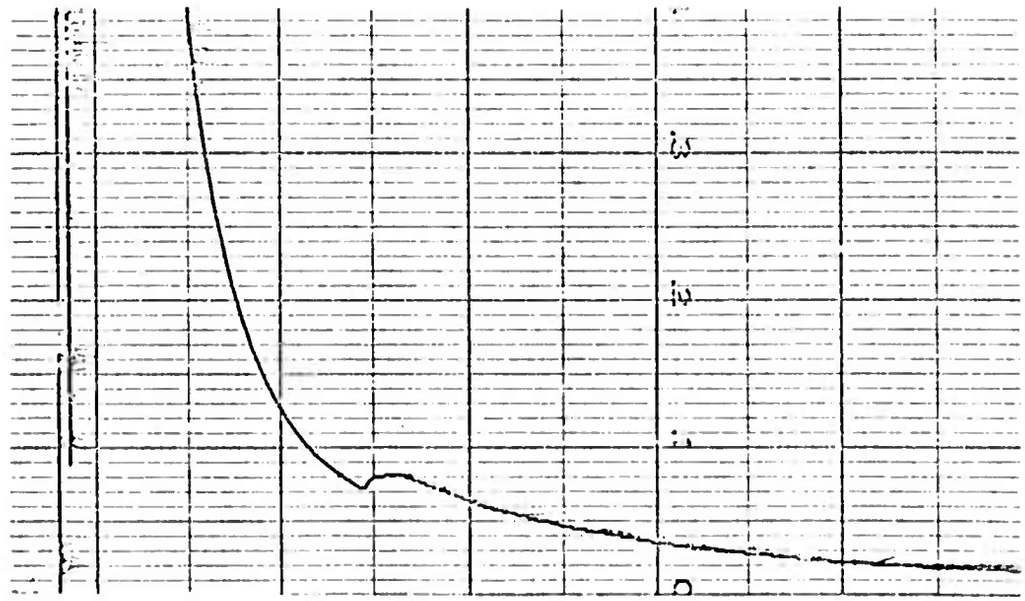

Figure 15 Chromatograms of naphthalene (Aerograph HY-F1, Model 600D, same column as used in camphor).

CHAPTER IV

RESULTS AND DISCUSSIONS

A systematic experimental study was originally planned to determine the effect of two important parameters--interfacial temperature gradient and stirring--on the critical trapping velocity. Many preliminary experiments were conducted to find a suitable particle-organic matrix pair. The ideal pair should have a measurable critical velocity, non-faceted solid-liquid interface and easy handling for sample preparations. The pair of carbon and naphthalene was found to fulfill most of the requirements.

Many phenomena, which help in the understanding of particle pushing, were discovered during the experiments and later treatment of the solidified products. Experiments were designed not only to provide quantitative data on the effect of temperature gradient and stirring, but also to assist in the discovery of new and important phenomena through direct microscopic observation.

The experimental results obtained from the vertical Bridgman growth method are discussed first. Those obtained from horizontal zone-refining with rotation follow. A summary of results is given at the end of the discussion for each experimental method.

A. Bridgman-Stockbarger Technique

1. General

Consider inert particles more dense than the organic melt added

into the upper portion of the growth tube (see Figure 6). The particles are acted upon by various forces (such as gravity, viscous drag and bouyancy) and settle in the melt. Most of them arrive on the horizontal solid-liquid interface, and a new steady-state interface in contact with the particles is formed. Very fine particles are suspended in the melt due to Brownian motion and gentle convective currents which exist in the melt about 1 cm above the freezing interface. As solidification starts at slow speeds, the particles covering the interface are swept along as the freezing interface advances. The moving interface also contacts the fine particles suspended in the melt and pushes them. As the growth rate is gradually increased, a speed is reached at which some particles cease to be pushed by the interface and are trapped in the growing crystal. With many different sizes and shapes of particles, the observed transition from pushing to trapping takes place over a wide range of velocities.

The significant experiments performed in the vertical Bridgman method are tabulated in Table 4 (salol) and Table 5 (naphthalene), together with the observed results.

2. Solid-Liquid Interface Morphology

The solid-liquid interface was maintained by heating the upper portion of the growth tube and cooling the lower portion of the tube. The shape of this interface was significantly affected by power input to the heater and by coolant temperature. Three kinds of interface shapes were observed in the vertical Bridgman growth method, as shown

TABLE 4

SUMMARY OF VERTICAL BRIDGMAN EXPERIMENTS FOR CARBON-SALOL SYSTEM[1]

Run	Stirring RPM	Circulator Temp. °C	Heater Input, w	Change of V, mm/hr.	Growth Length, mm	Observed Results
BSA-1	no	-20	5	3 to 8	33	1. V_c = 7 mm/hr. for the observed grain surface. 2. At high temperature gradient, the interface was planar and smooth when V was less than 6 mm/hr., but it became faceted when V increased to 8 mm/hr. 3. Many bubbles grew on the interface and produced tube "worms" in the crystal.
BSA-2A	160	-20	5	6	11	1. Particles were pushed. 2. Particles were suspended
BSA-3A	160	-20	3	6	20	1. The interface moved downward into the cooler and could not be observed. 2. The shape of interface was concave. Increase of stirring did not change the shape.
BSA-4A	160	-20	5	-	-	1. A brass cooler was used, which improved heat transfer and moved the interface upward into the heater. 2. Agitation made interface more faceted.

TABLE 4 (continued)

SUMMARY OF VERTICAL BRIDGMAN EXPERIMENTS FOR CARBON-SALOL SYSTEM[1]

Run	Stirring RPM	Circulator Temp. °C	Heater Input, w	Change of V, mm/hr.	Growth Length, mm	Observed Results
BSA-5A BSA-6A	160	-10	5	6	-	1. Motion picture was taken showing that particles were moving upward around the bulged interface at beginning of stirring. The interface became concave when it reached steady-state. 2. At the end of run, the melt was decanted. The corcave interface was faceted and consisted of many large grains.
BSA-7A	160	-10	6	6	18	1. Particles were added when the growth unit reached steady-state. Most of the particles were trapped immediately.
BSA-8A	160	-10	4	6	18	1. Small growth tube (13 mm O.D.) was used to give a higher temperature gradient and a smoother interface. 2. Most particles were trapped immediately after addition.
BSA-9A	160	-10	2	6	49	1. Three additions of particles were made. Each addition was trapped immediately and produced a black band in the crystal.

TABLE 4 (continued)

SUMMARY OF VERTICAL BRIDGMAN EXPERIMENTS FOR CARBON-SALOL SYSTEM[1]

Run	Stirring RPM	Circulator Temp. °C	Heater Input, w	Change of V, mm/hr.	Growth Length, mm	Observed Results
BSA-10A	160	-10	2-3	8-15	7.5	1. The interface moved away from the stirring blade when V was increased. The distance between the interface and the blade should be controlled.
BSA-12A	160	-10	2.5	6-12	37	1. Carbon was dispersed into the melt by an ultrasonic cleaner. The melt was dark and the solid was also dark.
BSA-13-1	No	-10	2.5	6	29	1. Different particles were used for the following runs. 2. Red iron oxide particles were added. They were trapped and the solid was light red.
BSA-13-2	No	-10	2.5	8-12	40	1. Zn dust was used, and particles were continuously trapped
BSA-14	No	-10	2.5	6-12	58	1. Si powder was used and trapped. 2. The structure of solidified salol appeared different from those of previous runs.

(1) Large growth tube (26 mm I.D.) was used for runs BSA-1 to 7A. Small tube (10.5 mm I.D.) for runs BSA-8A to 14. Each tube size had its own heater. Glass cooler was used for runs BSA-1 to 3A, but brass cooler was used for the remainder of the runs.

TABLE 5

SUMMARY OF VERTICAL BRIDGMAN EXPERIMENTS FOR CARBON-NAPHTHALENE SYSTEM(1)

Run	Stirring RPM	Change of V, mm/hr.	Growth Length, mm	Observed Results
BNA-1A	160	6-13	34	1. One grain pushed particles, while another grain trapped particles continuously. 2. Sometimes trapping was due to a bubble floating away causing momentary rapid freezing.
BNA-3A	200	8-16	50	1. The distance (about 1 mm) between the interface and the stirring blade was controlled by a support jack. 2. V_c for one grain was 15 mm/hr., while the other grain pushed particles until the end of the run.
BNA-4	No	8-24	80	1. Many bubbles grew on the interface when V exceeded 16 mm/hr. 2. V_c for one grain was 21 mm/hr.
BNA-5	No	13-38	85	1. V_c next to the wall was 18 mm/hr. 2. V_c for one grain was 21 mm/hr. 3. V_c for another grain was 26 mm/hr.

TABLE 5 (continued)

SUMMARY OF VERTICAL BRIDGMAN EXPERIMENTS FOR CARBON-NAPHTHALENE SYSTEM[1]

Run	Stirring RPM	Change of V, mm/hr.	Growth Length, mm	Observed Results
BNA-6V	No	15-30	60	1. The growth tube was evacuated at 0.3 Torr. Bubbles formed at 25 mm/hr. 2. V_c = 18 mm/hr. next to the wall. 3. V_c = 21 mm/hr. for one grain. 4. V_c = 25 mm/hr. for another grain.
BNA-7V	No	13-35	60	1. Same as BNA-6V, but had a larger vacuum space in the sealed tube. Bubbles grew at 27 mm/hr. 2. V_c = 17 mm/hr. next to the wall. 3. One grain trapped more particles than the other grain. V_c varied from 19 to 35 mm/hr.
BNA-8A	160	18-39	62	1. The distance between the interface and the stirring blade was controlled at less than 1 mm. 2. Some particles trapped at 30 mm/hr; most trapped at 39 mm/hr. 3. Some bubbles formed on the interface.

(1) The circulator temperature was -10°C.
The heater input was 6 watts. The heater (14 mm I.D.) was placed on the top of the brass cooler.
The growth tube was 13 mm O.D. and 14 to 23 cm long.
Carbon particles were dispersed into the melt by an ultrasonic cleaner, except for run BNA-1A.

in Figure 16. At a given growth rate, the freezing interface moved upward into the heating zone when the coolant temperature was lowered and became convex (Figure 16A). On the other hand, when the heater power was increased, the freezing interface moved downward into the cooling zone and became concave (Figure 16C). A planar interface could be obtained by adjusting conditions so that the interface was in the vicinity of the junction of the heater and cooler (Figure 16B).

The shape of the interface influences the critical trapping velocity. A convex interface caused most of the particles to fall into the groove created between the interface and glass wall. The particles at the glass-solid-liquid interface were trapped sooner than those in the center of the tube. The former gave a V_c of 18 mm/hour, and the latter a value of 21 mm/hour for ultrasonically dispersed carbon in naphthalene. Figure 17 shows carbon trapped between the crystal and the tube wall.

The freezing interface of naphthalene was always smooth under the imposed temperature gradients of this study, even though naphthalene has a large entropy of fusion (ΔS_f = 53.4 J/mole °K). The interface morphology of salol was influenced by the growth rate in addition to the temperature gradient. At high temperature gradients the interface became smooth when the growth rate was less than 6 mm/hour, but it was faceted when the growth rate increased above 8 mm/hour.

3. Temperature Gradients

Direct addition of carbon into the melt of naphthalene was used

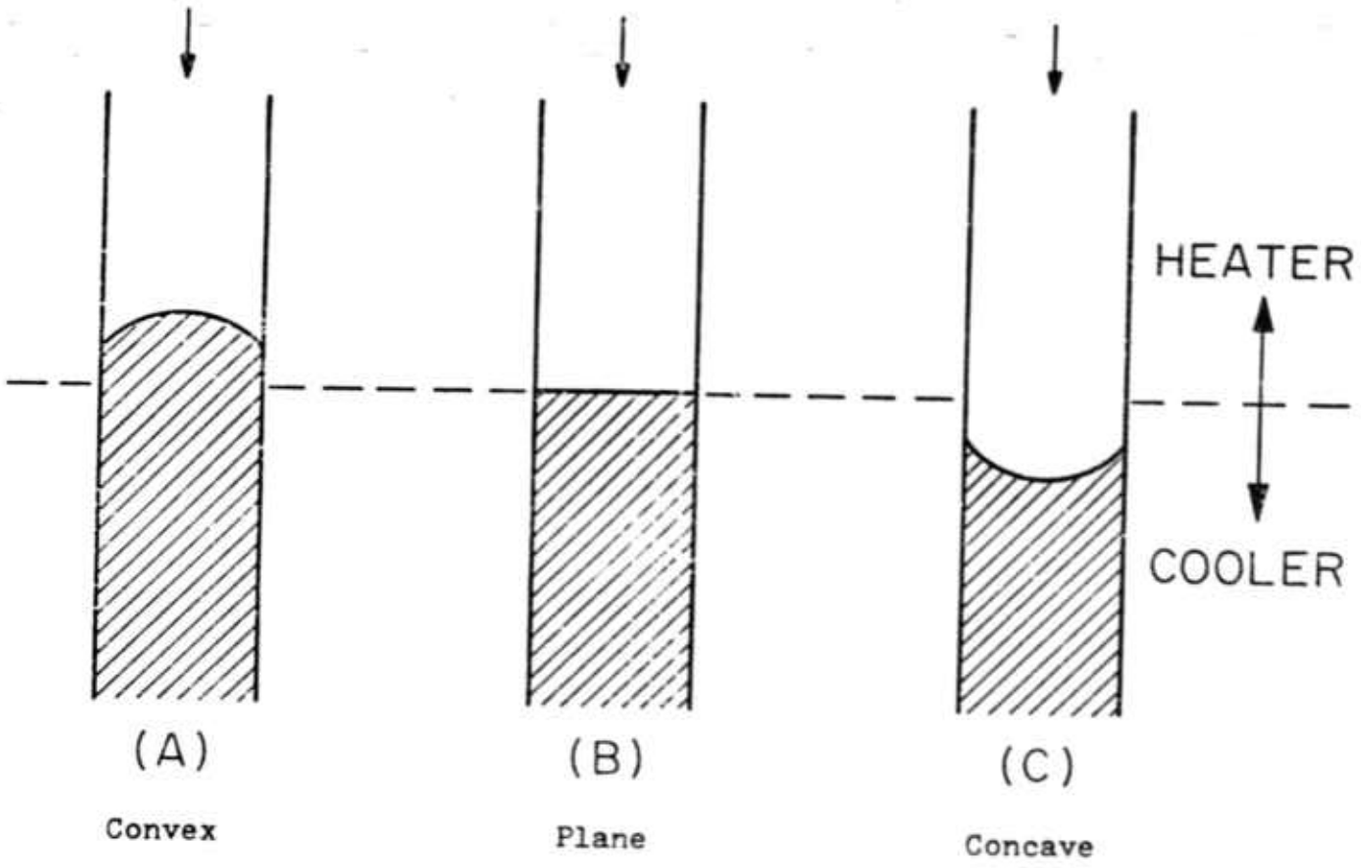

Figure 16 Shapes of the freezing interface in the Bridgman-Stockbarger experiments.

Figure 17 Carbon particles trapped next to the tube wall during Bridgman growth of naphthalene (13 mm OD tube, BN-5, V_c= 12 mm/hr).

to study the effect of temperature gradient on the critical velocity. With varied gradients, the critical velocities were all about 12 mm/hour as shown in Table 6. Higher gradients were obtained by means of decreasing the temperature of the cooling fluid and increasing the heater power input. The measured interfacial gradients are only approximate.

At the end of this preliminary study, Cisse and Bolling [9] presented similar results based on particle-water systems. Their results also indicated that the critical velocity does not depend significantly on the interfacial temperature gradient. Because of the foregoing evidence and similar conclusions based on the organic system, we did not pursue this subject further.

Theoretical studies of the factors influencing the interfacial temperature gradient were also made during this research. A paper was published based on part of this study and is attached as Appendix A. The influence of the length and radius of a crystal on the interfacial temperature gradient was estimated by use of a one-dimensional heat transfer calculation. It was found that the temperature gradient continues to change for quite long crystals when the Biot number $H = hR/k$ is small (where h is the heat transfer coefficient from the crystal surface, R is crystal radius, and k is the thermal conductivity), especially for good conductors, but does not depend on crystal length significantly when the Biot number is large. For our Bridgman growth of naphthalene, H was about 1 and the critical length was then equal to R. Therefore, a length of tube equal to its

TABLE 6

EFFECT OF TEMPERATURE GRADIENT ON CRITICAL VELOCITY

(Naphthalene-Carbon System)[1]

Run No.	Bath Temperature, °C	Heater Input, watts	Temperature Gradient, °C/cm[2]	Critical Velocity, mm/hr.
BN-5	-20	6.8	~27	~12
BN-3	0	5.0	~6	~12
BN-7	10	4.5	-	~12
BN-8	20	4.5	-	~12

[1] Carbon added directly into the melt.

[2] Measured interfacial temperature gradient in the melt at the interface.

diameter was submerged in the cooler at the beginning of each experiment, so that constant temperature gradients were maintained at the freezing interface during controlled solidification.

4. Stirring

It was hoped that stirring of the melt would increase the critical velocity. Stirring should enhance the supply of melt to the contact region between the particles and the interface, move particles along the interface giving them less time to be trapped, and keep many more of the particles in suspension and away from the interface. Because of its very low vapor pressure, salol was originally used for the stirring experiments with carbon. The experiment without stirring gave V_c = 7 mm/hour. However, the runs with agitation did not give satisfactory results. When carbon was added directly into the melt (BSA-9A), most of the carbon was immediately incorporated into the growing salol and made a dark band as shown in Figure 18 (three additions were made in this run). When the carbon was dispersed into the melt ultrasonically (BSA-12A), the interface trapped particles quite uniformly, resulting in a nearly uniformly dark solid. Other kinds of particles, Fe_2O_3 (BSA-13-1), Si (BSA-14) and Zn (BSA-13-2), were also used which were reported to be easily separated from salol by Uhlmann et al. [6]. However, we did not obtain the expected results even without stirring (see Table 4).

Therefore, the naphthalene-carbon system was used henceforth in the study of stirring, due to the ready separation. Inserting a

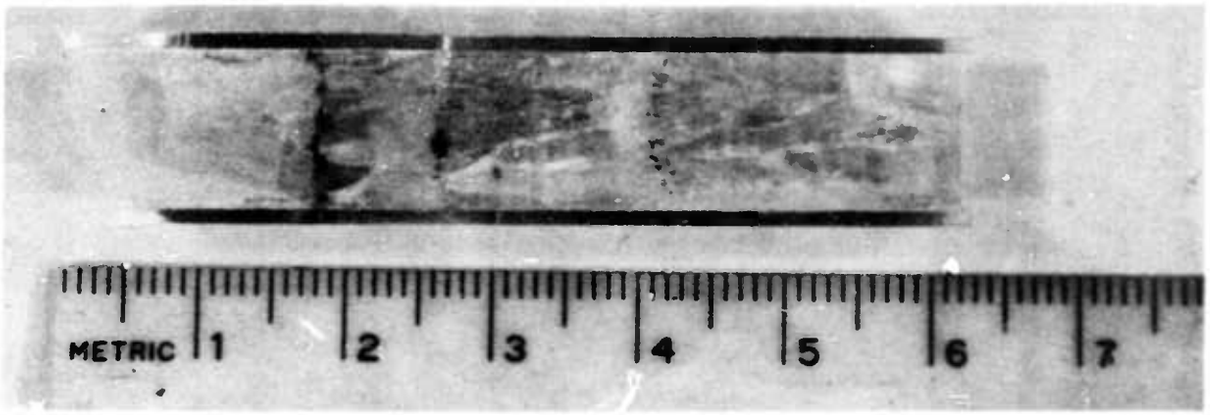

Figure 18 Carbon particles trapped immediately after each addition during Bridgman growth of salol with stirring (BSA-9A). Three additions made at V= 6 mm/hr.

stirrer in the growth tube made operation quite difficult. It was impossible to keep the distance between the stirrer and the interface constant. If the distance was large, stirring would not be expected to influence V_c. If the stirrer and the interface contacted each other, either the growth tube or the stirring rod were damaged. Although we used a stepless jack to adjust the position of the stirrer frequently during changes in the growth rate, this distance was very difficult to control and made the effect of stirring uncertain. However, one stirring run (BNA-8A) gave V_c = 30 mm/hour, which was quite encouraging.

Another phenomenon was observed as follows. When stirring was initiated, the shape and position of a steady salol interface changed drastically. The planar interface became convex into the solid due to higher heat transfer rates through the glass wall. Particles moved up the bulge and circulated into the melt (motion pictures were taken of this aspect). After the interface reached steady-state, it was concave into the solid making direct microscopic observation of particle pushing difficult. The melt was decanted (BSA-6A, 7A) and the interface was observed thereby to consist of many large facets, as shown in Figure 19. Some grains protruded up to 1.5 mm. The deepest point in the concave interface was about 9 mm from the periphery.

5. Matrix-Particle Dependence

Previous data [6] indicated that there were variations in V_c

Figure 19 The concave interface of growing salol containing many large facets (30 mm OD tube, BSA-7A).

among the particle materials in a given matrix material, and among the matrix materials for a given particle. We used a different, improved experimental method and observed that carbon particles were readily separated from naphthalene, but were very difficult to remove from camphor (V_c less than 2 mm/hour). A summary of results is listed in Table 7.

6. Gas Bubbles and Surface-Driven Flows

The solubility of gases in solids is normally much lower than in the corresponding melts. Segregation takes place at the freezing interface and increases the gas concentration next to the interface. As a result, gas bubbles often nucleate and grow on the interface during solidification [49]. Because temperature varies in the melt, the surface tension varies along the gas-liquid interface and can produce vigorous circulation. In the present experiments, bubbles gave rise to vigorous flows which circulated the particles around the bubbles. Figure 20 shows vigorous circulation of carbon particles around a bubble growing on the interface of naphthalene (frame from motion picture).

These gas bubbles had a large influence on the separation of foreign particles from the matrix materials. Gas "worms" were often created in the solid behind the bubbles on the interface, as shown in Figure 21. These bubbles sometimes floated away. Sometimes a bubble moved rapidly back into its gas worm or into a sudden crack in the solid and deposited a large number of particles in the solid. In such

TABLE 7

CRITICAL TRAPPING VELOCITIES IN VERTICAL BRIDGMAN CRYSTAL GROWTH

Organic Matrix	Particle	V_c mm/hour	Remarks
Naphthalene	C	21	Ultrasonically dispersed.
		16	Trapping next to glass wall.
		12	Agglomerate particles.
	Cu	18	
		14	Trapping next to glass wall.
Salol	C	7	
	Fe_2O_3	not pushed at 6	
	Zn	not pushed at 6	
	Si	not pushed at 6	
Camphor	C	not pushed at 2	

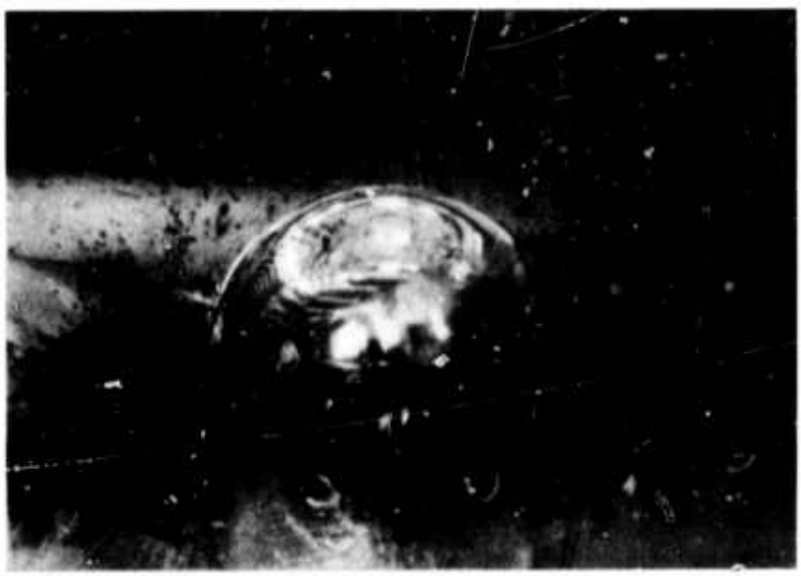

Figure 20 Surface-driven flows circulating particles around a gas bubble during freezing of naphthalene.

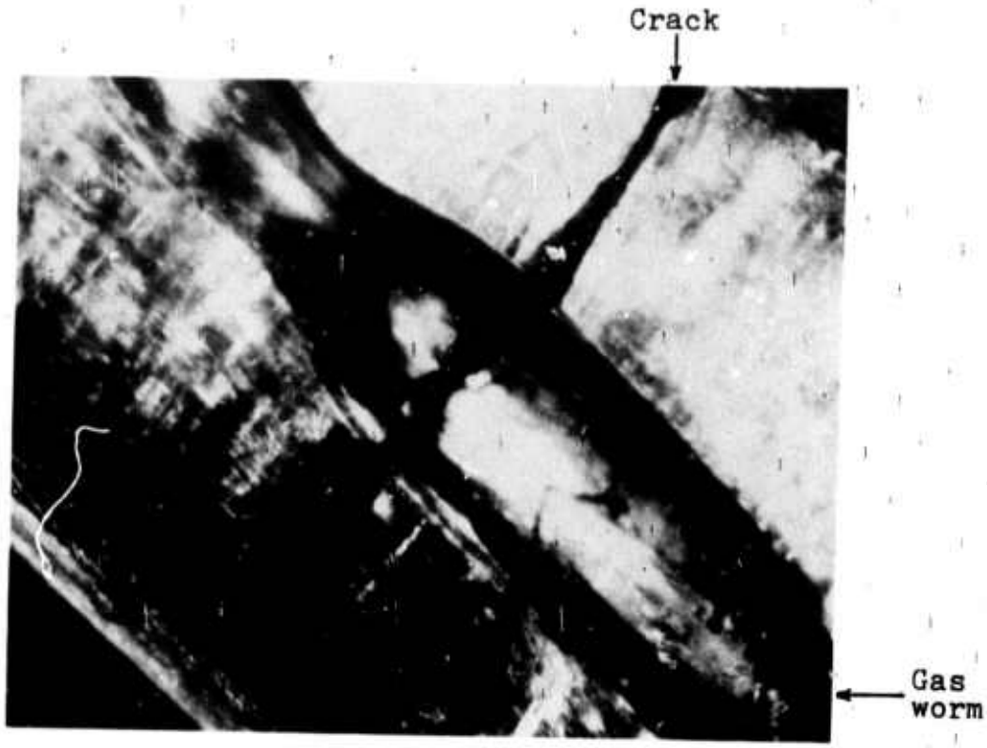

Figure 21 A large gas worm and a crack across the gas worm in solidified naphthalene (10X, BNA-4).

cases it was very difficult to know whether the particle incorporation was due to a true critical velocity or to the influence of bubbles.

Some interesting observations, not related to particle pushing, were also made on bubble nucleation and growth. In the carbon-naphthalene system, bubbles occurred at a change of crystal growth rate, or when the growth rate exceeded 16 mm/hour (BNA-4). When the growth tube was evacuated at 0.3 Torr, bubbles did not appear unitl V = 26 mm/hour (BNA-6V, 7V). However, no bubbles formed when copper foreign particles were employed in naphthalene with a 0.3 Torr evacuation even at V = 32 mm/hour (BNA-9V Cu). Hence, nucleation of bubbles depended on the type of particles present and the amount of gas in the matrix material.

Stirring the melt reduced bubble formation (BNA-1A, 2A, 3A), but did not eliminate the problem (BNA-8A). Bubbles also formed on the freezing interface of salol under some conditions.

A theoretical treatment of bubble nucleation during solidification is presented in Chapter VI.

7. Grain Surfaces

The solidified material in this study normally consisted of 2 to 4 grains for naphthalene and about 12 grains for salol when using a 13 mm O.D. glass tube. Several single grains were separated from one another and examined under a microscope. In salol, grain boundaries contained many steps, cavities, gas worms and preferentially

trapped particles, as shown in Figure 22. However, the surfaces of naphthalene grains primarily exhibited steps without preferential trapping of particles (Figure 23). The latter appears to confirm the results of Cisse and Bolling [9], in which they found particles on grain boundary grooves are pushed to higher velocities than those at flat grain surfaces of an ice water interface.

8. Growth Orientation

Examination of the solidified products of many runs indicated that one side of the interface began trapping particles much sooner than the other side, as shown in Figure 24A. This leads one to believe that certain grain orientations may push particles, while other grain orientations incorporate particles at the same growth rate. The transverse cut of the solidified ingot (BNA-8A) showed that one grain trapped particles, while the other grains rejected particles (see Figure 24B).

Incidentally, the rejection of soluble impurities was also observed to depend on growth orientation. In zone-refined camphor one grain was light yellow, while the adjacent grain was colorless.

9. Surfaces of Solidified Products

Like the surfaces of the grain boundaries, the cylindrical surfaces where the solid contacted the glass tube were not always smooth. Frequently, they were rough and contained steps, bumps, tiny crystals (Figure 25), and gas bubbles and worms (Figure 26). As

(A) Displaying many bumps and waves (100X).

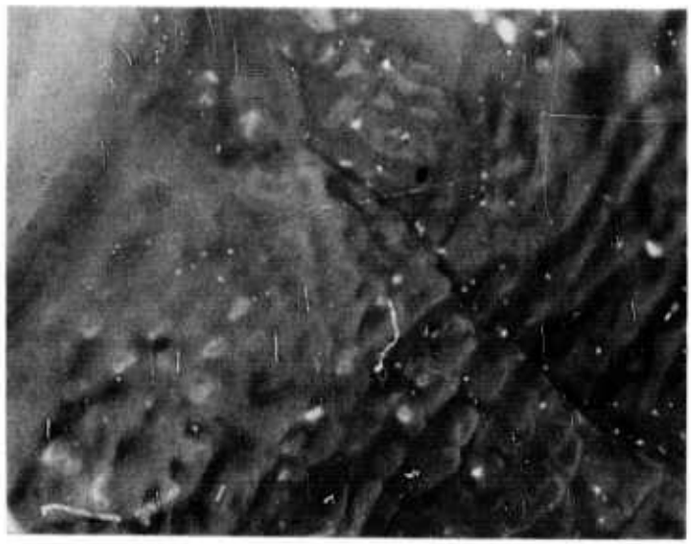

(B) Containing small gas worms (or cavities) and carbon particles (50X).

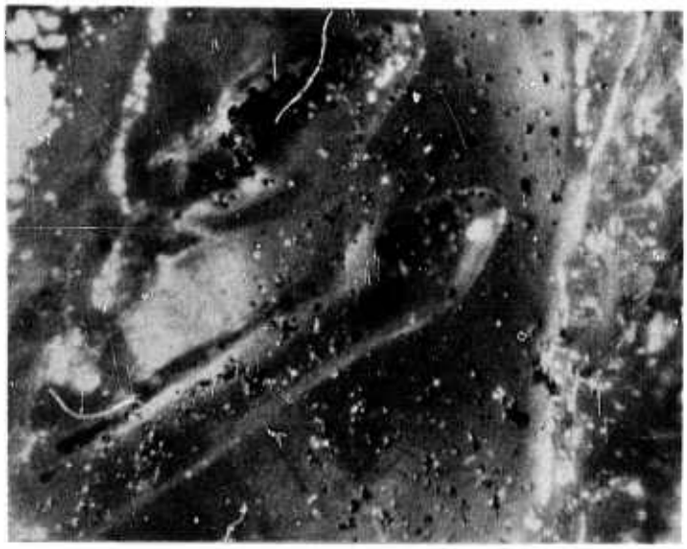

Figure 22 Surface of salol grains (BSA-10A).

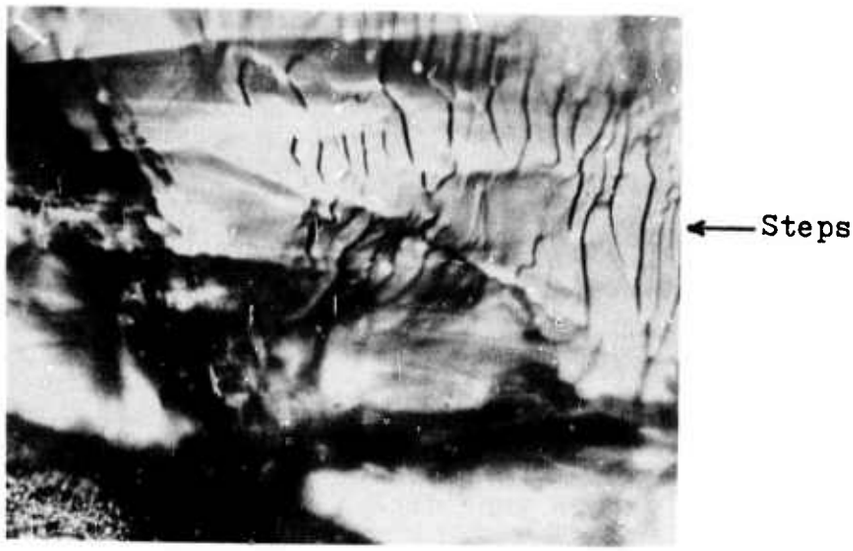

Figure 23 Surface of naphthalene grains containing many steps (50X, BNA-8A).

(A) Vertical Bridgman growth of naphthalene. Upper side trapped carbon earlier than lower side (The arrow at the right hand indicating the beginning of the run, BNA-6V).

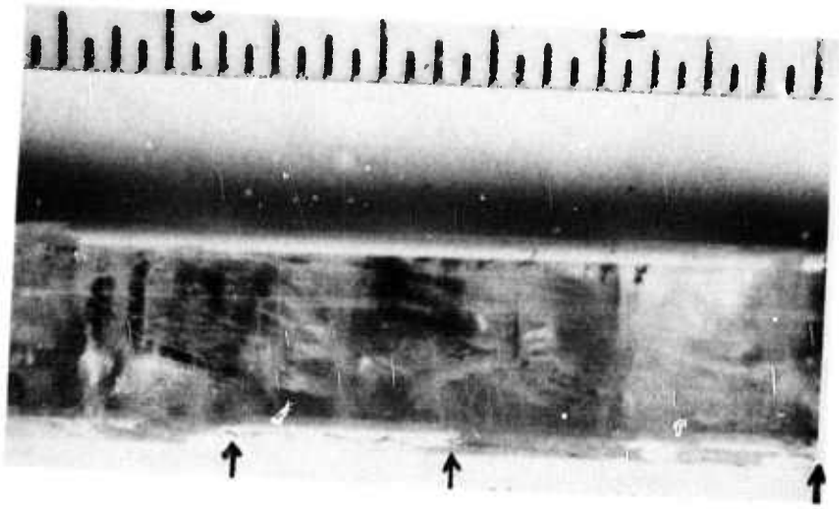

(B) Transverse section of solidified naphthalene (BNA-8A). One grain trapped carbon (dark grain with a gas worm) while the other grain did not (light grain).

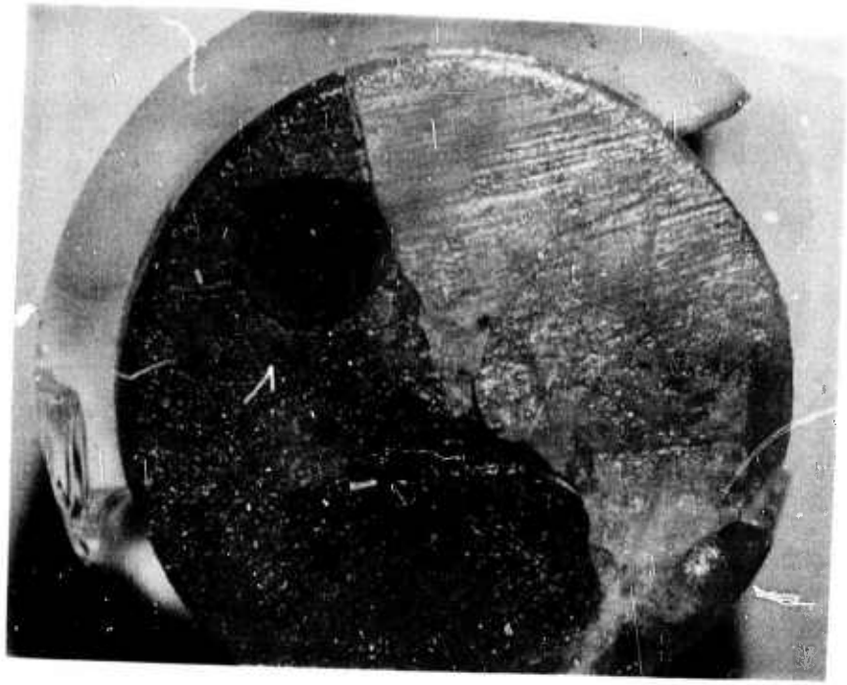

Figure 24 Effect of growth orientation on particle pushing.

(A) Containing many steps and waves, 100X.

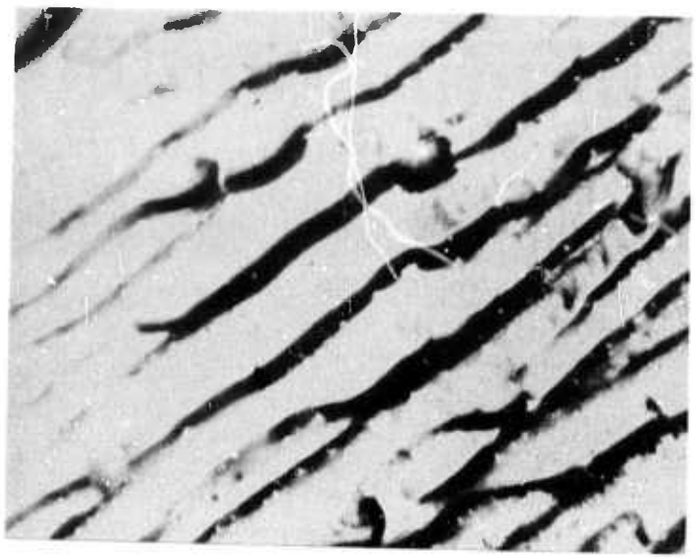

(B) Showing bumps and tiny crystals, 50X.

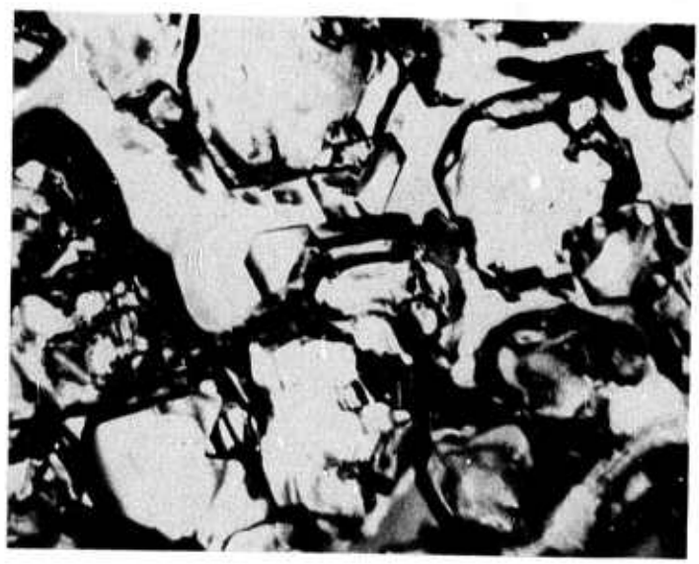

Figure 25 Surfaces of solidified naphthalene at tube wall.

Figure 26 Gas bubbles trapped between the solidified naphthalene and tube wall, 32X.

mentioned before, carbon particles were trapped between these surfaces and the glass wall at a lower critical velocity than at the advancing grain surfaces, especially with convex interfaces. This indicates that the results of Uhlmann, et al. [6] obtained with thin layers of melt held between microscope slides might have been strongly influenced by the glass slides and might not have been characteristic of a free interface.

10. Cracking and Healing

Because the coefficient of thermal expansion differs for a solid and its growth container, thermal stresses form during the period of cooling after solidification. Sometimes thermal stresses were sufficient to cause cracking of solidified material both in the horizontal and vertical directions. The cracks did not reach the freezing interface. Therefore, particles were not preferentially trapped at these locations. A vertical crack was sometimes difficult to distinguish from a grain boundary. Occasionally a horizontal crack healed to form a veil of microscopic gas bubbles, as shown in Figure 27. Similar observations were made in movement of inclusions in KI crystals [50].

11. Bouncing Particles

An interesting phenomenon was observed during zone-refining of camphor. Some of the small foreign particles originally present in the reagent bounced back into the melt as soon as they touched the

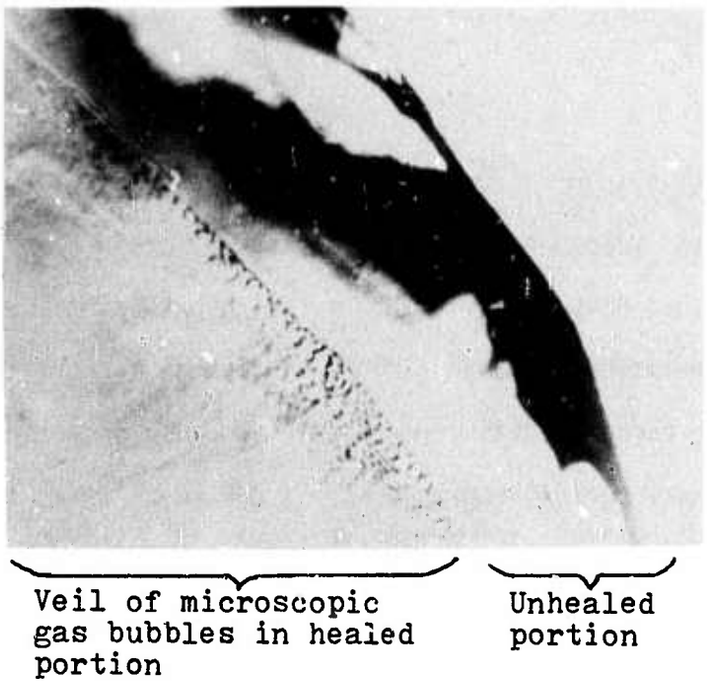

Figure 27 Crack (black area) and partially healed crack (a veil of microscopic gas bubbles) in solidified naphthalene (50X, NBA-4).

freezing interface. Others bounced into the melt following a rapid approach to the interface without actually touching it. This is suggestive of electrostatic effects or of irregular convection currents. Further study is warranted.

12. Summary

In addition to previously established parameters such as particle size and shape, particle roughness, and grain boundaries, we have found that bubbles, interface shape, growth container and the growth orientation all significantly influence the critical velocity in the carbon-naphthalene system. Because of this complex dependence, it was never observed that all particles were clearly incorporated at one location in the solidified products. In fact, the particles were trapped over a finite distance. The measured values of V_c varied from 21 to 35 mm/hour (BNA-7V) without stirring the melt. The growth of bubbles at the freezing interface was eventually prevented by evacuating the growth container. The freezing interface had to be kept slightly concave into the growing solid to prevent particles from being trapped between the crystal surface and the container. The interfacial temperature gradient did not affect the critical trapping velocity within the range investigated. The V_c for trapping of carbon by solidifying salol was 7 mm/hour, but particles of Zn, Si and Fe_2O_3 were not readily pushed. These results are contrary to data by others [6] in which a horizontal thin film held between two glass slides with a vertical freezing interface was

employed. Stirring might have increased V_c, but a new method to perform stirring was needed to replace the unsuccessful technique of inserting a stirrer.

B. Horizontal Zone-Refining with Rotation

1. Interface Shape

Tube rotation averaged out radial asymmetries. The shapes of the freezing and melting interfaces in a horizontal rotating zone depended on the growth rate. The variations of interface shapes are shown in Figure 28. Planar interfaces were obtained only at zero or very slow growth rates. When the growth rate was increased, the latent heat liberated at the freezing interface had to be conducted through the crystal. Since cooling took place only at the rotating tube wall, the freezing interface gradually became more and more concave. Meanwhile, the melting interface moved closer to the heater (heat power kept constant) and became increasingly convex, likewise because of latent heat consumption. At high growth rates (>90 mm/hour), insufficient time was available to completely melt through the feed and the melting interface began contacting the freezing interface, as illustrated in Figure 28D. Because of this, the critical velocities of certain particle-organic systems with high V_c were difficult to determine even when heating power was continuously increased during the experiment (for example, carbon-naphthalene in a 19 mm I.D. growth tube, HRL - 5 Cu).

As the freezing rate of naphthalene was increased, small

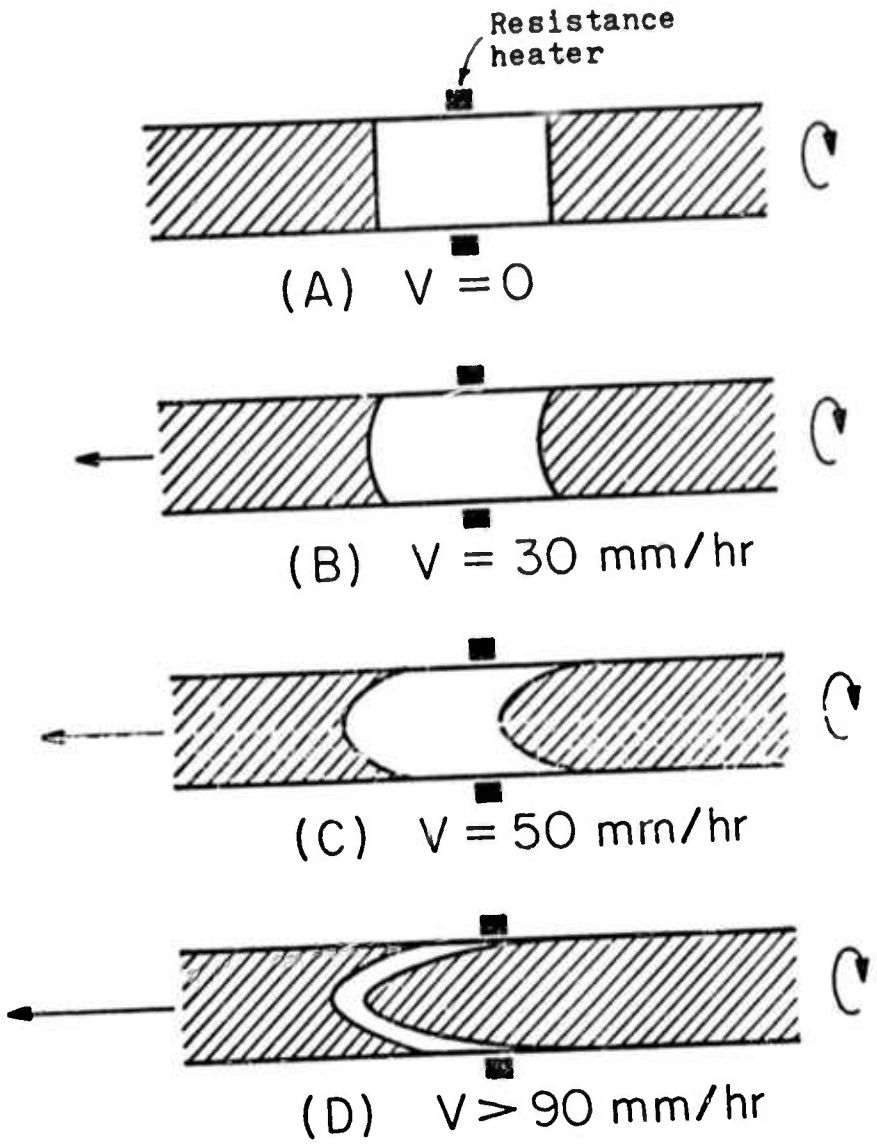

Figure 28 Change of zone shape with travel rate in horizontal zone-refining of naphthalene with rotation (50 RPM, 19 mm I.D. tube).

amounts of carbon particles gradually accumulated on the central portion of the concave interface and adhered there. These particles were then trapped into the growing crystal when the growth rate reached V_c. The length of crystal over which particles were entrapped depended on the growth rate after exceeding V_c. The trapping length was shorter as the growth rate was increased. Periodic trapping was observed over a finite length when the growth rate was kept at V_c. In other words, accumulation of particles on the concave interface and trapping of particles into the crystal took place alternatively at V_c until all particles in the rotating zone were incorporated. Figure 29 shows that carbon particles were pushed from the left end to the right end of a naphthalene ingot by the rotating zone-refining method.

Red iron oxide particles gave trapping characteristics similar to carbon. Both were entrapped along the axis of growing naphthalene. However, the pushing and trapping phenomena were different for copper particles. At V_c the particles did not accumulate at the central part of the interface, but were incorporated into the crystal rather uniformly.

The effect of interface shape on particle pushing was also studied. When the freezing interface was kept planar by means of a second heater, the results were slightly different from those obtained for a concave interface. Carbon particles were trapped uniformly into the growing naphthalene and V_c was increased from 30 to 35 mm/hour (HRT-6, 7 and 8). A planar interface was not easily obtained because

Figure 29 Horizontal zone-refined naphthalene with carbon particles pushed from the left to the right end (V_c=30 mm/hr and 5 RPM in a 13 mm OD tube).

each heater required a different heat input dependent on growth rate and rotation.

2. Rotation

A minimum speed of rotation was first established in order to keep most of the particles suspended in the rotating zone for each particle-organic matrix pair. The rotation was then increased to determine the effect of rotation speed on V_c. Tables 8, 9 and 10 are summaries of results for carbon, copper and red iron oxide in a naphthalene matrix.

Two kinds of V_c are shown in these tables. One is the V_c for particle trapping into the solid, the other is for trapping between the tube wall and the solid. Copper particles gave a strong dependence of V_c on rotation speed. Increase of rotation increased the critical trapping rate of copper into the solid. On the other hand, increase of rotation increased the centrifugal force causing some of the larger particles to stick to the tube wall. These particles were then engulfed next to the tube wall. Figures 30, 31 and 32 indicate the variations of V_c in the two positions with rotation speed for copper, iron oxide and carbon. For example, in the copper-naphthalene system V_c in the crystal increased with rotation, while V_c next to the wall decreased with rotation. The intersection of these two curves gives an optimum rotation speed under which a maximum V_c at the crystal is reached with no trapping next to the wall. The optimum rotation speeds and corresponding V_c are tabulated in Table 11.

TABLE 8

EFFECT OF ROTATION RATE ON CRITICAL FREEZING RATE V_c
FOR TRAPPING OF CARBON IN NAPHTHALENE
USING HORIZONTAL ZONE REFINING

Run	Tube Size mm I.D.	Rotation RPM	Critical Velocity, mm/hour	
			Crystal	Wall
HR-6	10.5	1.5	29	30
HR-8	10.5	1.4	28	30
HR-2	10.5	4	34	no
HR-5	10.5	4	30	no
HR-7	10.5	16	29	30
HR-3	10.5	33	32	32
HR-4	10.5	33	30	31
HR-15M	10.5	45	33	28
HR-16M	10.5	45	34	29
HR-23	10.5	80	30	20
HRL-1	19	10	24	28
HRL-2	19	30	36	36
HRL-3	19	60	37	trapped

TABLE 9

EFFECT OF ROTATION RATE ON THE CRITICAL FREEZING RATE V_c
FOR TRAPPING OF COPPER IN NAPHTHALENE
USING HORIZONTAL ZONE REFINING

Run	Tube Size mm I.D.	Rotation RPM	Critical Velocity, mm/hour	
			Crystal	Wall
HR-11	10.5	44	47	no
HR-12	10.5	44	51	no
HR-13	10.5	44	48	no
HR-19	10.5	50	66	80
HR-18	10.5	58	70	68
HR-17	10.5	70	77	65
HR-14	10.5	100	82	61
HRL-5	19	44	< 90	53
HRL-8	19	50	< 90	90

TABLE 10

EFFECT OF ROTATION ON V_c FOR IRON OXIDE-NAPHTHALENE IN HORIZONTAL ZONE REFINING

Run	Tube Size mm I.D.	Rotation RPM	Critical Velocity, mm/hour	
			Crystal	Wall
HR-21X	10.5	8	28	33
HR-20X	10.5	40	35	34
HR-22X	10.5	80	36	trapped
HRL-7X	19	8	32	no
HRL-6X	19	40	46	20

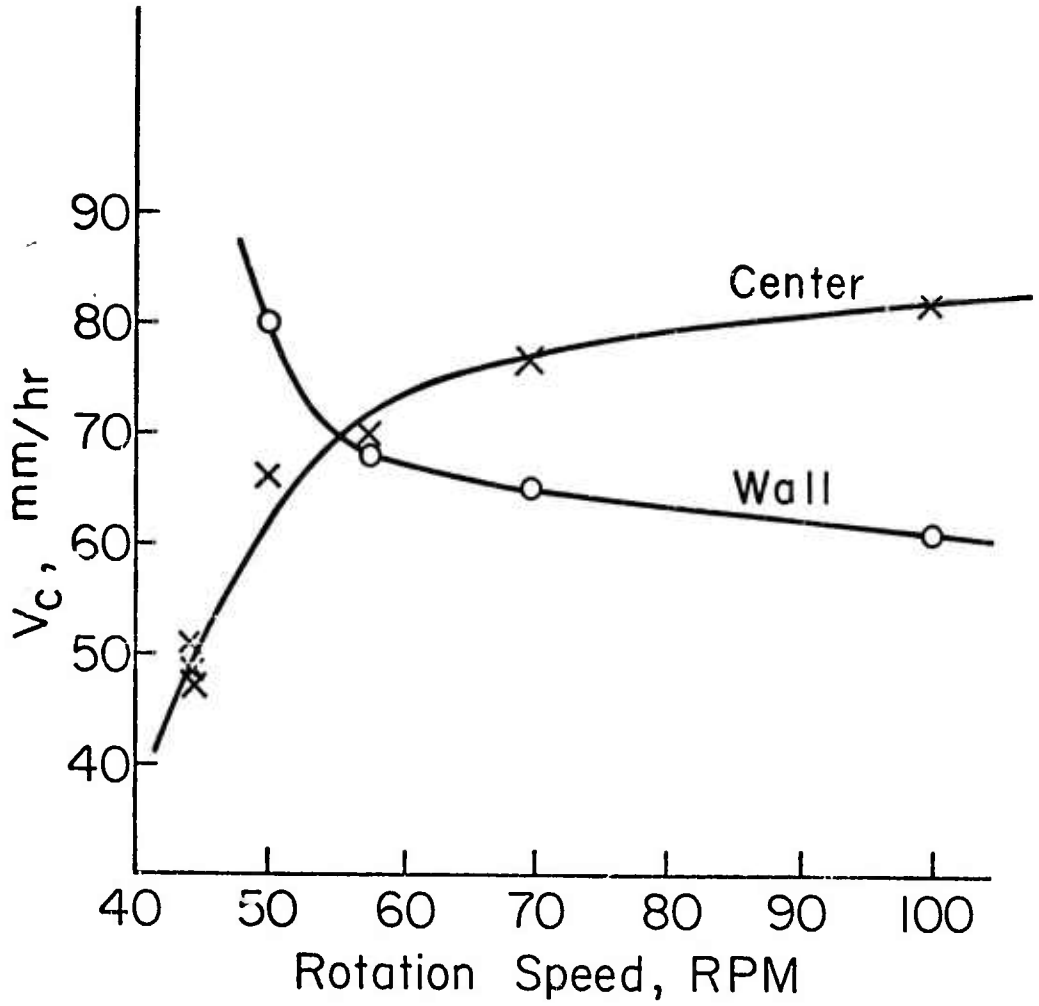

Figure 30 The influence of tube rotation on incorporation of copper particles by naphthalene during horizontal zone melting (10 mm I.D. tube).

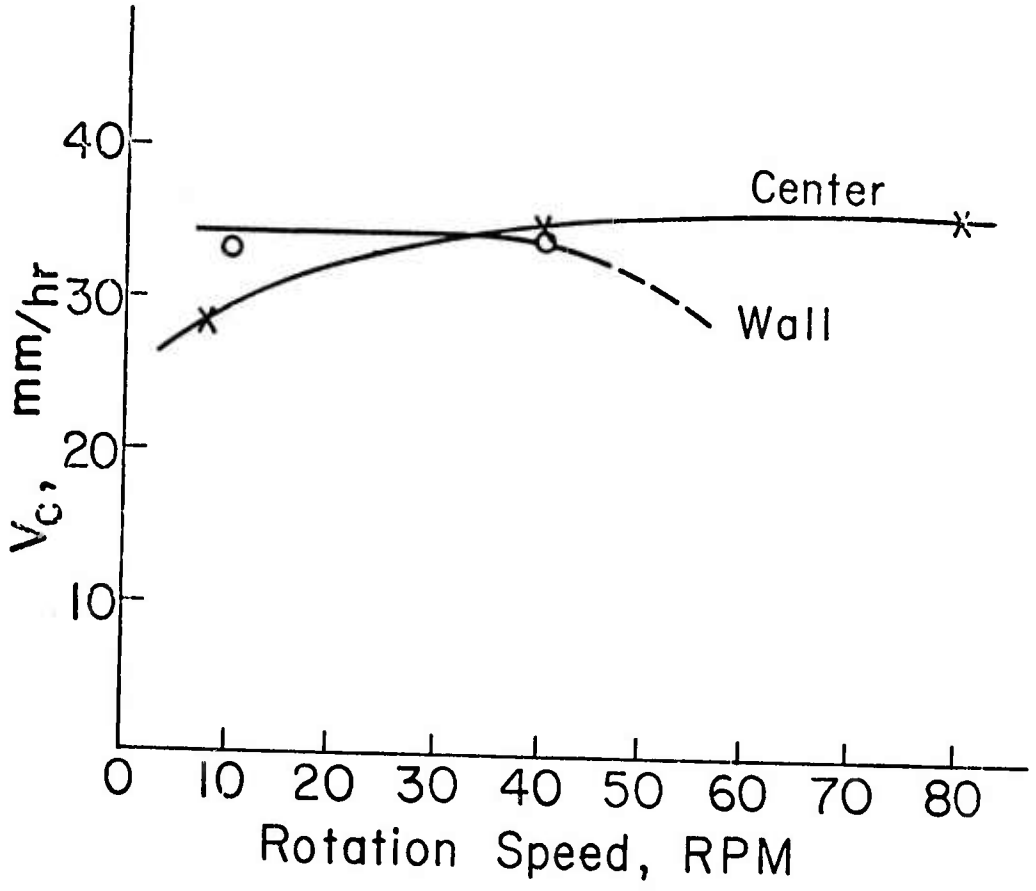

Figure 31 The influence of tube rotation on incorporation of iron oxide particles by naphthalene during horizontal zone melting (10 mm I.D. tube).

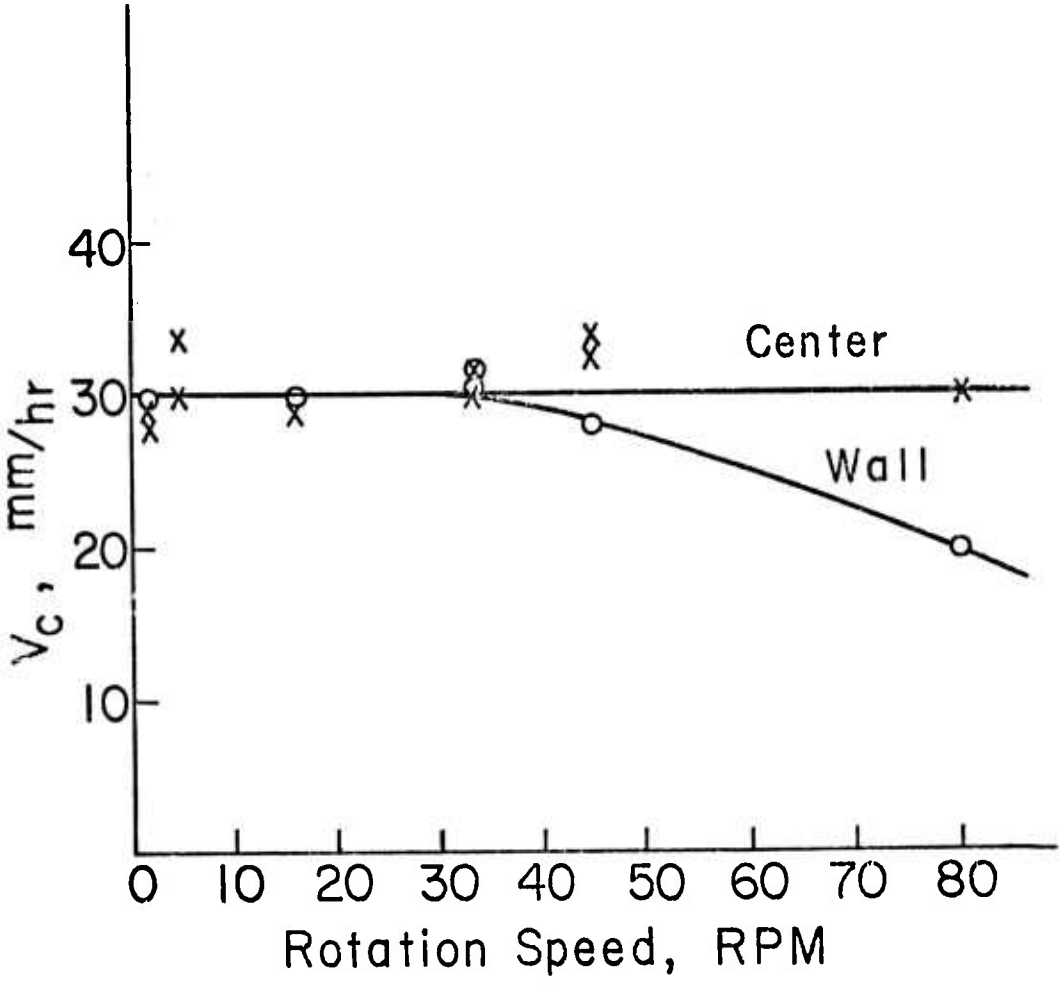

Figure 32 The influence of tube rotation on incorporation of carbon particles by naphthalene during horizontal zone melting (10 mm I.D. tube).

TABLE 11

OPTIMUM ROTATION RATES FOR SEPARATION OF PARTICLES FROM NAPHTHALENE BY A HORIZONTAL ZONE REFINER WITH ROTATION

Particles	Tube Size mm I.D.	Optimum Rotation RPM	V_c mm/hour
Carbon	10.5	33	30
	19	30	36
Copper	10.5	55	70
	19	50	< 90
Iron Oxide	10.5	40	35
	19	~ 25	~ 38

3. Tube Diameter

Tables 8, 9, 10 and 11 also give the experimental results obtained for a larger growth tube (19 mm I.D., 22 mm O.D.). By increasing the tube diameter by a factor of two, V_c was increased about 10% for iron oxide, 20% for carbon and more than 30% for copper under the respective optimum rotation rates. Furthermore, the optimum rotation rates for the large tube were reduced at least 10% from that of the small tube.

4. Bubbles and Void

The dissolved gases in the organic compound are continuously rejected into the melt during solidification. These gases grew into bubbles at the advancing interface in the vertical Bridgman experiments. In horizontal zone refining with rotation, however, the gases were transported into the melt sufficiently to avoid nucleation and growth at the interface. These gases were liberated in a gas space or void located at the top of the rotating zone. The void helped in observation of particles at the interface. Carbon and iron oxide particles always adhered at the center of the interface before they were incorporated into the crystal. Sometimes, adhesion of carbon particles on the interface gave a spiral pattern.

Bubbles appeared at the interface only at slow rotation rates and high growth rate during separation of carbon from naphthalene. They did not give difficulties in determination of V_c because they began occurring at about 30 mm/hour. Bubbles were not encountered at

the interface in any other horizontal zone melting experiments.

5. Summary

Horizontal zone refining with rotation achieved the goal of increasing the critical trapping velocity of particles. Sufficient data were gathered to permit design of a separation process and to make laboratory-scale production of particle-free organics. This new separation process is simple and effective and gives significant improvements and advantages over the vertical Bridgman method. The advantages are listed as follows: (1) V_c is increased about 50% for carbon particles and at least 300% for copper in naphthalene; (2) clear-cut separation is possible; (3) trapping between the crystal and the tube wall can be prevented; (4) bubbles do not grow on the freezing interface, so that the growth tube does not have to be evacuated; and (5) operation is simple, effective and economical. The economics of this separation process will be discussed in the next chapter.

An optimum rotation speed was determined for each particle-naphthalene system, above which a considerable amount of particles were trapped next to the glass wall and below which trapping was preferred in the crystal. Further discussion on horizontal rotation is given in Chapter VI.

CHAPTER V

POTENTIAL APPLICATIONS AND ECONOMICS

In addition to investigation of particle pushing and trapping by a freezing interface, the final goals of this work were to make particle-free organic chamicals, especially those which are solid at room temperature. In addition, several potential applications were discovered during the course of this work. Some of them were further studied experimentally. The results and economics of the developed process are given as follows.

A. Separation of Mixed Particles

The results shown in Chapter IV and previous data [6] have demonstrated that each kind of particle has a different freezing rate V_c in a given matrix material. In other words, a mixture of different kinds of particles may be separated in a properly selected organic compound if an increasing growth rate is employed during controlled solidification. The results of horizontal zone refining with rotation gave V_c = 30 mm/hour for carbon and V_c = 70 mm/hour at 55 RPM for copper in naphthalene. Because of their wide difference in V_c, it should be possible to separate a mixture of carbon and copper from one another by freezing of naphthalene. Run HR-15M accomplished this goal. When the freezing rate was progressively increased from 25 to 75 mm/hour at 44 RPM in a period of 4 hours, carbon particles started to be trapped at 34 mm/hour. All of the carbon was incorporated

into the central portion of the crystal over a length of 2 cm. Copper particles were then trapped uniformly at 54 mm/hour, until the end of the run (75 mm/hour). Figure 33 indicates that carbon particles were clearly separated from copper in solidified naphthalene.

The vertical Bridgman growth method was also used to separate mixtures of particles. Carbon and copper particles were ultrasonically dispersed into molten naphthalene (BNM-3). The growth tube (10.5 mm I.D.) was evacuated and sealed at 0.05 Torr. The growth rates were increased from 10 to 40 mm/hour. The solidified crystal was about 7 cm long at the end of a 3-hour run. Most of the carbon was trapped in the upper portion of the crystal, while copper was incorporated in the middle portion. Although the difference in their individual V_c was slight (about 21 mm/hour for carbon and 18 mm/hour for copper) in naphthalene, they were still separated from each other by programmed solidification. A mixture of red iron oxide and carbon was not separated appreciably in naphthalene (BNM-1). However, the growth tube was not evacuated and a growth of bubbles on the freezing interface adversely affected the separation.

Both growth methods have shown experimentally that a mixture of particles can be separated from one another by programmed solidification of a suspension in an appropriate liquid. We call our invention "particle chromatography". This new separation technique may be used to identify particles from a mixture of various kinds of particles, derived from drugs and particulate pollutants, as examples.

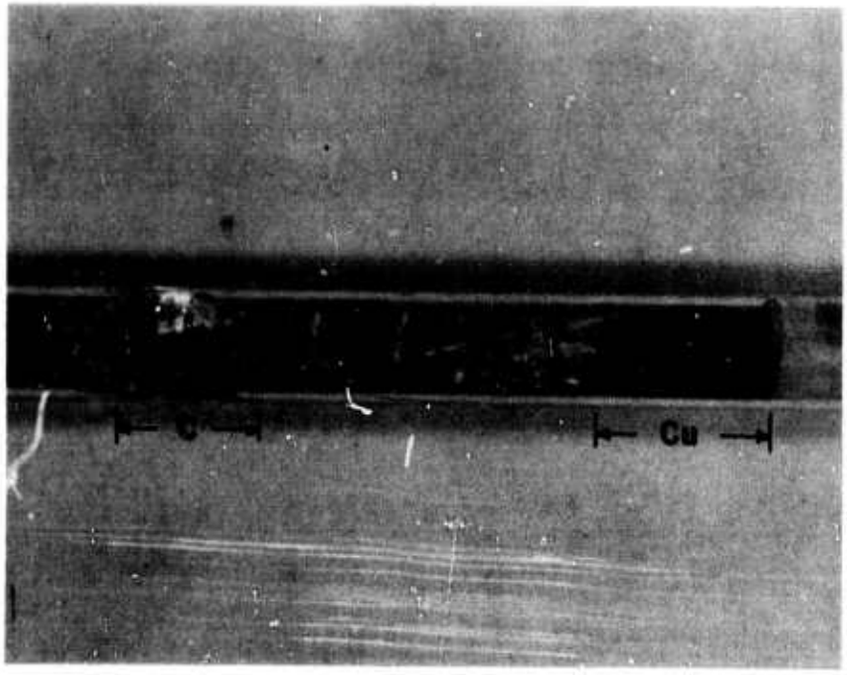

Figure 33 Carbon and copper particles were separated during programmed solidification of naphthalene in horizontal zone-refining with rotation (HR-16M).

B. Size Classification

Screen analysis is a simple and accurate method of fractionating materials into various sizes. It is widely used to determine the size distributions and to yield fractionated products which may be studied separately from the whole material. However, the method is applicable only to about 44 μm or 325 mesh. Below this size there are several methods to analyze the distribution of sizes, but it appears that only the method of elutriation may be employed to obtain fractionated products in the size range of 1 to 50 μm [51]. The basis of the elutriation method is that an upward velocity of fluid supports only particles smaller than a given size. The smaller particles are carried upward, while large particles settle in the stream. The collected particles may be further elutriated at different velocities to make finer size fractions and thus it is difficult to start with small amounts of particles. Here we have a method to make size fractions for a small quantity of particles.

Previous studies [5,6,7,9] indicated the dependence of the critical velocity on particle size. Larger particles have lower V_c, smaller particles have higher V_c. Therefore, particles with various sizes could be sieved in a matrix material by gradually increasing the freezing rates during controlled solidification. A mixture of silver powder and naphthalene (BNSC-3) was solidified by the Bridgman growth method. The freezing rates were increased from 6 to 26 mm/hour. The solidified crystal (5.2 cm) was transversely sliced into four equal sections. The silver particles in each section

were collected on a Millipore filter, and were examined under a microscope. The size distributions varied from the top to bottom sections. The micrographs of the top and bottom sections are shown in Figure 34. Small particles were dominant in the top section, but some large particles were also present in this section, which might have been pushed by grain boundary grooves and grain boundary triple points [9]. The bottom section contained many large particles as well as small particles These small ones were probably incorporated in the grooves between the crystal and glass tube where V_c was found to be substantially reduced in this study. The method could probably be improved by growing a single crystal with a slightly concave freezing interface so that the effects of grain boundary and grooves next to the wall can be eliminated.

C. Economics

The critical trapping velocity will have a major influence on the cost of making particle-free organic compounds since particles can only be separated from the matrix material at freezing rates below V_c. Because the value of V_c is different for each particle-organic system pair, the cost will be strongly dependent on the system being purified. An organic compound usually contains several different kinds of insoluble particles, the identities of which may or may not be known. This makes estimating the cost of producing particle-free ultrapure chemicals very difficult unless one knows (a) the kinds of particles and their values of V_c, and (b) the methods of determining

(A) Larger particles dominated in the bottom section, 200X.

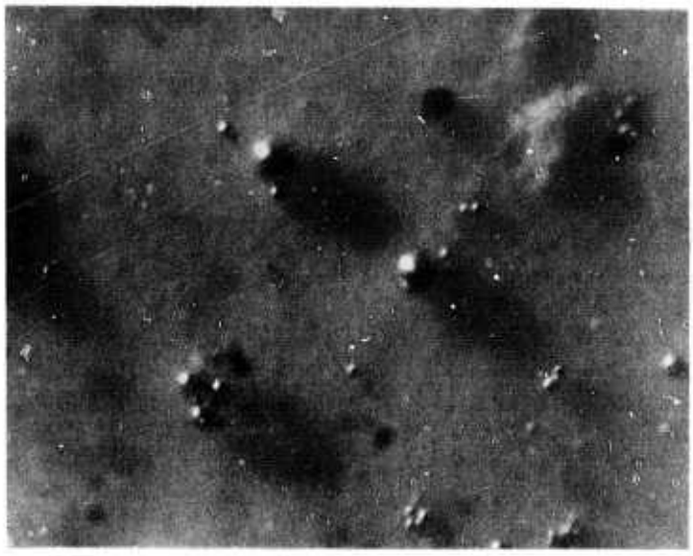

(B) Smaller particles dominated in the top section, 200X.

Figure 34 Size classification of spherical Ag particles (less than 50 μm) by vertical Bridgman growth of naphthalene.

the amount of particles in organic compounds.

Although carbon is a common insoluble impurity in solid organic chemicals, some other kinds of particles are also frequently present. To supply the first information one has to conduct experiments to determine the minimum value of V_c among the various kinds of particles present before a particle-free compound can be produced. Prediction of V_c might become possible if the foreign particles were identified. The second problem of determining the purity (in terms of insoluble impurity) may be qualitatively solved either by an optical microscope or by a filtration method as described in Chapter III. There is no accurate and convenient method available at the present time for quantitative measurements of particles in organic chemicals. With these limitations, we attempted to make particle-free naphthalene. The "native particles" present in naphthalene were difficult to remove by a Fisher zone-refiner as mentioned in Chapter III, but most of these particles were separated by means of a horizontal zone-refiner at 28 mm/hour with 5 RPM tube rotation. This V_c is close to the one for separation of carbon particles from naphthalene (see Table 8).

With our present knowledge of particle pushing and trapping, a crude cost estimate for producing particle-free naphthalene is made. Because the demand is not yet sufficient to warrant industrial-scale production, a laboratory-scale production is more realistic. Furthermore, it is recommended that a small group with one engineer and one technician be created in a chemical company which has established the market for ultrapure organic chemicals. With these assumptions, the

detailed economic calculations are shown in Appendix B. The total capital investment is about $68,000 and the total product cost is about $65,000 for an annual production of 300 Kg of particle-free ultrapure naphthalene. Therefore, the product cost is 22 cents per gram, if a reagent grade chemical is used as the feed material. This cost will be reduced if larger scale production is employed [52].

It is interesting to compare the present cost estimate with the price of zone-refined organic chemicals (removal of soluble impurities). Over 100 zone-refined organic products are available commercially. A few examples are given in Table 12 [53]. The price of zone refined naphthalene is about $1.42 per gram including profit, purification cost and the material cost (about 0.5 cent per gram for the reagent grade). One does not know the amount of profit made by the producers and suppliers, but the purification cost appears to be a substantial amount and is much higher than the present estimate. Zone melting of naphthalene [53-55] is typically conducted in a vertical zone-refiner which normally requires slower growth rates and numerous zone passes in order to reach ultrapure products. The reason is that the boundary layer next to the freezing interface is much thicker in vertical zone melting than in horizontal zone-refining with rotation. Therefore, the developed new separation process is economical to product particle-free ultrapure organic chemicals.

TABLE 12

PRICE OF SELECTED ZONE-REFINED ORGANIC COMPOUNDS
FOR PRIMARY STANDARDS [53]

Compound	Price (for 2-1/2 gr.)
Acetanilide	$ 3.55
Anthracene	4.70
Anthraquinone	3.55
Benzoic Acid	3.55
p-Bromoacetanilide	3.55
p-Chloroacetanilide	3.55
p-Fluorobenzoic Acid	12.25
o-Iodobenzoic Acid	4.70
Naphthalene	3.55
Salicylic Acid	3.55
Succinic Acid	3.55
Sulfanilamide	3.55
Vanillin	3.66

CHAPTER VI

INTERPRETATION

A. Pushing Mechanisms

1. Mass Transport

Theoretically, the steady-state pushing of a particle by an advancing solid-liquid interface demands a force to prevent incorporation of the particle into the growing crystal, and a supply of liquid to the contact area between the particle and the freezing interface. The repulsive force must equal the resultant of viscous drag [6,8], surface energies [6], electrostatic interaction [6], thermal forces [8,9], and external forces [6,8]. Crystallization pressure (Eq. (2-3)) is the maximum force that can be exerted by a growing crystal on the particle. On the other hand, Corren's phase-boundary force (Eq. (2-4)) is the minimum force needed to prevent the particle from adhering to the crystal. Neither of these two limits considers the transport of liquid which may limit the rate of pushing. In fact, the supply of material practically determines whether a growing crystal traps or repels a foreign particle.

The viscous drag is apparently a major force when a particle is in contact with a horizontal crystallization front. If the freezing interface is regarded as stationary, a crystallization flow [39] toward the interface is generated by the crystal growth. The drag force then results from the flow of fluid to the contact area between

particle and interface. This force interacts with the advancing interface through a thin film, and produces a repulsive force on the interface. In other words, the crystal growth rate determines the transport process which, in turn, produces a pushing force (Eq. (2-24)). Their relationship is derived in Chapter II. Equation (2-37) describes V_c, below which the particles are pushed by the freezing interface. The calculation of V_c for the present work is shown in the next section.

2. Heat Transfer

Theoretical developments for V_c described in Chapter II assumed that thermal conductivities of particle, melt and crystal are the same, and thus that there is no effect of heat transfer on the interface shape behind the particle. However, the thermal conductivity of the particle is in general different from those of melt and crystal. For instance, Figure 35 shows that a particle (air bubble) is present in front of an ice-water interface [56]. When the freezing interface approached the air bubble fixed under a small plate, the interface just under it rose up (Figure 35-1, 2, 3, 4 and 5). The thermal insulating effect of the air bubble ($k_p < k_\ell$) caused the water under the bubble to become colder than other portions of water at the same level. This caused the interface just under the bubble to freeze faster than other parts of interface, so that a bump was formed on the advancing interface. The air bubble escaped as soon as the plate above it was inclined (Figure 35-6). This suggested that a thin film

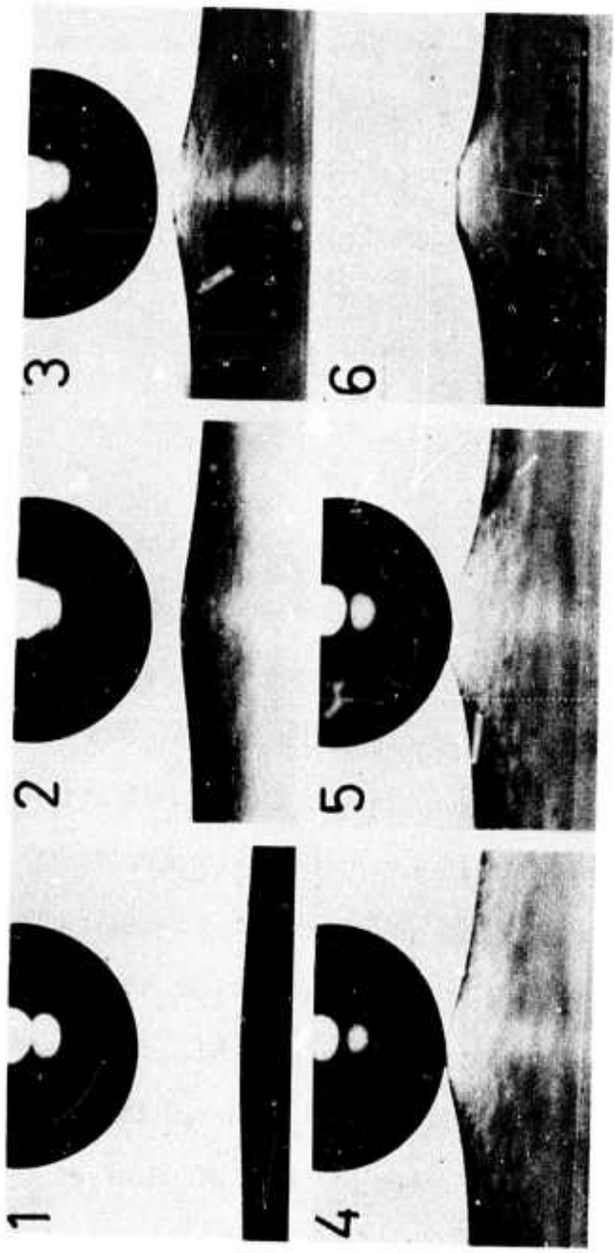

Figure 35 The presence of an air bubble in front of an advancing ice-water interface. The interface below the bubble rose up (from Reference 56).

of water existed between the bubble and the ice surface.

The schematic diagrams of isotherms and heat flows are illustrated in Figure 36 for the cases of $k_p < k_\ell$, $k_p = k_\ell$, and $k_p > k_\ell$. The presence of a particle on a solid-liquid interface with k_p different from k_ℓ changes the isotherms and thus distorts the uniform heat flow which would exist for $k_p = k_\ell$ or without the particle. Because the equilibrium interface normally approximates an isotherm, the interface shape behind the particle becomes convex for $k_p < k_\ell$ and concave for $k_p > k_\ell$. Among these three cases, the case with $k_p > k_\ell$ gives an effect similar to that due to the presence of a heavier particle. Both can cause an indentation on the interface below the particle and reduce the mass transport. Experimentally, copper particles gave a smaller V_c than carbon particles in the Bridgman growth of naphthalene.

The effect of particle conductivity on the interfacial temperature gradient is not exactly known [8,9], but the effect of interfacial temperature gradient on the particle pushing is discussed here. The heat flux q_z across a particle through a vertical central line can be expressed by

$$q_z = k_p \frac{dT}{dz} \cong k_p \frac{\Delta T}{\Delta z} = k_p \frac{\Delta T}{2T} \qquad (6\text{-}1)$$

The temperature difference between the top T_t and bottom T_b of the particle is then

$$\Delta T = T_t - T_b = \frac{2R}{k_p} q_z \ . \qquad (6\text{-}2)$$

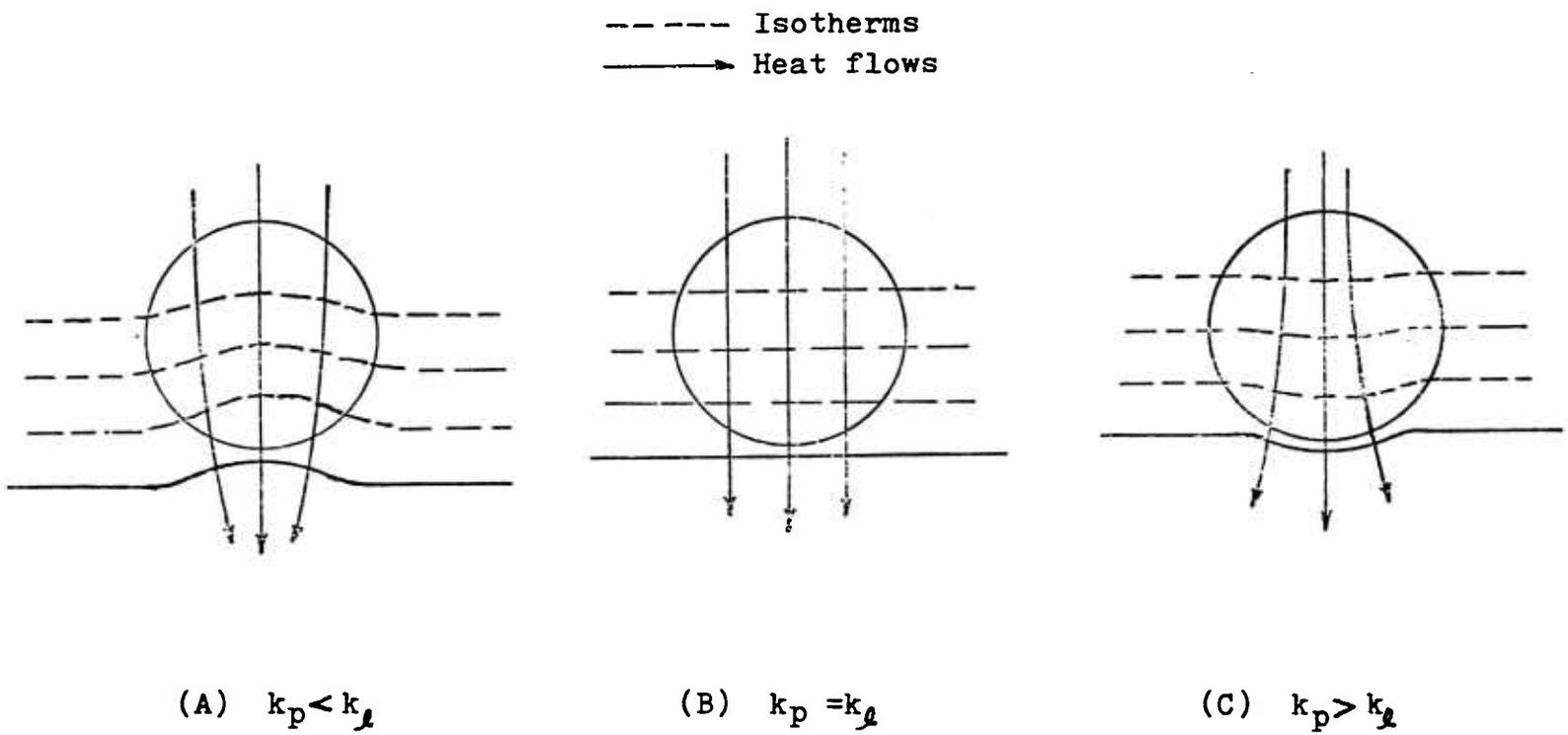

Figure 36 Effect of particle thermal conductivity on the shape of the equilibrium interface (assuming no gravity effect).

The above equation can also be used to explain the interface shapes behind the particles as shown in Figure 36. At a constant steady-state heat flux, ΔT is decreased as k_p increases. For the case $k_p > k_\ell$, T_b is higher than the temperature in the liquid at the same level and thus the interface melts back (Figure 36C). The reverse is true for the case of $k_p < k_\ell$ and the interface rises up (Figure 36A). When the imposed temperature gradient in the melt is increased, i.e., q_z is increased, ΔT increases. This means T_t increases while T_b remains approximately constant. In order for q_z to increase, either T_b must increase slightly, the interfacial temperature must decrease, or the thickness of the film must decrease. As a result, the well behind the particle becomes deeper for the case of $k_p > k_\ell$, and the bump becomes smaller for the case of $k_p < k_\ell$. The former is not favorable for particle pushing, while the latter may not affect V_c. This interpretation is based only on the above equation, and real situations may not be so simple. However, published data [9] indicated that V_c for pushing of copper particles by the ice-water interface ($k_p > k_\ell$) was decreased from 1.0 to 0.47 μm/sec. for 65 μm particles, from 1.2 to 0.6 μm/sec. for 40 μm particles, and from 2.4 to 1.7 μm/sec. for 10 μm particles when the temperature gradient in the water was increased from 1 to 10°C/cm. As shown in Table 6, V_c was not dependent on the temperature gradient for carbon particles pushed by freezing naphthalene ($k_p < k_\ell$).

Since the heat carried away into the growing crystal equals that conducted from the melt plus the latent heat liberated at the

freezing interface in a vertical Bridgman growth, the heat balance at the interface may be expressed by

$$-k_s \left(\frac{dT}{dz}\right)_{s,i} = -k_\ell \left(\frac{dT}{dz}\right)_{\ell,i} + V\rho_s \Delta H_f \qquad (6\text{-}3)$$

where the subscript s denotes solid, ℓ melt, and i at the solid-liquid interface. Both interfacial temperature gradients change with the rate of solidification. As the growth rate increases, heat generated by $V\rho_s \Delta H_f$ gradually dominates the conduction into the solid. Thus $(dT/dz)_{s,i}$ increases while $(dT/dz)_{\ell,i}$ decreases. Our experimental observations indicated that the position of the freezing interface moved downward in order to dissipate the increasing latent heat more easily into the coolant. Because the interface moved away from the heater, $(dT/dz)_{\ell,i}$ decreased in addition. We define "rapid solidification" as the situation when $(dT/dz)_{\ell,i}$ approaches zero or heat conduction from the melt becomes negligible in Eq. (6-3). Under this condition the interfacial gradient in the growing crystal can be directly calculated by

$$\left(\frac{dT}{dz}\right)_{s,i} \approx -V\rho_s \Delta H_f / k_s \ . \qquad (6\text{-}4)$$

Tien's temperature distributions measured during the normal freezing of naphthalene [57] were re-evaluated in light of the above. As shown in Table 13, the measured $(dT/dz)_{\ell,i}$ approached zero at the fast growth rate (66 mm/hour) and the measured $(dT/dz)_{s,i}$ agrees with the value calculated by Eq. (6-4) for two sizes of growth tubes. Thus, for rapid solidification $(dT/dz)_{s,i}$ may be directly estimated

TABLE 13

INTERFACIAL TEMPERATURE GRADIENTS FOR RAPID SOLIDIFICATION[1]

Growth Tube mm, I.D.	Growth Rate mm/hour	Temperature Gradient, °C/cm		
		Measured[2]		Calculated by Eq. (6-4)
		$(dT/dz)_{\ell,i}$	$(dT/dz)_{s,i}$	$(dT/dz)_{s,i}$
37	66	0	107	106.2
19	66	6.3	110	106.2

(1) Bridgman growth of naphthalene, 86°C hot bath and 0°C cooling bath for both cases (Tien [57]).

(2) Graphically measured from Tien's distributions by present author.

from the latent heat and does not depend on the crystal dimensions (this is not true in slow solidification; see Appendix A).

If the critical trapping velocity falls within the criterion of rapid solidification, V_c may not depend upon $(dT/dz)_{\ell,i}$ because the latter is actually always small. The latent heat of fusion is very high for naphthalene (35 cal/g) and water (80 cal/g) and thus one more readily reaches the condition of rapid solidification than with other transparent matrix materials. Our results on the carbon-naphthalene system and some of Cisse and Bolling's results on copper-water system indicated that V_c was not significantly affected by $(dT/dz)_{\ell,i}$.

3. Horizontal Rotation

The particle pushing or trapping process in horizontal zone-refining with rotation is different from that in the vertical Bridgman growth method. The former pushes particles by a vertical freezing interface, the latter pushes particles by an upward horizontal interface. (The interface is actually stationary. The motion referred to is that of the interface relative to the ingot.) Particle motion in the rotating zone eliminates two important factors. It prevents particles from continuous contact with the advancing interface, and also eliminates gravitational effects. Both of these are encountered in the vertical Bridgman technique and reduce V_c. This is particularly true for copper particles which possess a very high density (~ 9 g/cm^3). Therefore, V_c was increased at least 300% for copper in naphthalene

when the horizontal rotation method was employed.

Fluid motion in the rotating zone was not a simple solid-body rotation; it was complicated by the presence of radial and axial temperature gradients, air bubbles accumulating on the top, and solid particles moving in the melt under the influence of gravitational and centrifugal forces. In addition to local stirring effects, microscope observation revealed that two large-scale convective currents circulated from the bottom to the top in opposite directions and they met around the center of the melting zone. The flow patterns are sketched in Figure 37. These convective currents were not stable and fluctuated periodically.

The strength and duration of these currents seemed to depend on the temperature gradients and the size of the molten zone. In addition to the convective currents, two fluid streams moved toward the freezing interface. The first one was a crystallization flow [29], equal to $V(\rho_s/\rho_\ell)$. The second one was an axial flow (or secondary flow) resulting from the existence of density gradients and centrifugal forces [58]. Owing to friction, the melt next to the solid-liquid interface was carried by it and then forced to the tube wall by the centrifugal acceleration. Thus the mass of fluid which was driven outward by centrifugal forces was replaced by an axial flow, which was proportional to $\sqrt{\Omega\eta/\rho_\ell}$, where Ω is the angular velocity. These three fluid streams would have interacted with particles in contact with the interface when the growth rate approached V_c.

As soon as the particles were in contact with the interface,

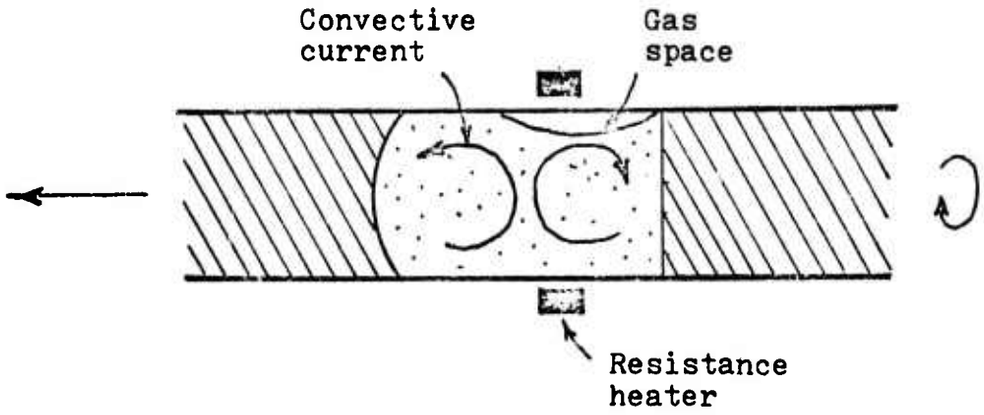

Figure 37 Flow patterns in a horizontal rotating zone (side view).

some of the particles would remain there through friction and adhesion. The centrifugal force acting on the particles was balanced by the shearing stress and viscous drag. After the particles attached to the rotating interface, the pushing and trapping mechanisms would then be similar to those in the vertical Bridgman method. In other words, transport is the limiting process. Without considering the convective currents, the radial velocity u in the boundary layer next to the interface is proportional to $r\Omega$ and the thickness of the boundary layer δ is proportional to $\sqrt{\eta/\Omega\rho_\ell}$. When the rotation speed is increased, u increases while δ decreases. This, in turn, serves to improve the mass transport in the contact area between the particle and the interface. Further, this mass transport is expected to be enhanced when the convective currents are considered which become stronger in a larger diameter tube. This explains why V_c was increased at higher rotation speeds (copper and iron oxide particles) and in a larger diameter tube (23 mm O.D.).

B. Calculations of V_c

In order to compare with the experimental results, calculation of V_c is made here by employing the simple Eq. (2-37) without considering effects of gravity and particle roughness. Some of the constants such as σ, η, a_o and $\phi(\alpha)$ needed for the calculation are not readily available from the literature. These constants are thus estimated first.

The direct measurement of the specific free energy $\sigma_{s\ell}$ of the solid-liquid interface was recently made for the transparent materials camphene, succinonitrile, water and white phosphorous by Jones and Chadwick [59]. Their experimental figures were in good agreement with the values predicted from Turnbull's theoretical equation, [60,61]

$$\sigma_{s\ell} = \left(\frac{3}{8} \text{ to } \frac{1}{2}\right) \Delta H_f / N^{1/3} V_m^{2/3} \qquad (6\text{-}5)$$

where ΔH_f is the heat of fusion, N is Avagadro's number, and V_m is the molecular volume. Because the calculated $\sigma_{s\ell}$ using the lower bound of the constant 3/8 in the equation gave better results for the above transparent materials, this constant is used to estimate $\sigma_{s\ell}$ of naphthalene, salol, camphor and benzophenone. The calculated results are shown in Table 14, along with Jones and Chadwick's data.

The physical properties of the supercooled thin film between the particle and interface are not known. (Data for properties of supercooled bulk liquid are even meager.) The viscosities of the supercooled melts for salol [62] and benzophenone [63,64] are shown in Figure 38. When the melts are above the melting temperature, the plots of $\ell n\ \eta$ versus 1/T give straight lines following the Arrhenius relation. But these lines become curved when the melts are supercooled. The viscosity of the supercooled melt is significantly higher than the melt at the melting point. Since the supercoolings of freezing organics for the present work were not measured, the viscosities at their melting points are used for the calculations of V_c. Experimental observations indicated that the supercoolings of

TABLE 14

ESTIMATION OF V_c FOR PARTICLES (1 and 10 μm)

Matrix Materials	ΔH_f, cal/mole	V_m, cm^3/mole	$\sigma_{s\ell}$, erg/cm^2		V_c, mm/hour	
			Theoretical	Experimental	10 μm	1 μm
Naphthalene	4500(1)	130	32.5		24.6	767
Salol	4650(2)	172	28		2.5	82
Camphor	1125(3)	154	7.3		2.7	85
Banzophenone	3860(1)	164	23.8		3.6	114
Camphene(4)			5	5.3		
Succinonitrile(4)			26	28		
Water(4)			38	41		
White Phosphorous(4)			7	10.3		

(1) Obtained from Reference 46.
(2) Obtained from Reference 25.
(3) Estimated by present author.
(4) Data from Reference 59.

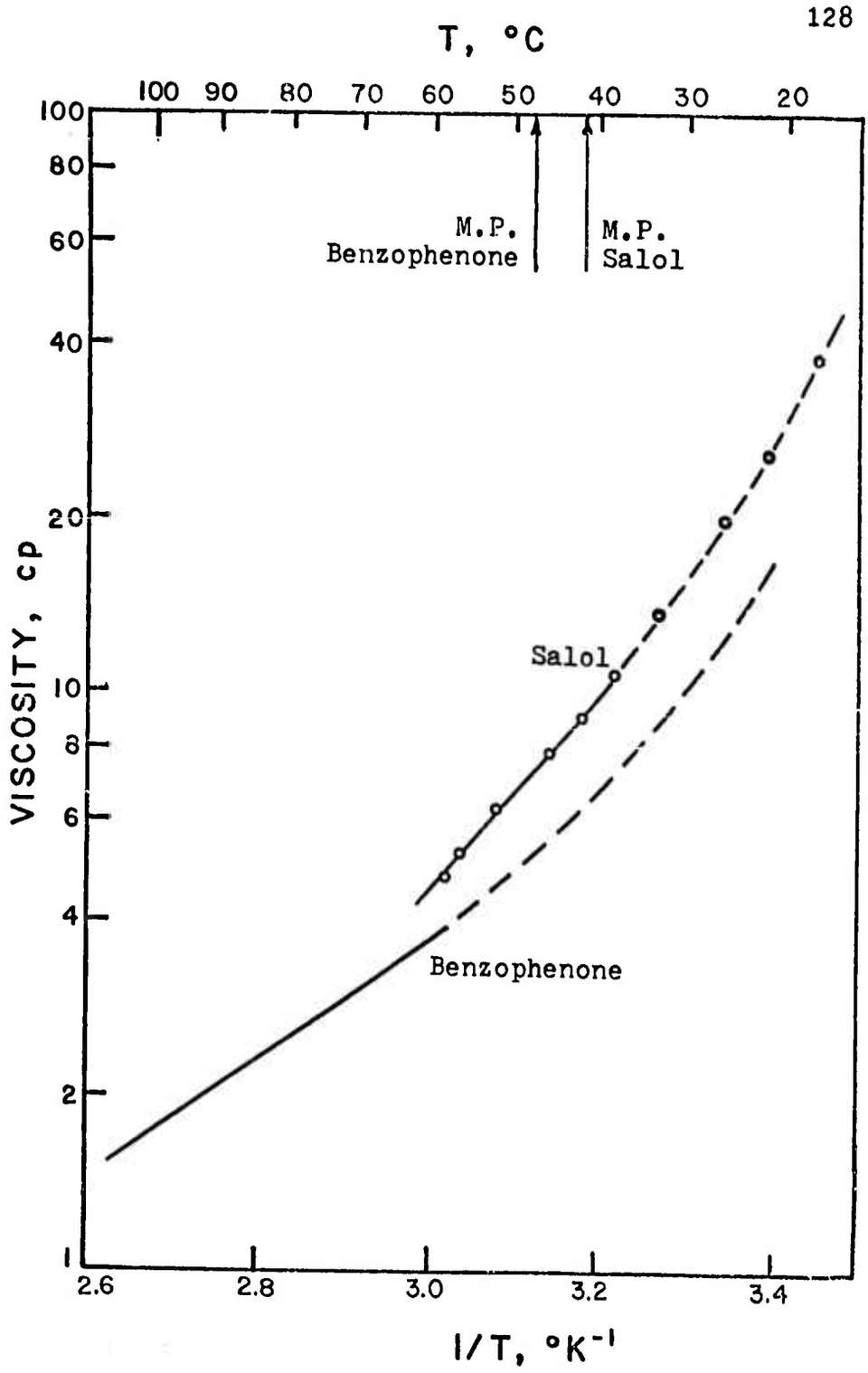

Figure 38 Viscosities of supercooled organic melts.

naphthalene and camphor were very small, but the supercoolings of salol and benzophenone seemed to be quite large.

The molecular volume V_m was obtained by dividing the molecular weight by the density of the liquid at the melting point. The molecular diameter a_o was then estimated from the molecular volume.

A plot of $\phi(\alpha)$ against α with β as a parameter is illustrated in Figure 39. For a given value of β, $\phi(\alpha)$ reaches a maximum value at $\alpha < 1/3$ (see Eq. (2-39)). By combining Eq. (2-26) with $\phi(\alpha)$, the separation distance d between the particle and interface can be calculated by the following equation.

$$d/a_o = \frac{\phi(\alpha)}{\alpha(1-\alpha)^2} \tag{6-6}$$

The calculated values of d/a_o are tabulated in Table 15. The variation of d/a_o is less than a factor of two when the α is increased from 0.05 to 0.3. Since α represents the curvature of the freezing interface which is generated due to the interaction between the particle and interface, it may approach a value of $0.2 \sim 0.3$ at the onset of particle trapping. In this practical range of α, the values of d/a_o are almost constant for a thin film existing between the particle and advancing interface. For the present calculations of V_c, $\beta = 1$ and $\phi(\alpha)$ max = 0.335 will be used.

Thus far the constants needed for prediction of V_c have been estimated. Calculated results of V_c are also presented in Table 14 for particles of 1 and 10 m diameter. Since the experimental results of V_c (Table 7) were determined for the smallest trapping velocities,

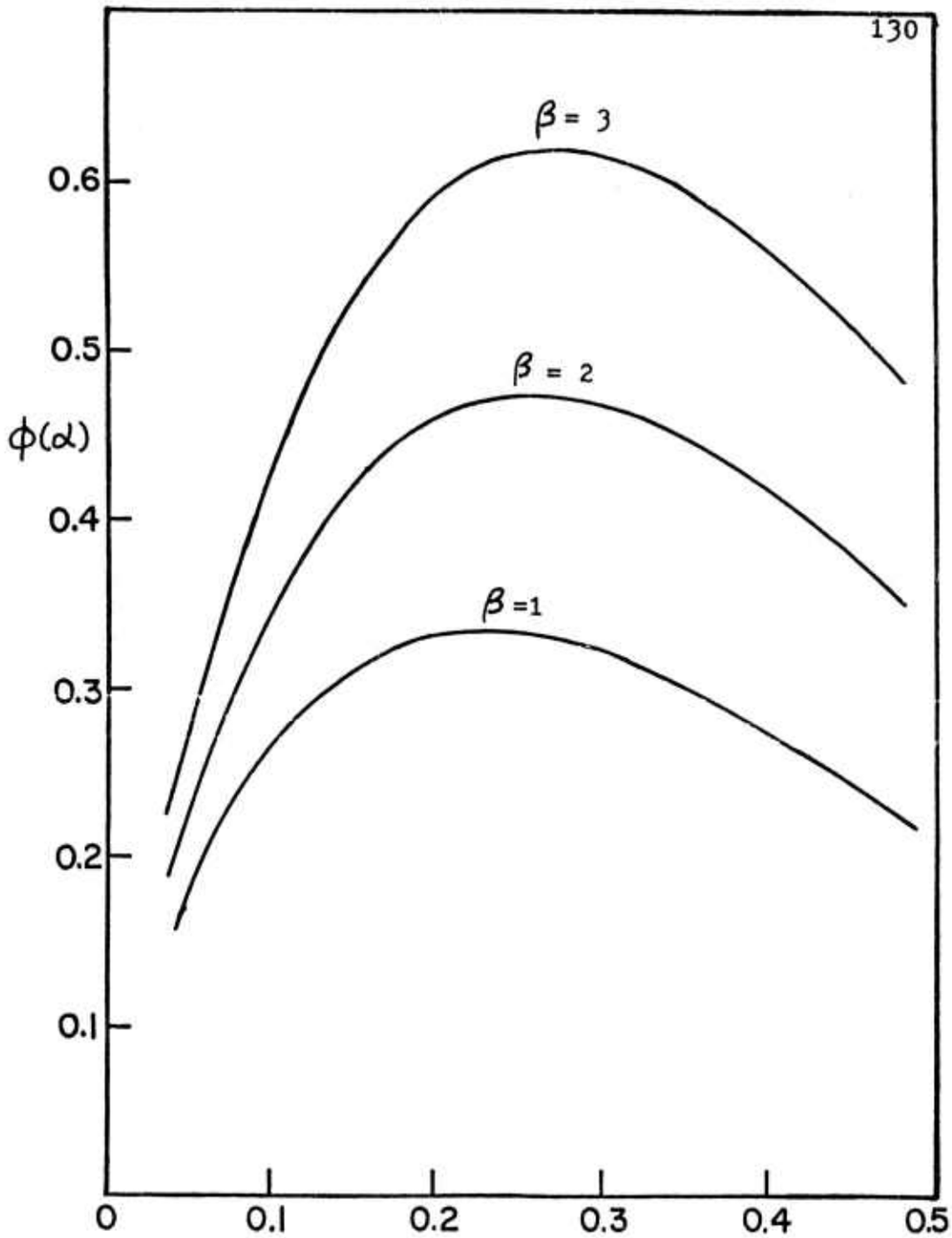

Figure 39 Plot of $\phi(\alpha)$ vs α with β as a parameter from $\phi(\alpha) = \alpha(1-\alpha)^2(\beta - \ln \alpha)$.

TABLE 15

VARIATION OF d/a_o WITH α AND β

	d/a_o		
α	$\beta = 1$	$\beta = 2$	$\beta = 3$
0.05	4.0	5.0	6.0
0.10	3.3	4.3	5.3
0.20	2.6	3.6	4.6
0.30	2.2	3.2	4.2

(or V_c for larger particles), they are, in fact, in good agreement with the calculated values.

C. Formation of Air Bubbles

The freezing interface can reject dissolved gas, exactly in the same way as any other solute for which the segregation coefficient k_o is less than unity. As the gas concentration increases at the interface, the melt may become sufficiently supersaturated to nucleate bubbles. The bubbles formed at the interface grow by diffusion of dissolved gas from adjacent supersaturated areas of the melt. The bubble nucleation may be either homogeneous or heterogeneous. Thorough treatment of nucleation theory for vapor to liquid, liquid to solid, and solid to solid transformation have existed in the literature for some time. Only recently has such a theory been presented for the liquid to vapor transformation [65-68]. The purpose of this section is to modify this theory and to make it applicable to nucleation of bubbles from the melt containing dissolved gases during controlled solidification.

The homogeneous nucleation rate of bubbles developed by Hirth and Pound [65] was estimated by multiplying the concentration of critical-sized bubbles n^* by the frequency of adding molecules ω. The equilibrium concentration was corrected by a non-equilibrium or Zeldovich factor Z because the process actually occurs at steady state rather than equilibrium. The nucleation rate equation is of the form

$$J = Z\omega n^* \ cm^{-3} sec^{-1} \quad . \tag{6-7}$$

The value of n^* is estimated from the metastable equilibrium between two phases of differing Gibbs free energy

$$n^* = n_o \exp(-\Delta G^*/kT) \tag{6-8}$$

where n_o is the total concentration of molecules in the liquid phase and ΔG^* is the free energy change for formation of a critical bubble.

The Gibbs free energy of formation of a spherical bubble in a supersaturated melt under a prevailing hydrostatic pressure P_h (the schematical diagram of bubble formation is shown in Figure 40) is

$$\Delta G^o = 4\pi r^3 \Delta G_v/3 + 4\pi r^2\sigma + 4\pi r^3 P_h/3 \tag{6-9}$$

in which ΔG_v is the volume free energy change and σ is the surface energy. Since ΔG_v is always negative for a supersaturated melt, Eq. (6-9) exhibits a maximum for a critical-sized bubble r^* where $(\partial \Delta G^o/\partial r) = 0$ and $\Delta G^o = \Delta G^*$. The relation between ΔG^* and r^* is obtained as

$$\Delta G^* = 4\pi\sigma(r^*)^2/3 \tag{6-10}$$

where $r^* = -2\sigma/(\Delta G_v + P_h)$.

The condition for mechanical equilibrium of a bubble applied to a critical-sized bubble may be expressed as

$$P^* = P_h + \frac{2\sigma}{r^*} \tag{6-11}$$

in which P^* is the total pressure in the critical bubble. An alternative form of ΔG^* is obtained through elimination of r^*, by Eq. (6-11)

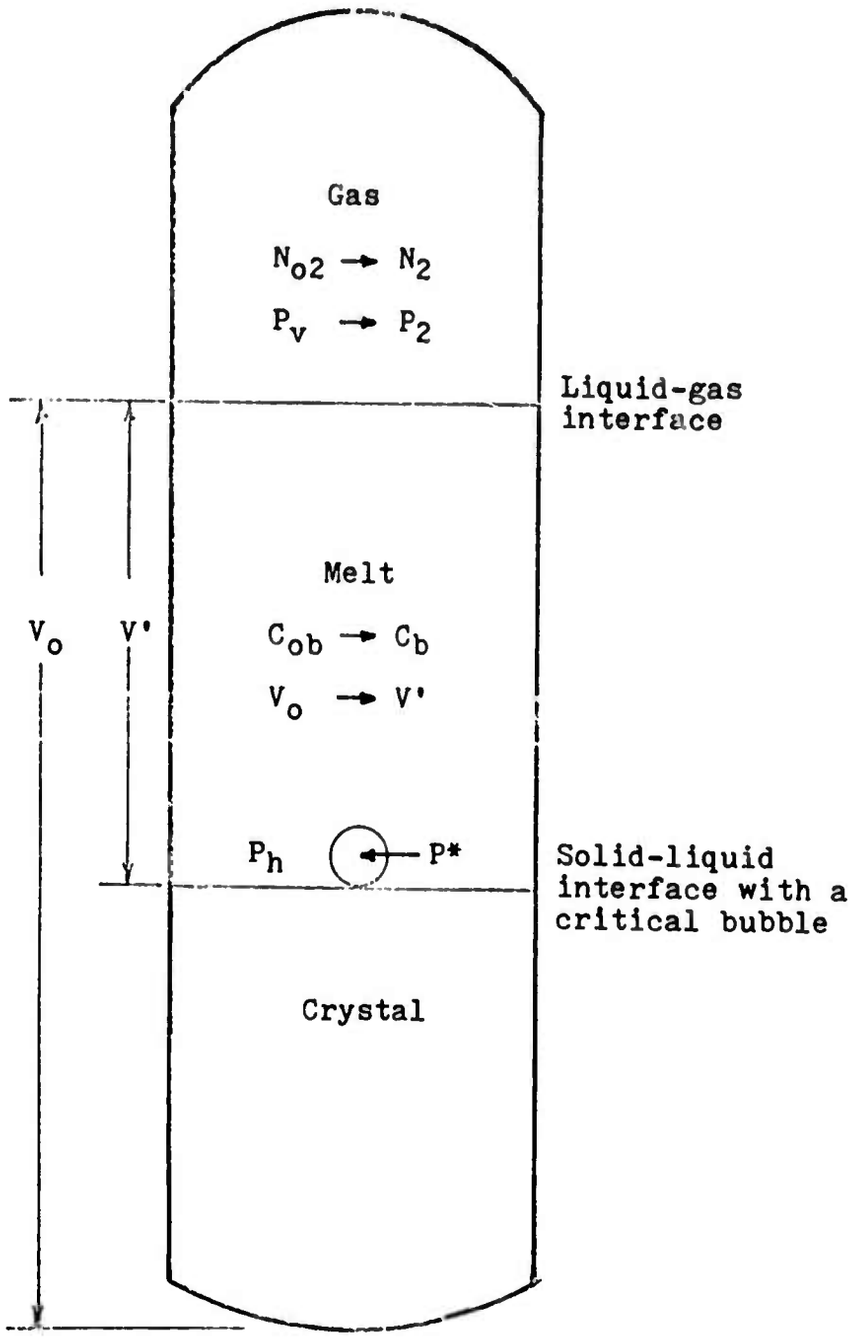

Figure 40 Schematic diagram of bubble formation at a freezing interface.

$$\Delta G^* = 16\pi\sigma^3/3\ (P^* - P_h)^2 \quad . \tag{6-12}$$

P^* represents the total pressure in a critical bubble. It is the vapor pressure if the liquid is a single component. It is the pressure of dissolved gas if the vapor pressure of the melt is negligible. It is the sum of partial pressure of dissolved gas p_2^* and partial pressure of the melt p_1^* when both the melt and dissolved air have considerable partial pressures, such as in the present experiments on naphthalene. The last situation is treated here. Assuming ideal gas behavior,

$$P^* = p_1^* + p_2^* \quad . \tag{6-13}$$

The usual Kelvin equation [23] deals only with a pure liquid and a nucleus of its vapor. The vapor pressure p_1^* of the solvent inside the critical bubble was related to the properties of a dilute solution surrounding the bubble by Ward, et al. [67]. The relation is derived here for dilute ideal solution. The chemical potentials for the solvent in the solution and vapor phases are given as [69],

$$\mu_1' = \mu_o'(P_h,T) - kTx_2' \tag{6-14}$$

and

$$\mu_1'' = \mu_o''(P^*,T) + kT\ \ell n\ x_1'' \tag{6-15}$$

where the subscripts 1 and 2 refer to the solvent and solute respectively. The single prime indicates the liquid phase and the double prime indicates the vapor phase. μ_o is the chemical potential of

the pure component and x is the concentration in mole fraction.

The chemical potential of the pure component μ_o is a function of pressure and temperature. At constant temperature, the Gibbs-Duhem equation reduces to

$$n d\mu_o = V dP \quad . \tag{6-16}$$

If the pure solvent is assumed to be incompressible, the above equation is integrated as

$$\mu_o'(P_h,T) = \mu_o'(P_\infty,T) + v_\ell(P_h-P_\infty) \quad . \tag{6-17}$$

Equation (6-16) is also integrated in the vapor phase and becomes

$$\mu_o''(P^*,T) = \mu_o''(P_\infty,T) + kT \ln \frac{P^*}{P_\infty} \tag{6-18}$$

where P_∞ is the vapor pressure of the pure solvent across a flat surface. Substituting Eqs. (6-17) and (6-18) into Eq. (6-14) and (6-15), respectively, the chemical potentials are

$$\mu_1' = \mu_o'(P_\infty,T) + v_\ell(P_h-P_\infty) - kT\, x_2' \tag{6-19}$$

and

$$\mu_1'' = \mu_o''(P_\infty,T) + kT \ln \frac{P^*}{P_\infty} + kT \ln x_1'' \quad . \tag{6-20}$$

Since $\mu_o'(P_\infty,T) = \mu_o''(P_\infty,T)$, the condition for equilibrium across the curved interface ($\mu_1' = \mu_1''$), using Eqs. (6-19) and (6-20), is

$$kT \ln \frac{P^* x_1''}{P_\infty} = v_\ell(P_h-P_\infty) - kT\, x_2'$$

or

$$p_1^* = P_\infty \exp\left[\frac{v_\ell}{kT}(P_h - P_\infty) - x_2'\right] \quad . \tag{6-21}$$

The nucleation of bubbles occurs at the freezing interface where the concentration of dissolved gases has the highest value C_i (or x_2' in mole fraction). The partial pressure of gas p_2^* in the critical bubble can be evaluated from C_i (or x_2') by the Henry's law $p_2^* = C_i H_i$ where H is an empirical constant.

Because the segregation of a dissolved gas by the freezing interface is analogous to the segregation of a solute, the segregation coefficient k_o is defined here as the ratio of the gas concentration in the solid to that in the liquid at equilibrium. Using a constant value of k_o in the quasi-steady-state stagnant film approach [70], the gas concentration at the interface during fractional solidification is found to be

$$\frac{C_i}{C_b} = \frac{1}{k_o + (1-k_o)\exp\left(-\frac{\delta V}{D}\frac{\rho_s}{\rho_\ell}\right)} \tag{6-22}$$

where C_b is the gas concentration in the bulk melt, and δ is the thickness of the boundary layer. The vapor pressure of dissolved gas at the interface is then

$$p_2^* = \frac{H_i C_b}{k_o + (1-k_o)\exp\left(-\frac{\delta V}{D}\frac{\rho_s}{\rho_\ell}\right)} \quad . \tag{6-23}$$

The importance of the gas concentration in the bulk melt C_b is

obvious, since it directly affects the gas concentration at the freezing interface. The value of C_b depends on the solidification conditions. If the growth tube containing a solidified organic is evacuated and sealed as described in Chapter III, the maximum number of air molecules remaining in the vacuum space is $N_{o2} = P_v V''/kT$ where P_v is the pressure and V" is the volume in the vacuum space. As soon as the organic is melted before beginning solidification, the amount of air in the vacuum space increases to $N_2 = p_2 V''/kT$ where p_2 is the partial pressure of air. The difference $N_2 - N_{o2}$ results from transport of dissolved air from the melt to the gas space. Assume C_{ob} is the gas concentration in the solid (its volume V_o) before melting, and C_b is the concentration of the bulk melt with a volume V', the material balance on the gases is

$$\frac{p_2 V''}{kT} - \frac{P_v V''}{kT} = C_{ob} V_o - C_b V' \quad . \tag{6-24}$$

Substituting $p_2 = H_b C_b$ into the above equation, the gas concentration in the bulk melt is expressed as

$$C_b = \frac{P_v V'' + C_{ob} V_o \, kT}{V' kT + H_b V''} \quad . \tag{6-25}$$

Using Eqs. (6-13), (6-21) and (6-23), the activation free energy for nucleation of a bubble is

$$\Delta G^* = \frac{16\pi\sigma^3}{3\left[\dfrac{H_i C_b}{k_o + (1-k_o)\exp\left(-\dfrac{\delta V}{D}\dfrac{\rho_s}{\rho_\ell}\right)} + P_\infty \exp\left(\dfrac{v_\ell}{kT}(P_h - P_\infty) - x_2'\right) - P_h\right]} \quad . \tag{6-26}$$

The growth process of a bubble consists of a molecule (dissolved gas or solvent) in the surface of the bubble evaporating into the critical bubble. The frequency of occurrence is equal to the frequency of condensation of a molecule from the bubble,

$$\omega = \frac{4\pi r^{*2}\nu}{s} \exp\left(\frac{-\Delta G^{*}_{vap}}{kT}\right) = \frac{\alpha P^{*}(4\pi r^{*2})}{(2\pi m kT)^{1/2}} \quad . \tag{6-27}$$

And the Zeldovich correction factor is

$$Z = \left(\frac{3\Delta G^{*} v_g}{16\pi^3 kT r^{*6}}\right)^{1/2} = \left(\frac{\sigma v_g}{4\pi^2 r^{*4} kT}\right)^{1/2} \tag{6-28}$$

where s is the surface area of a molecule at the interface, ν is the Debye maximum frequency of vibration of a liquid molecule, ΔG^{*}_{vap} is the activational free energy for evaporation, α is the condensation coefficient, and m is the molecular mass.

The factor ($Z\omega$) has been estimated for pure liquids [71]. Hirth, et al. [66] suggested that growth step of dissolved gas was the favored process due to ΔG^{*}_{vap} for desorption of gas being less than that for evaporation of the melt. We assume here that the growth frequency is the same for the solute and solvent, and the value of m can be estimated by the relation $1/\sqrt{m} = 1/\sqrt{m_g} + 1/\sqrt{m_\ell}$ where m_g is the gas molecular mass and m_ℓ is the solvent molecular mass.

An explicit expression for the nucleation of gas bubbles is obtained by substituting the Eqs. (6-26), (6-27) and (6-28) into Eq. (6-7),

$$J = n_o \alpha \left(\frac{2\sigma v_g}{\pi m}\right)^{1/2} \left(\frac{P^*}{kT}\right) \exp\left(-\frac{\Delta G^*}{kT}\right)$$

$$= \left(\frac{n_o \alpha}{kT}\right)\left(\frac{2\sigma v_g}{\pi m}\right)^{1/2} \left[\frac{H_i C_b}{k_o + (1-k_o)\exp\left(-\frac{\delta V}{D}\frac{\rho_s}{\rho_\ell}\right)} + P_\infty \exp\left(\frac{V_\ell}{kT}(P_h - P_\infty) - x_2'\right)\right]$$

$$\times \exp\left[\frac{-16\pi\sigma^3/3kT}{\frac{H_i C_b}{k_o + (1-k_o)\exp\left(-\frac{\delta V}{D}\frac{\rho_s}{\rho_\ell}\right)} + P_\infty \exp\left(\frac{V_\ell}{kT}(P_h - P_\infty) - x_2'\right) - P_h}\right] . \quad (6\text{-}29)$$

All parameters in the above equation are, in principle, known or experimentally measurable for a given system. The surface tension σ used in the above derivation may not be a constant but will be affected by solute adsorption at the interface. Hirth and Pound [65] pointed out in their ebullition (or boiling) studies that the size of critical bubble (of the order of a micron in diameter and containing millions of molecules) was sufficiently large that macroscopic thermodynamic quantities might be employed with some degree of confidence.

The above nucleation equation combining with Eq. (6-25) indicates that increase of C_b (decreasing V' or increasing P_v), or $\delta V/D$ is favorable for the formation of bubbles. Our experimental results qualitatively agree with the above theoretical development. In other words, evacuation of the growth tube (decreasing P_v), stirring or rotating the melt (reducing δ) and slow growth rate V hindered bubble occurrence, while bubbles formed at the end of the

Bridgman runs due to increase of C_b by decreasing V'.

Gas bubbles were also found in single crystal growth of paratellurite TeO_2 [72] by the pulling method. Formation of bubbles was prevented by the slow pulling rate (about 1.5 mm/hour) combined with high rate of the crystal rotation (40-50 RPM). This is in agreement with our theoretical predictions. The interpretations made in the referenced paper are unsound.

Recently Swanger and Rhines [73] made theoretical calculations for homogeneous nucleation of gas bubbles in the blood and found that homogeneous nucleation is impossible because the initial pressure of the gas must exceed 1900 ATM. Maeno's experimental observations [56] indicated that air bubbles did not form on a smooth ice-water interface unless the interface was scratched with a glass rod. Further, air bubbles could develop between the particles and the ice-water interface, depending on the types and surface conditions of particles. Thus, formation of air bubbles was practically the result of heterogeneous nucleation. Our results revealed that carbon particles could act as nucleation sites for air bubble formation, but copper particles had no nucleating ability for bubbles.

CHAPTER VII

CONCLUSIONS

At least three objectives have been accomplished from the research described in this dissertation. (1) Discovery of some important and interesting phenomena leading to improved understanding of the fundamental nature of particle pushing and trapping at a freezing interface. (2) The development of a new separation process enabling economical removal of foreign particles from organic chemicals. (3) The invention of a new method to separate mixtures of different particles by solidification, opening up a potentially new field -- particle chromatography.

The experimental results of the vertical Bridgman crystal growth indicate that interface shape, growth container, growth orientation, and the presence of bubbles all significantly influence the critical velocity for trapping. These variables, plus previously established parameters such as particle size and shape, particle roughness, grain boundaries, density and thermal conductivities, make the process of particles pushing and trapping extremely complicated. For example, particles were always trapped over a finite length of freezing crystal, i.e., over a range of velocities (21 to 35 mm/hour). Among the four organic compounds used, only naphthalene can push particles readily due to its low viscosity. The effects of particle properties on V_c appeared to be insignificent, although thermal conductivity, density and roughness are possible factors for the same

size particles. The measured values of V_c agreed with those calculated by Eq. (2-37). The V_c for the carbon-naphthalene system was reduced from 21 to 18 mm/hour by trapping between the glass wall and a convex interface. The formation of gas bubbles at the freezing interface was hindered by evacuating the growth container, stirring of the melt, and use of a slow growth rate. These observations are in good agreement with the theoretical treatment of bubble nucleation (Eq. (6-29)) developed here. Carbon particles provided nucleation sites for bubbles, but copper particles did not. The interfacial temperature gradient in the melt had no observable effect on V_c. A simple theory based on Eq. (6-2) predicts that increase of temperature gradient might reduce V_c if $k_p > k_\ell$, and would have no effect on particle pushing if $k_p < k_\ell$. For rapid solidification the gradient in the solid can be simply estimated from Eq. (6-4) with small and negligible heat conduction in the melt next to the interface, regardless of the crystal dimension.

Horizontal zone-refining with rotation enhanced mass transfer and eliminated the detrimental effects resulting from bubbles and high particle density, and thus significantly increased V_c over that obtained with the vertical Bridgman technique. The measured V_c was increased 300% for copper (ρ_s = 9 g/cc) and 50% for carbon (ρ_s = 2 g/cc) particles in naphthalene. With this new process it is possible to make clear-cut separation of particles. The cost estimate showed that product cost is only 22 cents per gram for particle-free naphthalene. Particle and fluid motion in the rotating zone was

found to be complex. Three fluid streams flow toward the freezing interface. They are crystallization flow, secondary flow, and convective current. The radial velocity in the boundary layer should have a direct effect on transport of liquid in the contact region between the particle and interface. This velocity is theoretically increased by increasing rotation speed and convective current. The present results indicated that the V_c was increased at higher rotation rates for copper and iron oxide particles and in a larger diameter tube.

Potential applications suggested by this work were also explored. Two applications were found to be feasible. Separation of a mixture of different particles (particle chromatography) and classification of particles were experimentally tested.

It is hoped that the results of these studies will contribute to better understanding of particle pushing and trapping by growing crystals, that the new separation process will be realized commercially and that the potential applications will be widely accepted. The suggested future work is briefly outlined in the next chapter.

CHAPTER VIII

SUGGESTED FUTURE WORK

Based on the results of this dissertation, further work on particle pushing and trapping might be continued along the following lines.

A. Czochralski Crystal Growth

In addition to the Bridgman crystal growth and zone melting, the Czochralski technique is widely used for the growth of single crystals. A seed is attached at the end of a rotating rod. The crystal grown on the seed is pulled vertically from the melt. Since the seed controls the orientation of growing crystal, the study of the effect of growth orientation on V_c is possible. This technique does not need a growth container which limits the rotation speed in horizontal zone-refining due to particles being trapped next to the tube wall at high rotation rates. Further, sectioning of solidified products without containers is easier for the purpose of microscopic investigation.

Like horizontal zone-refining with rotation, the Czochralski method also eliminated settling effects which produce continuous contact of particles with the interface during the process of particle pushing. However, the former pushes particles by a vertical interface; the latter will use a horizontal interface to reject particles. The rotation speed is an important factor in Czochralski crystal growth,

and can significantly affect the shape of growing interface and flow patterns in the melt [3,72,74,75]. At slow rates of rotation, natural convection currents dominate in the melt and the interface is normally convex. The interface becomes more concave at higher rotation rates owing to an axial flow (secondary flow) resulting from centrifugal acceleration. It would be interesting to study how rotation influences V_c in this geometry. A mixture of carbon particles and salol appears good materials to start investigating particle separation by this potential process.

B. Particle Chromatography

As described in Chapter V, horizontal zone-refining with rotation has proved to be a promising technique for separation of mixed particles. For instance, carbon particles were readily separated from a mixture of carbon and copper particles. This new technique should be explored further for a mixture containing several different kinds of particles, especially for metal or semiconductor materials. Since quantitative analyses of these materials have been well established, determination of separation efficiency is possible by analyzing each trapped band. The separation efficiency is expected to depend on the freezing rate, the speed of rotation and the matrix material selected.

C. Crystal Growth from Solution

This dissertation so far has been concentrated on particle

separation for crystal growth from the melt. However, crystallization from solution is a very common and important separation technique in the inorganic chemical process industries. As mentioned in the chapter on "Literature Studies", the evidence has shown that certain crystals growing from solution have a tendency to reject foreign particles. No information is available at the present time on what kinds of crystals tend to reject foreign particles more than the other kinds of crystals. It has been known that some inorganic salts can crystallize in different forms and habits under varied crystallization conditions. Sodium sulfate crystallizes $Na_2SO_4 \cdot 10H_2O$ from the aqueous solution by cooling it below 32°C, while anhydrous Na_2SO_4 is formed above 32°C by evaporation of water. If the solution is mixed with carbon particles, the results will indicate whether $Na_2SO_4 \cdot 10H_2O$ or anhydrous Na_2SO_4 rejects more particles. A similar experiment can be made for Na_2CO_3 solution. Sodium carbonate can crystallize in several different forms as $Na_2CO_3 \cdot 10H_2O$, $Na_2CO_3 \cdot 7H_2O$, $Na_2CO_3 \cdot H_2O$, and anhydrous Na_2CO_3. The form incorporating the least amount of particles should be crystallized during purification.

Further study may be carried out with a complex solution, such as the Great Salt Lake brine. Several companies are interested in recovery of saline minerals as well as magnesium from the brine of the Great Salt Lake by the solar evaporation processes [76]. Fractional crystallization by solar evaporation is under dynamic conditions. Certain salts are very difficult to crystallize, although they should be formed according to the phase equilibrium. Minerals such as NaCℓ,

epsomite ($MgSO_4 \cdot 7H_2O$), schoenite ($K_2SO_4 \cdot MgSO_4 \cdot 6H_2O$), kainite ($KC\ell \cdot MgSO_4 \cdot 3H_2O$) and carnallite ($KC\ell \cdot MgC\ell_2 \cdot 6H_2O$) may be consecutively crystallized in the individual solar ponds. However, if a considerable amount of SO_4^{--} is removed from brine at the beginning of solar evaporation, a different crystallization path is followed. Salts of $NaC\ell$, $MgSO_4 \cdot 7H_2O$, $KC\ell$ and carnallite are dropped out in the solar ponds. These solar salts are harvested and are further processed in the manufacturing plants to produce $KC\ell$ (potash), K_2SO_4, Na_2SO_4, Mg, etc. However, a considerable amount of the insoluble materials (such as sands, clays, muds, etc.) trapped in the salts have to be removed by several processing steps including thickening, flotation, centrifugation, and filtration. These separation steps increase the capital and operating costs, and thus influence the overall process economics and profitability. If one knows some crystals (likely kainite) trap more foreign particles than others, these crystals should be avoided in process development. An experimental study is needed to identify these crystals.

NOMENCLATURE

A	Area, cm^2
a	Molecular diameter, cm
a_o	Interatomic distance, cm
B	Weight of load, dyne
b	Height of a monoatomic layer, cm
C	Concentration, g/cm^3 or cm^{-3}
C_∞	Saturated concentration, g/cm^3 or cm^{-3}
c	A constant in Eq. (2-6)
D	Diffusion coefficient, $cm^2/sec.$
d	Separation distance or thickness of a thin film, cm
$E(r)$	Distance between a concave interface and its lowest point as a function of r, cm
F	Force, dyne
F_c	Viscous drag at a plane sink, dyne
$F(\alpha)$	Viscous drag at a curved sink, dyne
F_D	Force needed for diffusion, dyne
G	Gibbs free energy, erg
H	Biot number (= hR/k)
H	Henry's constant, dyne cm/g
ΔH_f	Latent heat of fusion, cal/g or erg/mole
h	Separation distance between the particle and interface at any value of r, cm
h	Heat transfer coefficient, cal/sec. cm^2 °K
J	Nucleation rate, cm^{-3} sec^{-1}

$\bar{K}$	Total curvature, cm^{-1}
k	Botlzmann constant, erg/molecule °K
k	Thermal conductivity, cal/sec. cm °K
k_o	Equilibrium segregation coefficient
L	Latent heat of fusion, erg/atom
m	Mass of a molecule, g/molecule
m	Slope of liquidus line in a phase diagram, °C cm^3/g
N	Number of molecules (or a number)
N	Avagadro's number, molecules/mole
n	A constant in Eq. (2-5)
n^*	Concentration of critical bubbles, cm^{-3}
n_o	Concentration of molecules in the liquid phase, cm^{-3}
P	Pressure, $dyne/cm^2$
P_h	Hydrostatic pressure at the freezing interface, $dyne/cm^2$
P^*	Total pressure in a critical bubble, $dyne/cm^2$
P_∞	Saturated pressure, $dyne/cm^2$
P_v	Pressure in the evacuated space, $dyne/cm^2$
p	Partial pressure, $dyne/cm^2$
q_z	Heat flux in the z direction, cal/sec. cm^2
R	Radius of a particle or crystal, cm
R	Gas constant, erg/°K mole
r	Distance in a radial direction, cm
r_o	Effective contact radius between a particle and an interface, cm
$\Delta\bar{r}$	Mean displacement, cm

S	Entropy, erg/°K
ΔS	Volume entropy of fusion, erg/°C cm^3
ΔS_f	Molar entropy of fusion, erg/°K mole
s	Surface area of a molecule at the interface, cm^2
T	Temperature, °C or °K
T_b	Temperature at the top of the particle, °C
T_t	Temperature at the bottom of the particle, °C
ΔT_c	Temperature depression due to curvature effect, °C
ΔT_i	Temperature change due to interaction of a particle and interface, °C
ΔT_s	Supercooling for growth of crystal, °C
U	Flow velocity in the contact area, cm/sec.
u	Radial velocity in a boundary layer, cm/sec.
V	Volume, cm^3
V	Crystal growth velocity, cm/sec.
V_c	Critical trapping velocity, cm/sec.
V_m	Molar volume, cm^3/mole
v	volume, cm^3/molecule
W	Work, erg
w	A parameter (= $r^2(1-\alpha)/2R$)
x	Concentration in mole fraction
Z	Non-equilibrium or Zeldovich factor
z	Distance in a z-axis direction, cm

Greek Symbols

α	A parameter for the shape of interface.
α	Condensation coefficient
β	A constant in Eq. (2-25)
δ	Thickness of a boundary layer, cm
η	Viscosity, g/cm sec.
θ	Angle
λ	Mobility, cm/sec.
μ	Chemical potential, erg/molecule
μ_o	Chemical potential for a pure substance, erg/molecule
ν	Debye maximum frequency, sec^{-1}
ρ	Density, g/cm^3
σ	Interfacial free energy, erg/cm^2
$\phi(\alpha)$	A parameter $(= \alpha(1-\alpha)^2(\beta-\ell n\ \alpha))$
ω	Growth frequency, sec^{-1}
ω	Angular velocity, radian/sec.

Subscripts

1	Solvent
2	Solute
b	Bulk liquid
i	Interface
g	Gas phase
ℓ	Liquid phase
o	Original condition

p	External body or particle
s	Solid phase

Superscripts

*	Critical nucleus conditions
'	Liquid phase
"	Vapor or gas phase

REFERENCES

(1) K. A. Jackson, Phil. Mag., 7 (1962) 1615.

(2) H. E. Buckley, "Crystal Growth," Wiley, New York, 1951, p. 468.

(3) M. Zief and W. R. Wilcox, editors, "Fractional Solidification," Dekker, New York, 1967.

(4) Y. Ya Khaimov-Mal'kov in "Growth of Crystals," A. V. Shubnikov and N. N. Sheftal', editors, Consultants Bureau, Inc., New York, Vol. 2, 1959, p. 14.

(5) A. E. Corte, J. Geophysical Research, 67 (1962) 1085.

(6) D. R. Uhlmann, B. Chalmers, and K. A. Jackson, J. Appl. Phys., 35 (1964) 2896.

(7) P. Hoekstra and R. D. Miller, J. Colloid. & Interface Sci., 25 (1967) 166.

(8) G. F. Bolling and J. Cisse, J. Crystal Growth, 10 (1971) 56.

(9) J. Cisse and G. F. Bolling, J. Crystal Growth, 10 (1971) 67.

(10) J. Cisse and G. F. Bolling, J. Crystal Growth, 11 (1971) 25.

(11) K. A. Jackson and J. D. Hunt, Acta Metallurgica, 13 (1965) 1212.

(12) D. P. Grigor'ev, "Ontogeny of Minerals," Daniel Davey, New York, 1965, p. 94.

(13) G. Becker and A. Day, Proc. Washington Acad. Sci., 7 (1905) 283, through Ref. 4.

(14) G. Becker and A. Day, Zentralbl. Miner., (1916) 337, 364, through Ref. 21.

(15) C. W. Correns, Sitz. Ber. Preuss. Akad. Wiss., Phys.-Math., 11 [illegible] 1, through Ref. 4.

(16) E. Schi[illegible], Z. Metallkunde, 27 (1935) 4, 76, through Ref. 4.

(17) A Shubnikov, Z. Krist., 88 (1934) 466, through Ref. 4.

(18) I. N. Fridlyander and N. A. Vysotskaya, Doklady Akad. Nauk SSSR, 62 (1948) 1, 71, through Ref. 4.

(19) C. W. Correns and W. Steinborn, Z. Krist., A101 (1939) 117, through Ref. 4.

(20) G. B. Bokii, Trudy Inst. Kristall. Akad. Nauk SSSR No. 5 (1940) 143, through Ref. 21.

(21) V. Ya Khaimov-Mal'kov in "Growth of Crystals," A. V. Shubnikov and N. N. Sheftal', editors, Consultants Bureau, Inc., New York, Vol. 2, 1959, p. 3.

(22) C. W. Correns, Faraday Society, Discussion, 5 (1949) 267.

(23) A. W. Adamson, "Physical Chemistry of Surfaces," Wiley, New York, 1967, Chapter 7.

(24) M. V. Pikunov, Metalloved. i Obrabotka Tsvetnykh Metal. i Splavov, Sbornik State i, 1957, 55; through CA, 52 (1958) 16826c.

(25) D. R. Uhlmann, Ph.D. Dissertation, Harvard University, Cambridge, Massachusetts, 1963.

(26) R. B. Bird, W. E. Stewart and E. N. Lightfoot, "Transport Phenomena," Wiley, New York, 1960, Chapter 3.

(27) W. Jost, "Diffusion in Solids, Liquids, Gases," Academic Press, New York, 1960, Chapter 1.

(28) J. W. Cahn, W. B. Hillig and G. W. Sears, Acta Metallurgica, 12 (1964) 1421.

(29) K. A. Jackson, D. R. Uhlmann and J. D. Hunt, J. Crystal Growth, 1 (1967) 1.

(30) K. A. Jackson, in "Liquid Metals and Solidification," American Society for Metals, Cleveland, 1958, 174.

(31) K. A. Jackson and J. D. Hunt, Acta Metallurgica, 13 (1965) 1212.

(32) J. W. Cahn, Acta Metallurgica, 8 (1960) 554.

(33) F. D. Rosi, RCA Review, 19 (1958) 349.

(34) C. Hulse and J. Batt, Tech. Report K910803-5, United Aircraft Corp., May 1971.

(35) G. A. Chadwick, in "Fractional Solidification," M. Zief and W. R. Wilcox, editors, Dekker, New York, 1967, Chapter 4.

(36) W. R. Wilcox, J. Crystal Growth, 7 (1970) 203.

(37) J. W. Rutter and B. Chalmers, Can. J. Phys., 31 (1953) 15.

(38) W. A. Tiller, K. A. Jackson, J. W. Rutter, and B. Chalmers, Acta Metallurgica, 1 (1953) 428.

(39) W. R. Wilcox, J. Crystal Growth, 12 (1972) 93.

(40) W. A. Tiller and J. W. Rutter, Can. J. Phys., 34 (1956) 96.

(41) T. S. Plaskett and W. C. Winegard, Can. J. Phys., 37 (1959) 1955.

(42) W. G. Pfann, C. E. Miller and J. D. Hunt, Rev. of Scient. Inst., 37 (1966) 649.

(43) S. Ruben, "Handbook of the Elements," 2nd Edition, Howard W. Sams and Co., Indiana, 1967.

(44) R. H. Perry, editor, "Chemical Engineering Handbook," 4th Edition, McGraw-Hill, New York, 1963.

(45) J. S. Glass, Chem. Engr. Progress, 68 (1972) 59.

(46) R. C. Weast, editor, "Handbook of Chemistry and Physics," 53rd Edition, The Chemical Rubber Co., Cleveland, 1972.

(47) P. G. Stecher, editor, "The Merck Index of Chemicals and Drugs," 7th Edition, Merck and Co., New Jersey, 1960.

(48) N. B. Tsederberg, "Thermal Conductivity of Gases and Liquids," the M.I.T. Press, Cambridge, Massachusetts, 1965, through Reference 25.

(49) B. Chalmers, "Principles of Solidification," Wiley, New York, 1964, Chapter 6.

(50) W. R. Wilcox and P. J. Shlichta, J. Appl. Phys., 42 (1971) 1823.

(51) J. M. Dallavalle, "Micromeritics," Pitman, New York, 1948, Chapter 4.

(52) M. S. Peters and K. D. Timmerhaus, "Plant Design and Economics for Chemical Engineers," 2nd Edition, McGraw-Hill, New York, Chapters 2, 3 and 4, 1968.

(53) Fisher Scientific Co., Product Bulletin 5-712-100.

(54) M. J. Joncich and D. R. Bailey, Anal. Chemistry, 32 (1960) 1578.

(55) E. F. G. Herington, R. Handley and A. J. Cook, Chemistry and Industry, (London) (1956) 292.

(56) N. Maens, in "Physics of Snow and Ice," Proc. of Int. Conf. on Low Temp. Sci., 1966, The Institute of Low Temp. Sci., Hokkaido University, Sapporo, Japan, Vol. 1, p. 207.

(57) L. Tien, "Freezing of a Convective Liquid in a Crystal Growth Tube," Ph.D. Dissertation, Univ. of Michigan, Ann Arbor, 1968.

(58) H. Schlichting, "Boundary Layer Theory," McGraw-Hill, New York, 4th Edition, 1960, Chapter 5.

(59) D. R. H. Jones and G. A. Chadwick, Phil. Mag., 22 (1970) 291.

(60) D. Turnbull, J. Appl. Phys., 21 (1950) 1022.

(61) D. Turnbull, "Liquids: Structure, Properties, Solid Interactions," T. J. Hughel, editor, Elseiver, New York, 1965, p. 16.

(62) O. Jantsch, Zeit. Krist., 103 (1956) 198.

(63) R. R. Dreisbach, "Physical Properties of Chemical Compounds," Advances in Chemistry Series, No. 15, American Chemical Society, Washington, D.C., 1950, p. 354.

(64) F. Giordani, in "International Critical Tables,", E. W. Washburn, editor, McGraw-Hill, New York, Vol. 7, 1930, p. 211.

(65) J. P. Hirth and G. M. Pound, "Condensation and Evaporation," in Progress in Material Science, Pergamon Press, Oxford, Vol. 11, 1963, Chapter F.

(66) J. P. Hirth, G. M. Pound and G. S. St. Pierre, Met. Trans., 1 (1970) 393.

(67) C. A. Ward, A. Balakrishnan and F. C. Hooper, J. Basic Engr., 695, Oecember 1970.

(68) W. D. Weatherford, J. Colloid and Interface Sci., 34 (1970) 197.

(69) L. D. Landau and E. M. Lifshitz, "Statistical Physics," Addison-Wesley, Reading, Massachusetts, 1969, Chapter IX.

(70) J. A. Burton, R. C. Prim and W. P. Slichter, J. Chem. Phys., 21 (1953) 1987.

(71) O. Turnbull and J. C. Fisher, J. Chem. Phys., 17 (1949) 71.

(72) S. Miyazawa and H. Iwasaki, Japanese J. Appl. Phys., 9 (1970) 441.

(73) L. A. Swanger and W. C. Rhines, J. Crystal Growth, 12 (1972) 323.

(74) T. Arizumi and N. Kobayashi, Japanese J. Appl. Phys., 8 (1969) 1091.

(75) N. Kobayashi and T. Arizumi, Japanese J. Appl. Phys., 9 (1970) 361.

(76) G. Flint, in Kirk-Othmer's "Encyclopedia of Chemical Technology," 2nd Edition, Wiley, New York, Suppl. Vol., 1971, p. 438.

APPENDIX A

INFLUENCE OF CRYSTAL DIMENSIONS ON THE INTERFACIAL TEMPERATURE GRADIENT

Reprinted from:
Journal of Crystal Growth 12 (1972) 191–194 © *North-Holland Publishing Co.*
Printed in the Netherlands

INFLUENCE OF CRYSTAL DIMENSIONS ON THE INTERFACIAL TEMPERATURE GRADIENT

VINCENT H. S. KUO and WILLIAM R. WILCOX

Chemical Engineering and Material Science Departments, University of Southern California, Los Angeles, California 90007, U.S.A.

Received 26 February 1971; revised manuscript received 29 November 1971.

The influence of the length and radius of a crystal on the interfacial temperature gradient was estimated by use of a one-dimensional heat transfer calculation. It was found that the temperature gradient is substantially independent of crystal length only when the Biot number hR/k is large (where h is the heat transfer coefficient from the crystal surface, R is crystal radius, and k is thermal conductivity).

1. Introduction

The temperature gradient at the solid–liquid interface of a solidifying crystal is an important parameter. It influences the microscopic shape stability of the interface, the generation of dislocations, the macroscopic shape of the interface, eutectic structures, and free convection in the adjacent melt. In directional solidification techniques such as Czochralski and Bridgman growth the geometry of the crystal changes during growth, i.e., the crystal grows longer. As the crystal grows the interfacial temperature gradient changes as well.

In this paper we estimate the interfacial temperature gradient and in particular examine its dependence on crystal geometry. A cylindrical crystal is assumed which loses heat to its surroundings which are at constant temperature T_a. The heat transfer coefficient h for the cylindrical surface is assumed constant, but different from that at the cold end of the crystal h_L*. The problem is solved for a non-growing crystal, but the error caused by neglecting the heat carried by the moving crystal is estimated. A one-dimensional approximation is employed, with the geometry and heat transfer parameters as shown in fig. 1.

* The heat transfer coefficient is defined as the rate of heat loss per unit area from the surface divided by the temperature difference between the surface and the surroundings (ambient gas for convective heat transport, heat shields or cooling surfaces for heat transport by radiation).

2. Theory

The non-dimensionalized differential equation governing heat transfer in a moving thin rod is [1,2]

$$\frac{\partial^2\theta}{\partial\eta^2} - \alpha\frac{\partial\theta}{\partial\eta} - 2H\theta = \alpha\frac{\partial\theta}{\partial\tau}, \qquad (1)$$

where $\theta = (T-T_a)/(T_i-T_a)$, $\eta = z/R$, $\alpha = V\rho C_p R/k$ (Péclet number), $H = hR/k$ (Biot number for cylindrical surface), and $\tau = tV/R = L/R$. Here T is the temperature at distance z from the interface, T_i is the interface temperature, R is the radius of the crystal, V is the growth rate, ρ is the crystal density, C_p is the heat capacity, k is the thermal conductivity, and L is

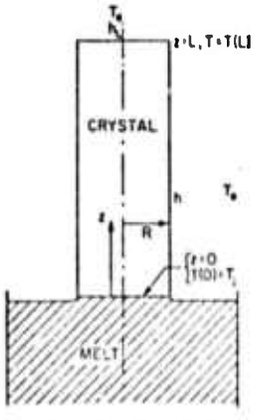

Fig. 1. Geometry and parameters of problem.

the length of the crystal. The boundary conditions are

at $\eta = 0$ (the solid–liquid interface), $\theta = 1$; (2)

at $\eta = L/R = \tau$ (the cold end of the crystal),

$$\partial\theta/\partial\eta = -\frac{h_L R}{k}\theta = -H_L\theta; \quad (3)$$

at $\tau = 0$ (infinitesmally short crystal), $\theta = 1$. (4)

When $H_L = H$ the thermal conditions at the cold end of the ingot are the same as on the cylindrical surface, while $H_L = 0$ corresponds to an insulated crystal end and $H_L \to \infty$ to a perfectly cooled end, $T(L) = T_s$.

We have been unable to solve these equations analytically because of the moving boundary condition, eq. (3). Although a numerical solution could be obtained this is thought to be unprofitable since the equations only approximate reality. Therefore, we first examine the solution for $\alpha = 0$, which is*.

$$\theta = \left[\frac{H_L}{H}\sinh(2H)^{\frac{1}{2}}(\tau-\eta) + \left(\frac{2}{H}\right)^{\frac{1}{2}}\cosh(2H)^{\frac{1}{2}}(\tau-\eta)\right] \times \left[\frac{H_L}{H}\sinh(2H)^{\frac{1}{2}}\tau + \left(\frac{2}{H}\right)^{\frac{1}{2}}\cosh(2H)^{\frac{1}{2}}\tau\right]^{-1}. \quad (5)$$

From this the dimensionless interfacial temperature gradient is found to be

$$-\left(\frac{\partial\theta}{\partial\eta}\right)_0 = (2H)^{\frac{1}{2}}\left[\frac{H_L}{H}\cosh(2H)^{\frac{1}{2}}\tau + \left(\frac{2}{H}\right)^{\frac{1}{2}}\sinh(2H)^{\frac{1}{2}}\tau\right] \times \left[\frac{H_L}{H}\sinh(2H)^{\frac{1}{2}}\tau + \left(\frac{2}{H}\right)^{\frac{1}{2}}\cosh(2H)^{\frac{1}{2}}\tau\right]^{-1}. \quad (6)$$

Curves calculated from this equation are shown in fig. 2. It is seen that the predicted temperature gradient is independent of length only for $H = H_L = 2$. As the crystal length increases, the dimensionless temperature gradient approaches $-(2H)^{\frac{1}{2}}$. The fractional deviation from this asymptotic value is

$$f_L = [|(2H)^{\frac{1}{2}} - (\partial\theta/\partial\eta)_0|](2H)^{-\frac{1}{2}} = \left[\left|\frac{H_L}{H} - \left(\frac{2}{H}\right)^{\frac{1}{2}}\right|\exp(-(2H)^{\frac{1}{2}}\tau)\right] \times \left[\frac{H_L}{H}\sinh(2H)^{\frac{1}{2}}\tau + \left(\frac{2}{H}\right)^{\frac{1}{2}}\cosh(2H)^{\frac{1}{2}}\tau\right]^{-1}. \quad (7)$$

* Reed considered this problem for radiation into zero temperature with a perfectly cooled end ($H_L = \infty$, $T_s = 0$ and $h = \sigma\varepsilon T^3$, where ε is the emissivity and σ is the Stefan–Boltzmann constant)[3].

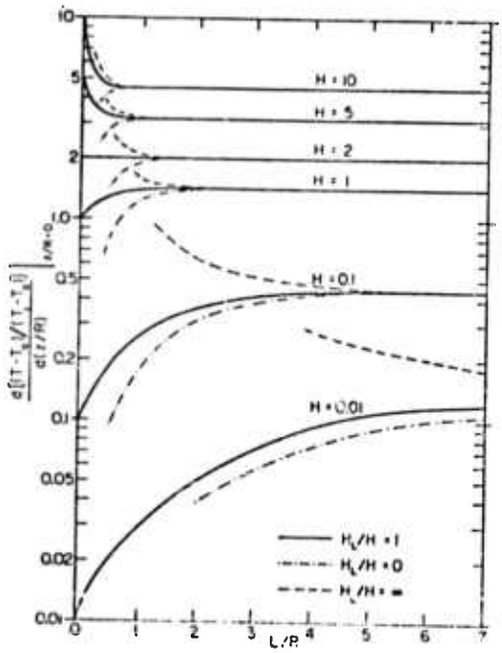

Fig. 2. Predicted dependence of the dimensionless interfacial temperature gradient on the length of the crystal and on the Biot number $H = hR/k$ for the cylindrical surface for $H_L = 0$ (cold end insulated), $H_L = H$, and $H_L = \infty$ (perfectly cooled end, $T(L) = T_s$); eq. (6).

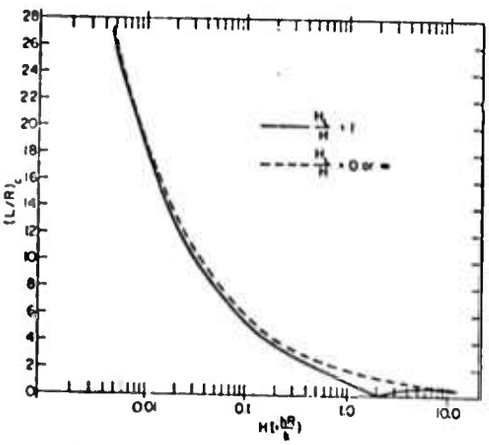

Fig. 3. Length of the crystal for which the interfacial temperature gradient deviates by 1% from that for a long crystal, for $H_L/H = 1$ and 0 or ∞ (same result for 0 and ∞); eq. (8).

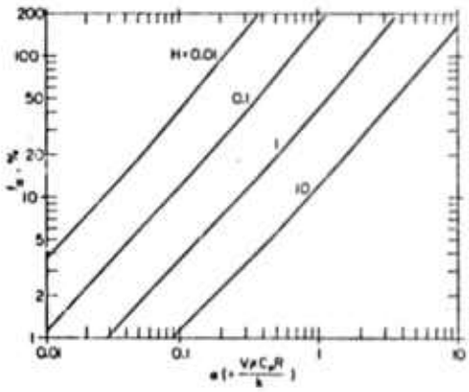

Fig. 4. Percentage error in the interfacial temperature gradient of a long crystal caused by neglecting the heat carried by the crystal motion due to growth; eq. (11).

From this we may find the length of crystal for which the interfacial temperature gradient differs from the asymptotic value by any chosen amount. If $f_L \ll 1$, we note that

$$\sinh (2H)^{\frac{1}{2}}\tau \approx \cosh (2H)^{\frac{1}{2}}\tau \approx \tfrac{1}{2}\exp [(2H)^{\frac{1}{2}}\tau],$$

and we find that the length at which the error is f_L is given by

$$\tau_e = (L/R)_e = -\frac{1}{2(2H)^{\frac{1}{2}}}\ln\left\{\tfrac{1}{2}f_L\left[\frac{H_L}{H}+\left(\frac{2}{H}\right)^{\frac{1}{2}}\right]\times\left[\left|\frac{H_L}{H}-\left(\frac{2}{H}\right)^{\frac{1}{2}}\right|\right]^{-1}\right\}. \quad (8)$$

This is plotted in fig. 3 for a 1% deviation from the asymptotic gradient, i.e., $f_L = 0.01$. τ_e may be regarded as the dimensionless length below which the interfacial temperature gradient depends on length.

The influence of crystal motion on the interfacial temperature gradient can only be determined analytically for a very long crystal ($L \to \infty$). The steady state solution ($\partial\theta/\partial\tau = 0$) of eq. (1) for $L \to \infty$ is[2])

$$\theta = \exp\{\tfrac{1}{2}[\alpha-(\alpha^2+8H)^{\frac{1}{2}}]\eta\}, \quad (9)$$

which yields the dimensionless interfacial temperature gradient

$$(d\theta/d\eta)_0 = \tfrac{1}{2}[\alpha-(\alpha^2+8H)^{\frac{1}{2}}]. \quad (10)$$

Thus the fractional error in the interfacial temperature gradient of a long crystal caused by neglecting the motion of the crystal is found to be

$$f_e = \left|\frac{-(8H)^{\frac{1}{2}}-\alpha+(\alpha^2+8H)^{\frac{1}{2}}}{\alpha-(\alpha^2+8H)^{\frac{1}{2}}}\right|, \quad (11)$$

which is plotted in fig. 4.

3. Discussion

These results show that when a crystal's length exceeds its diameter, its interfacial temperature gradient depends on its length only for small values ($\lesssim 1$) of the Biot number H. This is reasonable since the Biot number is the ratio of the surface to the longitudinal thermal conductivity, or the ratio of the ease of losing heat from the surface to the ease of conducting heat down the crystal. Thus, for example if a crystal's length is twice its diameter, then for large H ($\gtrsim 0.15$) its interfacial temperature gradient is influenced only by the thermal conditions at the cylindrical surface, while for small H ($\lesssim 0.15$) the thermal conditions at the other end of the crystal also influence the interfacial temperature gradient. Values of H can be estimated for typical crystal growth situations. For good

Table 1

Comparison of the present results (using $H_L/H = \infty$, $T_\infty = 0$ K, $R = 1$ cm, and $h = \sigma\varepsilon T_i^3$) with those of Reed[3])

Material	Ge	Cr_2O_3	W
Melting point, T_i (K)	1210	2538	3640
Thermal conductivity, k (W/cm °K)	0.4	0.04	1.4
Emissivity, ε	0.2	0.8	0.36
Heat transfer coefficient, h (W/cm² K)	0.002	0.075	0.099
Biot number, $H = hR/k$	0.005	1.87	0.071
Present estimate of critical length L_c beyond which interfacial gradient constant (fig. 3) (cm)	26	1.4	7.2
Reed's critical length, L_c (cm)	15	0.8	3.9
Deviation of the interfacial gradient from value for semi-infinite crystal using Reed's L_c in eq. (8), f_L (%)	10	9.1	10.8
Present estimate of interfacial gradient for semi-infinite crystal, $(dT/dz)_0 = -(2H)^{\frac{1}{2}}T_i/R$ (K/cm)	121	4880	1365
Reed's estimate of $(dT/dz)_0$ (K/cm)	76	3000	865
Experimental $(dT/dz)_0$ from ref. 6 (K/cm)	115	–	–

conductors we generally find[2]) $H < 0.1$. For an organic compound with $h = 10^{-3}$ W/cm^2 °C for free convection to air[5]), $k = 10^{-3}$ W/cm °C, and $R = 4$ cm, we find $H = 4$.

At this point it is worthwhile to examine the validity of the various assumptions that have been made. It has previously been shown[2-4]) that the one-dimensional approximation used here is valid for $H \lesssim 0.2$. Fortunately it is for these low values of H that our results are significant in that a dependence of interfacial temperature gradient on length is predicted then. For $H \gtrsim 0.2$ we expect our results to be inaccurate primarily in the sense that the interfacial temperature gradient will be a function of radial position. Our conclusion that the interfacial thermal conditions are substantially independent of crystal length is expected to remain valid.

We have assumed h is constant, whereas in almost all real crystal growth systems h will be a function of z and T, both for convective heat transfer and for radiative heat transfer. When one estimates h, it is done for conditions near the interface, which have the primary influence on interfacial temperature gradients. It is of interest to compare the present results with those of Reed, as shown in table 1.

The error caused by neglecting the heat carried by the movement of a growing crystal is estimated in eq. (11). The worst possible case is that of a rapidly growing insulator. Thus for an organic with $V = 5$ cm/hr, $R = 2$ cm, $H = 2$ and $x = 1.3$, the error is about 20%, i.e., the interfacial temperature gradient of a long organic crystal is 20% lower than the quasi-steady state estimate.

Acknowledgement

The authors are grateful to the Petroleum Research Fund (administered by the American Chemical Society) for its financial support.

References

1) H. C. Carslaw and J. C. Jaeger, *Conduction of Heat in Solids*, 2nd ed. (Clarendon Press, Oxford, 1959) p. 148.
2) W. R. Wilcox and R. L. Duty, J. Heat Transfer 88c (1966) 45.
3) T. B. Reed, in: *Crystal Growth*, Ed. H. S. Peiser (Pergamon, Oxford, 1967) p. 39.
4) W. M. Rohsenow and H. Y. Choi, *Heat, Mass and Momentum Transfer* (Prentice-Hall, Englewood Cliffs, N.J., 1961) ch. 6.
5) W. H. McAdams, *Heat Transmission* (McGraw Hill, New York, 1954) ch. 7.
6) J. C. Brice and P. A. C. Wiffin, Solid-State Electron. 7 (1964) 183.

APPENDIX B

ECONOMIC CALCULATIONS

Following are the detailed calculations for the cost estimate for producing particle-free naphthalene. The assumptions made for the calculation are as follows:

(1) The production group consists of one engineer and one technician. This group works independently in a large company.

(2) The engineer is responsible for research, development, and administration. The technician is responsible for production and maintenance.

(3) The feed material is a reagent grade chemical, such as Baker's analyzed grade naphthalene.

A. Annual Production

In the two-man production group, the technician can handle five of six units of horizontal zone-refiners with rotation in routine production. Each unit is equipped with automatic control, not requiring much attention. The growth tube is 25 mm O.D. and 40 cm long. (The purified ingot is 22 mm in diameter and about 30 cm long.) The freezing rate is assumed to be 25 mm/hour (<28 mm/hour). Because two heaters are on each refiner, two zone passes are assumed to ensure particle-free naphthalene.

$$\text{Travel time} = \frac{40 \text{ cm}}{25 \text{ mm/hour}} = 16 \text{ hours}$$

Zone-refining operation can be conducted overnight so that most of the technician's time is spent in preparations for zone-refining and handling of zone-refined products. Thus, daily production of this group is about five purified ingots. Assuming 250 working days per year, the annual production is

$$5 \times (\pi \times 2.2 \times 30\ cm^3) \times (1.145\ gr/cm^3) \times 250$$
$$= 5 \times (207)(1.145) \times 250 = 300\ Kg/year\ .$$

B. Total Capital Investment

(1) Fixed-Capital Investment

(a)	Six units of horizontal zone-refiners with rotation. Design and fabrication by the production group or modification of the Fisher zone-refiner ($800/unit):	$12,000
(b)	Building with auxiliary facilities:	30,000
(c)	Laboratory equipment:	10,000
(d)	Indirect costs (design, engineering and contingency):	10,000
	Fixed-Capital Cost:	$62,000

(2) Working Capital, 10% of the Fixed-Capital cost: $ 6,000

Total Capital Investment (1) and (2): $68,000

C. Total Product Cost

(1)	Wages with 100% overhead (for one engineer and one technician):	$50,000
(2)	Depreciation (10 years) $62,000 x 0.1:	$ 6,000

(3) Feed materials (400 Kg):	$ 3,000
(4) Utilities (electricity, water and fuel):	$ 1,000
(5) Maintenance and repairs:	$ 1,000
(6) General expenses (administrative costs, research and development):	$ 2,000
(7) Miscellaneous (interest, insurance, taxes, etc.):	$ 2,000
Total Product Cost:	$65,000

D. Cost of Production

$65,000/300 Kg = 22¢/g.